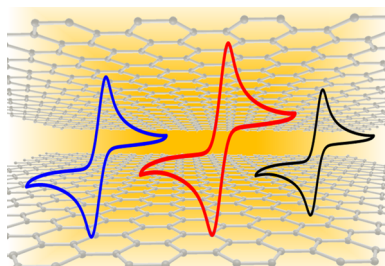


## Electrochemistry of Graphene and Related Materials

Adriano Ambrosi, Chun Kiang Chua, Alessandra Bonanni, and Martin Pumera\*

Division of Chemistry & Biological Chemistry, School of Physical and Mathematical Sciences, Nanyang Technological University, Singapore 637371, Singapore



### CONTENTS

1. Introduction	7150
2. Preparation of Graphene and Its Properties	7152
2.1. Top-down Methods	7152
2.1.1. Mechanical Exfoliation of Graphite	7152
2.1.2. Solution-Based Exfoliation of Graphite	7153
2.1.3. Electrochemical Exfoliation of Graphite	7154
2.1.4. Chemical Oxidation of Graphite, Exfoliation, and Reduction	7154
2.1.5. Opening/Unzipping Carbon Nanotubes: Graphene Nanoribbons	7154
2.1.6. Graphite and Carbon Nanotubes: Source of Impurities	7156
2.2. Bottom-up Methods	7157
2.2.1. Chemical Synthesis	7157
2.2.2. Epitaxial Growth on SiC	7157
2.2.3. Chemical Vapor Deposition	7159
2.2.4. 3D Graphene	7159
2.3. Processability of Graphene Materials	7160
2.4. Characterization Methods	7160
3. Electrochemistry at Graphene Surfaces	7161
3.1. Graphene and Heterogeneous Electron Transfer	7161
3.2. Inherent Electrochemical Activity of Graphene-Related Materials	7163
3.3. Influence of Dopants and Impurities on Graphene Electrochemistry	7164
3.4. Spectroelectrochemistry of Graphene	7165
4. Graphene in Electrochemical Sensing and Bio-sensing	7166
4.1. Voltammetric and Amperometric Graphene Sensors and Biosensors	7166
4.1.1. Analysis of Biomarkers	7166
4.1.2. DNA Analysis	7167
4.1.3. Protein Analysis	7169
4.1.4. Cell Analysis	7169
4.1.5. Analysis of Heavy Metals	7169
4.1.6. Graphene in Security Applications	7170
4.2. Impedimetric Graphene Sensors and Biosensors: Toward Label-Free Detection	7170
4.2.1. DNA Analysis	7171
4.2.2. Protein Analysis	7171
4.2.3. Cell Analysis	7171
4.3. Potentiometric Graphene Sensors and Biosensors	7172
5. Graphene in Energy Systems	7172
5.1. Graphene for Capacitors and Supercapacitors	7172
5.2. Oxygen Reduction Reaction on Graphene	7174
5.3. Graphene-Based Solar Cells	7175
5.4. Graphene-Based Lithium Ion Batteries	7177
6. Conclusion and Future Perspectives	7179
Appendix 1: IUPAC Definitions of Graphite, Graphene, and Amorphous Carbon	7180
Appendix 2: Overview of the Electrochemistry of Graphene, Graphite, and Graphene-Related Materials	7180
Author Information	7180
Corresponding Author	7180
Notes	7180
Biographies	7180
Acknowledgments	7181
References	7181

### 1. INTRODUCTION

Sustainable energy production, environmentally sustainable development, and affordable healthcare are three major challenges of the current global community. Electrochemistry is at the heart of many chemical and biological sensors, as well as energy storage and generation technologies. Electrochemistry utilizes energy in the cleanest possible form, as electricity, to collect or inject electrons through electrodes. New advanced materials are always sought after to improve the performances of existing devices or to create new disruptive technologies. Graphene and related materials bring new perspectives and prospects to electrochemical systems. The advantages of graphene for electrochemical devices are manyfold. The overall aim of this review is to provide a critical overview of our understanding on the electrochemistry of graphene and related materials. We will first discuss the way how the graphene and related materials are prepared, since the methods have strong influences on the materials properties. Consecutively, we describe how the fundamental electrochemical properties of graphene are influenced by the materials properties of graphene. Spectroelectrochemistry and its insight into graphene structure and function are discussed. We will demonstrate the role of dopants and impurities on graphene electrochemistry. We then focus on numerous application of

Received: January 15, 2014

Published: June 4, 2014

graphene in electrochemical devices, starting with sensors and biosensors and continuing with energy storage and generation applications. We critically discuss the advantages and disadvantages of graphene-based systems and we outline future challenges.

Carbon is the fourth most common element in the universe (after hydrogen, helium, and oxygen). However, carbon is not the most abundant element in the Earth's crust, as elements such as iron, silicon, or even titanium are found in higher quantities. Nevertheless, carbon constitutes the very fundamental building block of life. It is also widely applied in most technologies, since it is often found in its pure elemental forms (i.e., coal, graphite, and diamond) in large deposits and requires only minimal processing for subsequent applications. Specifically in electrochemical applications, carbon materials are of enormous industrial importance for already more than 100 years.<sup>1</sup> Carbon electrodes are frequently utilized on an industrial scale for metallurgy; production of silicon, yellow phosphorus, and calcium carbide; or in batteries (the zinc–carbon battery is the most popular low-cost battery available). These applications are largely made possible by the excellent physical and chemical properties of carbon-based materials. These include the ability to carry a large amount of electrical current, withstand very high temperatures, exhibit fast heterogeneous electron transfer (in the case of amorphous carbon and graphite), and exhibit good mechanical properties, even under the aforementioned extreme conditions. Graphite and amorphous carbon are able to remain as solids up to a temperature of 3825 °C before sublimation occur. This is highly unique to carbon materials, as only a few other elements show almost similar properties, with tungsten (mp 3414 °C), osmium (mp 3033 °C), and tantalum (mp 3017 °C) being able to withstand such thermal conditions [cf. metals such as iron (mp 1538 °C), silicon (mp 1414 °C), and platinum (mp 1768 °C)].<sup>2</sup> Moreover, graphite exhibits excellent electrical and thermal conductivities. Conductivity in graphite is highly anisotropic, which means that it differs along the different axes of the crystal. The electrical resistivity of graphite (in highly ordered pyrolytic graphite) is 0.04 mΩ cm along the graphene sheets ( $\text{sp}^2$ -hybridized carbon atoms) and 150 mΩ cm across the stacked graphene sheets.<sup>3</sup> The resistivity of a single crystal of graphite is  $\sim 10^{-6}$  mΩ cm along the graphene sheet.<sup>4</sup> In comparison, the electrical resistivity of copper is  $1.68 \times 10^{-3}$  mΩ cm and mercury is  $1.47 \times 10^{-3}$  mΩ cm.<sup>5</sup> The thermal conductivity of graphite along the graphene sheets is  $4.2 \text{ W cm}^{-1} \text{ K}^{-1}$ , while across the stacked graphene sheets is  $0.04 \text{ W cm}^{-1} \text{ K}^{-1}$  at 20 °C (cf. iron at  $15.4 \text{ W cm}^{-1} \text{ K}^{-1}$  and platinum at  $4.95 \text{ W cm}^{-1} \text{ K}^{-1}$ ).<sup>6</sup> Even though these values pertain to graphite, they have large significances and implications for graphene research, as will be further discussed below. More importantly, these values provide a rough idea and serve as a starting point of appreciation for the properties of a single graphitic layer—graphene.

Graphene is defined by the International Union for Pure and Applied Chemistry (IUPAC) as “*a single carbon layer of graphite structure, describing its nature by analogy to a polycyclic aromatic hydrocarbon of quasi-infinite size*”.<sup>7</sup> However, this definition is hardly adhered to in the current literature. The word “graphene” is used to label a wide variety of carbon materials instead; these materials can deviate in various ways from the IUPAC definition of graphene. There are four common deviations: (i) The number of layers of graphene is often more than one; i.e., the definition of “single layer” parameter is

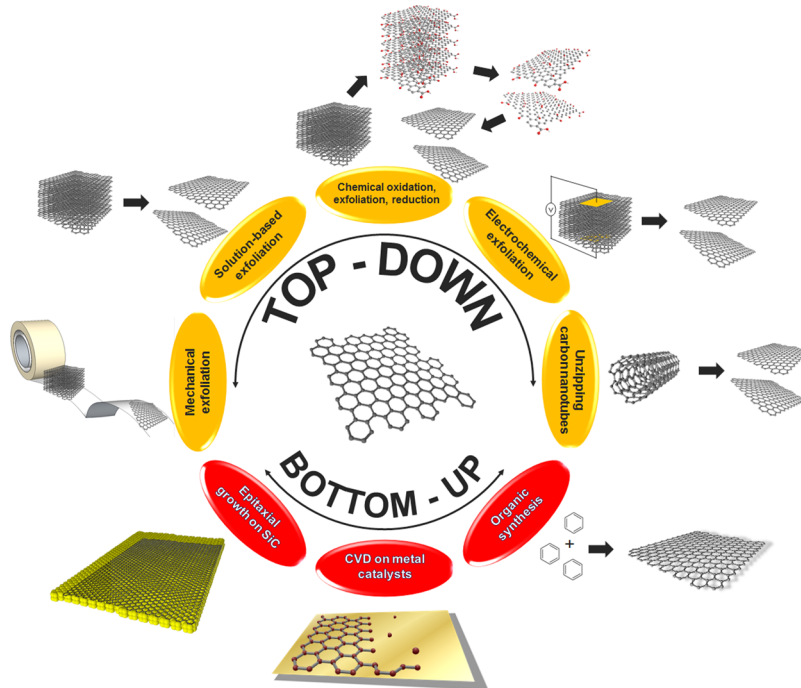
violated. Such “graphene” can consist of single, few (two to nine layers), or even multiple layers ( $\geq 10$  layers; in some cases, these multilayer graphene can be called ultrathin graphite; note, however, that the IUPAC definition of graphite<sup>7</sup> requires long-range stacking of graphene layers along the *c*-axis in ABA or ABC order, a condition which is quite often not fulfilled for multilayer graphene<sup>8,9</sup>). (ii) A large sheet of “graphene” is often build up from fragments of small (tens of nanometers) single or few layer graphene “stitched” together at grain boundaries; thus, the definition of “quasi-infinite size” parameter defined by IUPAC<sup>7</sup> is violated. This is typical for the so-called CVD graphene (for details see section 2.2.3). (iii) Chemically modified graphene materials (consisting of various thickness) are often laden with a large amount of heteroatoms, mostly oxygen-containing groups. (iv) Finally, heavily damaged graphene sheets with a crystallite size of nanometers contain a large amount of  $\text{sp}^3$ -hybridized carbon defects, adatoms, and physical holes in the structure with close resemblance to amorphous carbon (for the IUPAC definition of amorphous carbon, see Appendix 1).

The aforementioned graphene materials differ significantly in terms of the materials properties, including electrochemistry. Such properties are strongly influenced by the preparation methods of the materials. The oversimplified naming of all these different graphene materials under a single umbrella of “graphene” contributes to further confusion among scientists who are not involved in graphene research but may have expected that all graphene materials reported so far will follow the IUPAC definition, which is often not the case. We wish to emphasize here that even though the trend of classifying all graphene-related materials as “graphene” is most likely irreversible, all “graphene” materials must always be accompanied by full characterizations and descriptions so that the research community is well-informed of the exact nature of the discussed materials. However, for simplicity sake, we will refer all graphene-related materials in this review as “graphene” when discussing the materials collectively and we will attempt to be as specific as possible in the following discussions of individual cases.

The history of the discovery of graphene is rather interesting. Similar to carbon nanotubes, which were “rediscovered” several times, graphene was reported for the first time as a single layer back in 1968.<sup>10</sup> Single or few layers of graphene oxide were reported in the 1960s by Boehm, who made significant contributions to the field (Boehm is also behind the 1995 IUPAC definition of graphene).<sup>7</sup> In 2010, Andre Geim and Konstantin Novoselov received the Nobel Prize in Physics, not for the discovery of graphene, which is often misunderstood, but for the “groundbreaking experiments regarding the two-dimensional material, graphene”,<sup>11</sup> based on their study published in 2004.<sup>12</sup> For an intriguing history of graphene, please refer to the suggested specialized reviews and commentaries.<sup>13,14</sup>

Here, we wish to provide a comprehensive discussion on the rich electrochemistry of graphene materials. As mentioned above, real world “graphene” materials are not just simple and well-defined molecules but are materials of complex and variable structures that consequently define the inherent electrochemical properties. Since the structures and compositions of graphene materials are intimately linked to the preparation methods, we will proceed in this review by first describing the various methods of preparation, generally subdivided to top-down or bottom-up methods, followed by

Scheme 1. Illustration of the Current Preparation Methods for Graphene and Graphene-Related Materials



descriptions of analytical techniques commonly used for their characterizations. Consequently, we will discuss the fundamentals of electrochemistry at the various graphene surfaces as well as their inherent electrochemistry. Lastly, we will wrap up this review with comprehensive descriptions on the applications of graphene materials in electrochemical sensing, energy storage and energy production devices.

## 2. PREPARATION OF GRAPHENE AND ITS PROPERTIES

Several synthetic routes have been established to prepare graphene, but each one of them, besides possessing different scalability, generates graphene with very different characteristics, which strongly influence its properties. The preparation methods of graphene can be classified into two distinct approaches: (i) top-down and (ii) bottom-up (Scheme 1). The top-down methods generally include the exfoliation of graphite as starting material through mechanical (e.g., Scotch tape), chemical (e.g., solution-based exfoliation, graphite oxide exfoliation/reduction), or electrochemical (oxidation/reduction and exfoliation) processes, which aim at weakening the van der Waals forces between the graphene layers. A special category of process under the top-down approach comprises the fabrication of graphene nanoribbons, which can be achieved by opening/unzipping carbon nanotubes through chemical or thermal routes.

On the other hand, the bottom-up methods generate graphene by assembling small molecular building blocks into single or few layer graphene structures by means of catalytic (e.g., CVD), thermal (e.g., SiC decomposition), or chemical (organic synthesis) processes.

### 2.1. Top-down Methods

Graphite is a highly anisotropic material. Within the respective graphene sheets, carbon atoms are linked by  $sp^2$  bonds in a honeycomb lattice network with interatomic distance of 1.42 Å; however, along the *c*-axis of graphite crystal, the graphene

sheets are only held by weak van der Waals forces with an interlayer distance of 3.35 Å. It is, therefore, possible to mechanically or chemically exfoliate graphite into smaller units, to ultimately obtain a single graphene layer. In the following subsections, we will describe the most common top-down preparation methods of graphene with an emphasis on the different features of the resulting graphene materials and how these features may affect the electrochemical properties. Moreover, by using graphite or carbon nanotubes as a starting material in the top-down methods, a further subsection is also included in the discussions to describe how the impurities (e.g., carbon, metallic) present inherently in graphite or carbon nanotubes remain intimately embedded in the resulting graphene. The implications of these impurities on the electrochemical properties of the graphene materials will be discussed as well.

**2.1.1. Mechanical Exfoliation of Graphite.** Micro-mechanical cleavage of highly oriented pyrolytic graphite (HOPG) is the first proposed method to isolate a single layer graphene. It was described for the first time by Geim and Novoselov in 2004.<sup>12</sup> This method involves repeatedly peeling off layers of graphene from HOPG by means of an adhesive tape to eventually give single graphene layers that can be transferred successively onto an appropriate surface (e.g.,  $\text{SiO}_2$  wafers) through a wet or dry transfer technique. More commonly referred to as the “Scotch-tape method”, such micromechanical cleavage has facilitated the initial experimental measurements on the extraordinary electronic,<sup>12,15–17</sup> mechanical,<sup>18</sup> and thermal conductivity<sup>19</sup> properties of graphene, which subsequently triggered a burst of interest for graphene in several branches of science.<sup>20</sup> The Scotch-tape method is extremely simple, enables the isolation of single layer graphene with a dimension up to 1 mm<sup>21</sup> in size and causes minimal or no alteration to the graphene sheet in the process (Figure 1A). In fact, graphene obtained by this method is considered pristine and is of the highest quality achievable thus far. However, it can only be adopted for fundamental studies and basic research due

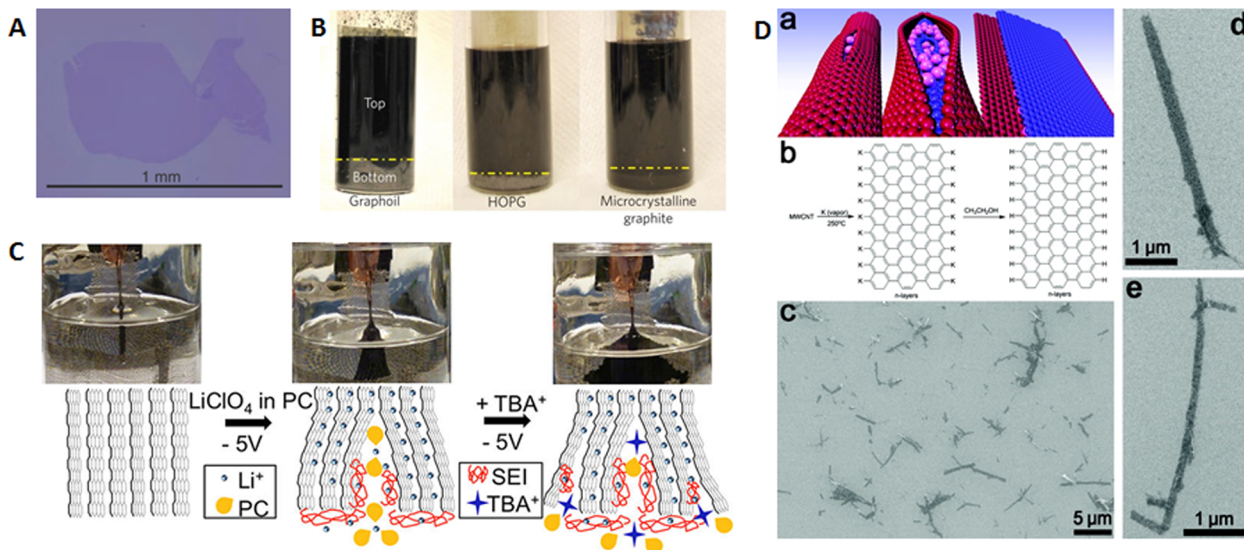


**Figure 1.** (A) Large graphene crystal prepared on an oxidized Si wafer by the Scotch-tape technique. Reprinted with permission from ref 21. Copyright 2009 The American Association for the Advancement of Science. (B) Comparison of chlorosulfonic acid dispersion of graphite (25 mg mL<sup>-1</sup> initial concentration) obtained from different sources as indicated below the vials. A dark upper portion (top) is obtained for all the sources after 12 h of centrifugation (5000 rpm), with a gray-colored lower portion (bottom). The yellow line on the vials indicates the interface between the top and bottom phases in the three vials. Reprinted with permission from ref 35. Copyright 2010 Nature Publishing Group. (C) Schematic and images of electrochemical expansion of graphite. Reprinted with permission from ref 52. Copyright 2012 American Chemical Society. (D) Schematic of the splitting process and SEM images on a Si/SiO<sub>2</sub> surface of GNRs produced by potassium splitting. (a) Schematic of potassium intercalation between the nanotube walls and sequential longitudinal splitting of the walls followed by unraveling to a nanoribbon stack. (b) Chemical schematic of the splitting processes where ethanol is used to quench the aryl potassium edges; only a single layer is shown for clarity, while the actual number of GNR layers correlates with the number of concentric tubes in the MWCNT. (c) Overview of a large area showing complete conversion of MWCNTs to GNRs. (d, e), Images of isolated GNR stacks demonstrating characteristic high aspect ratios and predominantly parallel edges. Reprinted with permission from ref 90. Copyright 2011 American Chemical Society.

to the low reproducibility and the impossibility of large-scale implementation. Pristine graphene isolated by such micro-mechanical exfoliation of graphite is expected to possess poor electrochemical activity, most likely comparable to the basal plane of graphite.<sup>22</sup> Although recent studies showed an improved electron transfer kinetic for pristine graphene with certain redox probes compared to the basal plane of graphite, such improvement was possibly attributed to the presence of corrugations on the graphene sheets.<sup>23,24</sup>

Since electrochemical applications normally require bulk quantities of materials for electrode fabrications, the mechanical exfoliation method is, therefore, unsuitable for this purpose. In addition, the extremely low density of defects present on pristine graphene may present a significant drawback when it comes to the electron transfer properties. It is, in fact, documented that the electron transfer events occur about 10<sup>6</sup> times faster at defects or edgelike portions of carbon materials as compared to basal or defect-free planes.<sup>25,26</sup> For more practical applications, in particular with regard to electrochemical applications, other fabrication methods should be considered, as we will discuss in the following subsections.

**2.1.2. Solution-Based Exfoliation of Graphite.** Considering the high quality of graphene that can be obtained by the mechanical exfoliation of HOPG, attempts have been made to develop a chemical method that is able to facilitate the separation of the graphene sheets with minimal alteration. Excellent solution-based exfoliation of HOPG can be achieved when the energy loss during exfoliation is minimized, specifically in organic solvents with surface tensions of ~40 mJ m<sup>-2</sup>.<sup>27</sup> Moreover, good organic solvents have a Hildebrand solubility parameter close to 23 MPa<sup>1/2</sup> and nonzero values for

the polar and H-bonding parameters of Hansen solubility parameters.<sup>28</sup> Concurrent ultrasonication treatment is generally adopted to drive the exfoliation process. Coleman and co-workers obtained good quality graphene sheets at about 1% concentration in *N*-methylpyrrolidone (NMP) solvent.<sup>27</sup> Similarly, Novoselov and co-workers prepared a graphene suspension by ultrasonication of HOPG for 3 h in *N,N*-dimethylformamide (DMF).<sup>29</sup> Numerous other organic solvents ranging from polar to nonpolar types have been investigated as well.<sup>28</sup> The liquid-phase exfoliation of graphite is certainly appealing, since this method can be scaled-up for larger production volume. However, the maximum achievable yield is still quite low at the moment. An improvement was obtained by Dai and co-workers, who ultrasonicated tetrabutylammonium hydroxide (TBA) and oleum intercalated graphite in DMF to achieve about 90% of single layer graphene.<sup>30</sup>

The exfoliation of graphite was also achieved in aqueous solutions with the use of ultrasound in the presence of surfactants such as sodium dodecyl benzenesulfonate (SDS), sodium cholate (SC),<sup>31,32</sup> and 1-pyrenecarboxylic acid.<sup>33</sup> The use of ultrasonication is necessary to facilitate the separation of graphene sheets but has a major drawback of breaking them into very small and inhomogeneous flakes. In an attempt to circumvent that, an ultrasonication-free exfoliation was performed by means of a preliminary intercalation of graphite with potassium, followed by a spontaneous exfoliation in NMP.<sup>34</sup> A high concentration of single layer graphene up to 2 mg mL<sup>-1</sup> was also obtained by the spontaneous exfoliation of HOPG in chlorosulfonic acid (Figure 1B).<sup>35</sup>

Solution-based exfoliation of graphite is certainly an appealing approach considering the possibility to produce good-quality graphene and the ease for large-scale adoption. However, several drawbacks should be taken into consideration. The majority of the exfoliated flakes remain in a multilayer structure, thus giving rise not only to low yields but also to a large variety of flakes consisting of different number of layers that are difficult to further separate.<sup>36</sup> More importantly, prolonged ultrasonication treatments damage the graphene sheets to result in small-sized graphene flakes and nanometric graphitic impurities. The presence of such impurities is capable of altering the density of edgelike planes, thus dramatically affecting the electrochemical properties of the graphene.<sup>37</sup>

The usage of exfoliating agents, such as surfactants, can also alter the properties of the resulting graphene, since they remain embedded on the graphene sheets. For example, the application of sodium cholate surfactant has demonstrated adverse effects on the electrochemical properties of the resulting graphene.<sup>38–40</sup>

**2.1.3. Electrochemical Exfoliation of Graphite.** Electrochemical methods aiming at the intercalations of ions and compounds within graphite are known since the 1980s when sulfuric acid,<sup>41</sup> Li<sup>+</sup>,<sup>42</sup> F<sup>-</sup>,<sup>43,44</sup> and Ni<sup>2+</sup><sup>45</sup> intercalated graphite were prepared in both aqueous and organic solvents. After the development of micromechanical cleavage of HOPG in 2004, electrochemical methods of isolating graphene from exfoliated graphite have regained much interest.<sup>46</sup>

The electrochemical exfoliation method involves the application of cathodic (reduction) or anodic (oxidation) potentials or currents in aqueous or organic electrolytes to a graphite-based (i.e., HOPG) working electrode in the presence of auxiliary (usually Pt) and reference (SCE, Ag/AgCl, etc.) electrodes. When a positive potential is applied, the graphite electrode is oxidized and the intercalation of negatively charged ions from the solution into the graphitic layers takes place. This is then followed by the application of a negative potential that facilitates the exfoliation process. The exfoliation of graphite into graphene sheets has been achieved by using sulfuric acid<sup>47</sup> and poly(styrenesulfonate) (PSS)<sup>48</sup> as electrolytes among others. More recently, SDS surfactant in aqueous solution was used for the graphite intercalation process by applying a positive potential of +2 V to intercalate the SDS molecules into the graphitic layers followed by a negative potential of -1 V to drive the exfoliation process. Graphene flakes with an average size of 500 nm and a thickness of 1 nm (one or two layers) were successfully obtained.<sup>49</sup>

The use of high anodic potentials produces oxidized graphene (graphene oxide), which is rich in oxygen functional groups and structural defects. Although the reversal of the applied potential eliminates a portion of the oxygen functional groups, the process cannot recreate a defect-less graphene structure.<sup>47</sup> Therefore, a cathodic reduction/intercalation method was attempted to generate nonoxidized graphene sheets with a more intact graphene structure. By first applying a negative potential, an intercalation process can be achieved with positive ions without any oxidation and formation of oxygen functionalities on the graphene sheets. Remarkable results have been obtained by Morales et al. with perchloric acid electrolyte in a study on both the intercalation of H<sub>3</sub>O<sup>+</sup> ion at negative potential and perchlorate anion at positive potential. After the electrochemical process, a microwave treatment was performed to thermally expand the intercalated graphite to provide graphene flakes that formed stable dispersions in NMP.<sup>50</sup> To

improve the yield of the exfoliation process, Li<sup>+</sup> ions in propylene carbonate electrolyte were used while a highly negative potential (-15 V) was applied. As a result, over 70% of the obtained graphene flakes had a thickness of less than five layers.<sup>51</sup> More recently, a further improvement was achieved using a two-stage process, with an initial expansion of graphite in a Li<sup>+</sup>-containing electrolyte followed by a second expansion step in a tetra-*n*-butylammonium electrolyte, at which a potential of -5 V was applied for both stages. In this way, besides the use of less extreme potentials, ultrasonication treatment was not required at all to obtain a dispersion of graphene (Figure 1C). On top of that, a direct electrochemical functionalization with aryl diazonium salt was also demonstrated on the expanded graphite to provide functionalized graphene sheets.<sup>52</sup>

Electrochemical exfoliation methods of graphite have several advantages as compared to other methods. These methods are certainly more environmental friendly, can be performed under ambient conditions, can be precisely tweaked by controlling the applied potential or current, and are generally fast. However, it is still very difficult to fabricate graphene with a homogeneous size and layer distribution. Moreover, the use of anodic potentials to intercalate ions causes unwanted oxidation of graphite and the introduction of oxygen functional groups disrupt the sp<sup>2</sup>-hybridized carbon network. This process is highly irreversible, since neither electrochemical nor chemical processes are able to regenerate the sp<sup>2</sup>-hybridized carbon network to the state of pristine graphene. Moreover, the presence of both structural damage and oxygen functional groups has profound influence on the electrochemical properties of the resulting graphene. Similar to the solution-based exfoliation methods, the use of surfactants may cause an irreversible “functionalization” of the graphene flakes that may ultimately result in the alteration of the electrochemical behaviors.<sup>38–40</sup>

**2.1.4. Chemical Oxidation of Graphite, Exfoliation, and Reduction.** While micromechanical exfoliation of graphite relies on the strong interaction between graphene layers and sticky tape to overcome the cohesive interlayer van der Waals forces of graphite, a chemical route based on a similar principle can also be carried out to facilitate the exfoliation process. This involves the intercalation of chemical species within the graphitic layers followed by a subsequent expansion/decomposition process that forces the layers apart. One of the most well-known approaches to expand graphitic layers is through oxidative intercalation by means of strong oxidizing agents in the presence of concentrated sulfuric and nitric acids. Brodie, in 1859, used potassium chlorate as an oxidant in his attempt to determine the exact formula of graphite by generating highly oxidized graphite. The newly oxidized graphite contained several oxygen functional groups disseminated all over the graphitic structure, which therefore introduced sp<sup>3</sup>-hybridized carbon atoms within the sp<sup>2</sup>-hybridized carbon network of graphite.<sup>53</sup> This method was then perfected and improved, in the following chronological order, by Staudenmaier (1898),<sup>54</sup> Hofmann and König (1937),<sup>55</sup> Hummers and Offeman (1958),<sup>56</sup> and lately Tour and co-workers (2010),<sup>57</sup> to obtain what is now called graphite oxide (GO).<sup>58</sup> The methods introduced by Staudenmaier, and Hofmann and König applied potassium chlorate as an oxidizing agent, while Hummers and Offeman, and Tour and co-workers applied potassium permanganate instead to avoid the formation of dangerous, explosive ClO<sub>2</sub> gas. The formation of several oxygen functional

groups within the graphitic layers increased the interlayer distance from 3.35 Å in graphite to over 6 Å in graphite oxide (humidity dependent). As a result of that, the cohesion strength between graphene layers is weakened such that even a simple ultrasonication treatment can further separate the layers.<sup>13</sup> Isolated sheets from GO, called graphene oxide, is an attractive material, because it can be obtained in a solution form and offers great opportunities for large-scale production of graphene.<sup>59</sup> In contrast to pristine graphene, graphene oxide demonstrates several interesting and unique properties. Graphene oxide exhibits high electrical resistivity due to the disrupted  $sp^2$ -hybridized carbon network by oxygen functional groups and also exhibits photoluminescence due to band gap opening as a result of quantum confinement effect from small  $sp^2$  domains. Apart from being an excellent fluorescence quencher, the oxygen functionalities can be exploited for chemical functionalizations to produce novel supporting materials for composites or sensor interfaces. If graphite oxide (and graphene oxide) is prepared as a precursor to graphene, further processes are required to eliminate the majority, if not all, of the oxygen functional groups and to reestablish the planar  $sp^2$ -hybridized carbon structure. Specifically, three main approaches, namely, thermal, electrochemical, and chemical methods, have been performed to accomplish such a task. On the basis of the thermal reduction method, GO is thermally shocked at about 1000 °C to generate gaseous species within the interlayers of the GO structure. This results in an increase of internal pressure that leads to the exfoliation of GO with the concomitant elimination of oxygen functional groups.<sup>60,61</sup> It has been recently discovered that, in addition to simple inorganic CO<sub>2</sub>, CO, and H<sub>2</sub>O molecules, more complex organic molecules are generated during the thermal exfoliation process.<sup>62</sup> Such thermally reduced graphene shows an improved conductivity, but it suffers from extended structural damage and defects. This method is simple and easily scalable, and the resulting graphene is advantageous for applications such as composite materials, ink, paint reinforcement, and electrochemical devices. A recent study highlighted the importance of the parent graphite particle size on the formation of oxygen functionalities during oxidation and the extent of structural defects upon thermal exfoliation.<sup>63</sup> These structural variables are directly reflected in the electrochemical properties of the prepared graphene materials.<sup>63</sup> Apart from that, the electrochemical reduction method is another interesting approach, since it can be easily controlled, can be performed under ambient conditions, does not require toxic or dangerous chemical agents, and requires only simple instrumentations. Several examples have shown how the application of negative potentials can eliminate most, but not all, electrochemically reducible oxygen functionalities to restore the graphene-like properties of GO.<sup>64–68</sup> Our group has recently investigated the chemical changes that occur during the application of cathodic potentials on GO films that subsequently allow for a precise control of C/O ratios between 3 and 10.<sup>69</sup> Despite the practice of thermal and electrochemical reduction methods, the usage of chemical agents to eliminate oxygen functional groups is the most widely applied approach. After the dispersion of GO in aqueous solution to obtain graphene oxide, a chemical reaction/reduction is performed to eliminate most oxygen functional groups. The dispersibility of the reduced graphene sheets is often retained whenever possible. One of the first and most widely applied reducing agents is hydrazine, which was already tested back in 1937 by Hofmann and König, who

documented a significant increase of C/O ratio after the reaction of GO with hydrazine hydrate.<sup>55</sup> They also tested FeCl<sub>2</sub> as a reducing agent.<sup>55</sup> The usage of hydrazine was then reproposed more recently to obtain reduced graphene with a C/O ratio of over 10.<sup>70</sup> Consequently, an exponential growth on the types of reducing agents was observed, which includes sodium borohydride, lithium aluminum hydride, hydroquinone, hydroxylamine, and more ecofriendly L-ascorbic acid, saccharides, tea extract, wild carrot root, and even bacteria, to name only a few.<sup>71–79</sup> More recently, even a camera flash<sup>80</sup> and laserscribes from a commercial optical drive<sup>81</sup> were used for the reduction of GO films (Figure 2).

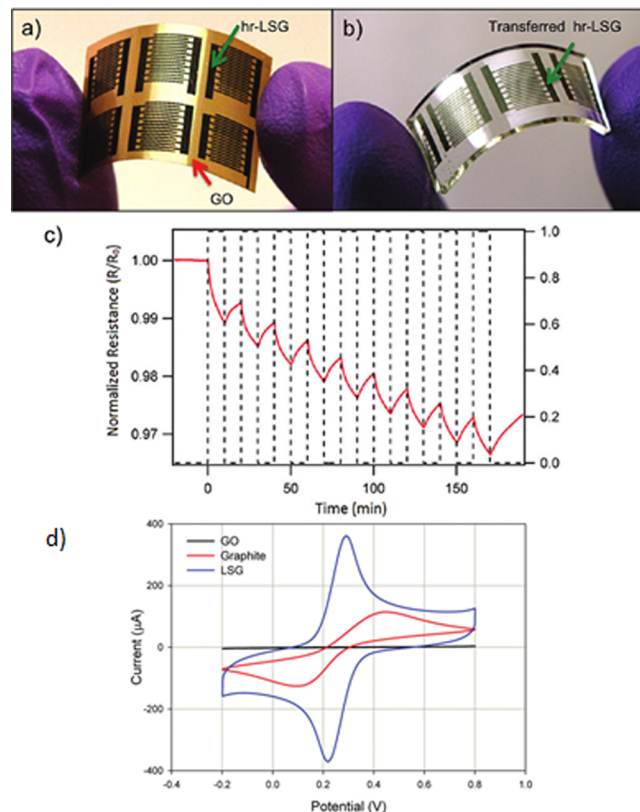


**Figure 2.** Laser scribing reduction of graphene oxide. (a) All-organic flexible set of interdigitated electrodes generated from highly reduced laser scribed graphene (hr-LSG). (b) Same interdigitated electrodes transferred onto polydimethylsiloxane (PDMS). (c) NO<sub>2</sub> detection using the same all-organic flexible interdigitated electrodes. Here the sensor uses hr-LSG as the active electrodes and marginally laser-reduced graphite oxide as the detecting media. The NO<sub>2</sub> concentration is 20 ppm in dry air gas. (d) CV profiles of graphite oxide (GO), graphite, and hr-LSG electrodes in an equimolar mixture (5 mM) of K<sub>3</sub>[Fe(CN)<sub>6</sub>]/K<sub>4</sub>[Fe(CN)<sub>6</sub>] dissolved in 1.0 M KCl solution at a scan rate of 50 mV/s. The hr-LSG electrode approaches the behavior of a perfect reversible system with a peak-to-peak potential of 59.5 mV at 10 mV/s, which is close to the theoretical Nernstian value of 59 mV. The hr-LSG shows high electron transfer rates. Reprinted with permission from ref 81. Copyright 2012 American Chemical Society.

It is important to know that chemical reduction procedures cannot completely remove the oxygen functional groups from GO. Although the chemically reduced graphene materials exhibit better and improved characteristics than GO, they are still very different from pristine graphene. This is due to the presence of residual oxygen functional groups and the high density of defects created during the oxidation of graphite.

Despite that, the chemical reduction method is an attractive and highly scalable synthetic route that allows for the fabrication of graphene materials with unique characteristics that can be exploited in electrochemical sensors, energy storage devices, transparent conductive films, and composites. As a matter of fact, the surface compositions and structural properties of the graphene materials obtained from this fabrication method can be very different. Starting from GO, which is nonconductive, highly defective, and rich in oxygen functional groups (C/O ratio ~2), a wide variety of chemically reduced graphene materials with different electrical properties, surface compositions, and density of defects can be obtained by varying the types of reducing agents, the starting GO material, and the synthetic conditions. It is, thus, possible to obtain chemically reduced graphene materials with distinctive electrochemical properties. If we were to examine GO, it is not an ideal material to be used as an electrochemical interface due to its low conductivity. However, the abundance of oxygen functional groups provides GO with an inherent redox activity, as some of the oxygen functional groups can be reduced and regenerated electrochemically.<sup>82</sup> This allows GO to be exploited as a signal carrier in certain electrochemical sensing schemes.<sup>83,84</sup> On the other hand, chemically reduced graphene materials can be used as transducer materials in electrochemical devices due to better electrical properties, a high density of defects, and edgelike planes, which facilitate fast electron transfer. Moreover, well-defined graphene oxide platelets (defined by dimensions of the nanofiber base) that can disperse as colloidal solutions can be fabricated from the oxidation of graphite nanofibers.<sup>85</sup>

**2.1.5. Opening/Unzipping Carbon Nanotubes: Graphene Nanoribbons.** Another top-down approach is represented by the opening/unzipping of carbon nanotubes (CNTs) instead of graphite as a starting material. This method generates the so-called graphene nanoribbons (GNRs), which differ from graphene due to its higher aspect ratio (at least 10) with a typical width of <50 nm.<sup>86</sup> One of the most significant properties of GNRs is the ability to engineer the band gap by varying the width of the nanoribbons. As such, large-scale fabrication of GNRs with a controlled width and length will facilitate their rapid usage and adaptation in electronic devices.<sup>16</sup> In the light of this, the longitudinal opening of CNTs is an interesting approach, since the circumference of the nanotubes defines the width of the produced nanoribbons. Various methods have been proposed to unzip/open the CNTs. Dai and co-workers partially embedded multiwalled CNTs (MWCNTs) on a layer of poly(methyl methacrylate) (PMMA), followed by an Ar plasma treatment which only etched the exposed portion of the CNTs to leave behind embedded GNRs.<sup>87</sup> A more scalable method was proposed by Tour and co-workers, who treated MWCNTs with concentrated sulfuric acid and potassium permanganate<sup>88</sup> to unzip the nanotubes longitudinally while, at the same time, introducing oxygen functionalities. This method was later improved by introducing H<sub>3</sub>PO<sub>4</sub> in the oxidation process to substantially reduce the formations of vacancies.<sup>89</sup> The oxygen functional groups introduced using these methods can be removed much later by a reductive treatment. However, the electronic properties of the nanoribbons are often compromised, since any structural damages introduced during the first step of oxidative longitudinal unzipping cannot be repaired. In order to avoid the oxidative treatment, the same group proposed a reductive process by heating MWCNTs in a glass tube at 250

°C in the presence of potassium. GNRs with a much lower defect density were obtained and demonstrated comparable electrical and electronic properties to pristine graphene (Figure 1D).<sup>90</sup>

Other groups have proposed the use of Li–NH<sub>3</sub> for the intercalation of MWCNTs followed by a thermal exfoliation step<sup>91</sup> or the use of metal nanoparticles for catalytic unzipping.<sup>92</sup> More recently, the acidic oxidation treatment have been applied on flattened double-walled CNTs to achieve a good control over the unzipping process along the folded edges.<sup>93</sup> It has also been observed that the oxidative treatment on MWCNTs, in some cases, resulted in the “unscrolling” of the nanotubes to provide large graphene sheets.<sup>94</sup> A recent study compared the electrochemical properties of nanographene sheets and graphene nanoribbons obtained from an oxidative treatment followed by a thermal exfoliation/reduction on stacked graphene nanofibers (SGNFs) and MWCNTs, respectively.<sup>95</sup>

As largely discussed in the aforementioned studies, the electronic properties of GNRs prepared by the unzipping of CNTs are strongly influenced by the density of defects, presence of oxygen functionalities, structural vacancies, and aspect ratios. In addition, the electrochemical properties are also influenced by similar parameters that were previously mentioned on graphene materials prepared by solution-based exfoliation or chemical oxidation/exfoliations and reduction methods. Apart from that, since CNTs are applied as a starting material, the presence of metallic or carbonaceous impurities has a profound influence on the electrochemical behaviors of the resulting GNRs. This aspect will be discussed in a broader and more general perspective, including both graphite and CNTs as starting materials in the top-down methods, in the following subsection.

**2.1.6. Graphite and Carbon Nanotubes: Source of Impurities.** Graphite material applied in the top-down methods can be obtained from two different sources, predominantly natural and synthetic origins. Natural graphite is mined and extracted as a mineral from ore rock, while synthetic graphite is produced by a graphitization process of a carbon source (coal etc.) at temperatures >2500 °C.<sup>96</sup> The graphitization method is regularly used to produce the aforementioned HOPG, which is a synthetic graphite of the highest purity and quality used for micromechanical exfoliation to obtain pristine graphene. It is important to mention that, in both production methods, absolute pure graphite cannot be obtained. Natural graphite, the preferred starting material for graphene production due to its low cost and large availability, generally has purity levels between 80 and 98% depending on the geographical location of the mines and the performed purification procedures. Nickel (Ni) and iron (Fe) are among the most abundant impurities found.<sup>97</sup> Synthetic graphite can reach purity levels as high as 99.9% depending on the type and purity of the starting carbon source, although impurity levels of up to 2% have been measured previously.<sup>98–100</sup> In addition, further milling processes to manufacture specific sizes of graphite flakes (natural or synthetic) prior to commercialization is another important source of contamination, especially pertaining to metallic impurities.<sup>101</sup> Most purification procedures are able to eliminate weakly bonded impurities but cannot remove strongly bonded or intercalated impurities in between the graphitic layers.

Since most metallic impurities present in the graphite starting material are not removed during the fabrication processes, the

impurities will most likely remain in the consequent graphene materials. As a result of that, the electrochemical properties of the produced graphene materials can be dramatically altered by the impurities. Our group has demonstrated, for example, that the metallic impurities (Ni and Fe) present in either synthetic or natural graphite remained strongly embedded in graphene materials produced from GO via chemical oxidation of graphite.<sup>97,102</sup> Subsequent thermal exfoliation<sup>102</sup> or chemical reduction<sup>97</sup> processes failed to eliminate the metallic impurities, resulting in permanently altered electrochemical behaviors of the graphene materials.

On the other hand, the use of carbon nanotubes as a starting material is specific to the fabrication of graphene nanoribbons. However, it is well-known that CNTs are grown at high temperatures over metal nanoparticle catalysts and that such metal catalysts remain trapped within the nanotubes structures with up to 30% in weight.<sup>103,104</sup> In addition, carbonaceous impurities, such as amorphous carbon<sup>105</sup> and nanographitic flakes, are also generated during the synthesis of CNTs. Although several purification procedures have been proposed to eliminate both the metallic and carbonaceous impurities from the CNT samples, only a substantial reduction was achieved but not a complete removal.<sup>103,104,106</sup> The influences of such impurities on the electrochemical properties of CNTs have been largely documented.<sup>107</sup> In relation to the fabrication of GNRs, it can be immediately perceived that the metallic impurities present within CNT samples can ultimately affect the electrochemical properties of GNR as a consequence of contaminations. The first demonstration of such adverse effect was recently published by our group and showed that the oxidative treatment to unzip MWCNTs did not remove the metallic impurities initially present in the CNTs and that such impurities altered the electrocatalytic behaviors of the resulting GNRs toward the oxidation of sulfides and hydrazine.<sup>108</sup>

## 2.2. Bottom-up Methods

The bottom-up approach of graphene production involves building up graphene sheets from small organic molecules that combine by means of catalytic processes. Special conditions are required to allow for the carbon-containing molecules to combine into an sp<sup>2</sup>-hybridized carbon network. Organic syntheses methods have also been proposed to build up small graphene molecules of a few nanometers in size using solution-based catalytic reactions. Alternatively, the use of solid supports such as Pt, Cu, and Ni can also facilitate the deposition of carbon atoms into planar structures on the metal surfaces using high-temperature chemical vapor deposition (CVD). Higher temperatures can be used to sublime Si atoms from silicon carbide (SiC) wafers, with consequent rearrangement of the remaining carbon atoms into graphitic layers. In the following subsections, we will discuss the technical aspects of the three main bottom-up methods used to synthesize graphene in detail, specifically, chemical synthesis, epitaxial growth on SiC, and chemical vapor deposition methods. As before, for each methodology, the properties of the produced graphene will be highlighted particularly from an electrochemical point of view.

**2.2.1. Chemical Synthesis.** The synthesis of small "graphene molecules" represents a very interesting route because it allows for the preparation of graphene with well-defined shape and controlled edge structures. Considering graphene as a polycyclic aromatic hydrocarbon (PAH) of infinite size, it only makes sense to combine small PAH

molecules to create graphene. The main drawback of this method is that graphene molecules that are larger than a few nanometers become highly insoluble in most organic solvents, which impedes further synthetic growth and facilitates uncontrolled side reactions instead. The pioneers and main actuators of this synthetic route are Müllen and co-workers, who demonstrated the synthesis of graphene nanoribbons of 30 nm in length<sup>109</sup> and the largest graphene molecule consisting of 222 carbons with a size of 3.2 nm,<sup>110</sup> among others which are well-described in another recent review.<sup>86</sup> Although the chemical synthesis method has to deal with several challenges, with the size limitation of graphene being the main obstacle, it represents a promising route for a clean and scalable fabrication method of graphene.

**2.2.2. Epitaxial Growth on SiC.** Graphene growth has been achieved on SiC substrates by heat treatment at high temperatures under ultrahigh vacuum (UHV) conditions.<sup>111</sup> During the process, Si atoms sublimate to leave an exposed layer of carbon atoms that will rearrange to form graphitic layers (epitaxial graphene). Precise control of the sublimation temperatures may lead to the formation of very thin graphitic layers, occasionally of single sheets.<sup>112</sup> A wafer-scale coating of monolayer graphene was recently achieved by annealing at a higher temperature (1650 °C) in Ar atmosphere rather than at a lower temperature (1150 °C) under UHV conditions.<sup>113</sup> The properties of graphene grown on SiC are somehow different than those of mechanically exfoliated graphene. This is mainly due to the presence of substrate-induced corrugations and irregular orientations of the graphene layers, which alter the electronic properties.<sup>111,114</sup> The use of SiC wafers to grow graphene is very promising due to the fact that it can be easily integrated into current industrial procedures used in the electronics industry. However, the high cost of single-crystal SiC wafers is the main limiting factor for large-scale fabrication. The electrochemical properties of epitaxial graphene were investigated by Loh and co-workers, who concluded that as-prepared epitaxial graphene possessed poor electrocatalytic properties, specifically, slow electron transfer rates. The application of an anodizing potential increased the density of defects and introduced oxygen functionalities on the epitaxial graphene that substantially enhanced its electrochemical performance.<sup>115</sup>

**2.2.3. Chemical Vapor Deposition.** Large area, single or few layer, high-quality graphene has been produced recently by using chemical vapor deposition (CVD), which makes this one of the most promising techniques for industrial-scale fabrication of graphene.<sup>116</sup> Although CVD graphene has poorer electronic and structural properties than mechanically exfoliated graphene, it still demonstrates excellent performances in applications such as electronic transistors,<sup>117</sup> transparent conductive electrodes,<sup>118</sup> electrochemical devices,<sup>119</sup> and corrosion-inhibiting coatings.<sup>120–122</sup> CVD is a well-known procedure that has been previously used to fabricate carbon nanotubes. The procedure involves a high-temperature decomposition step of a carbon source (feedstock) in the presence of a transition-metal catalyst on which carbon atoms will deposit and rearrange into sp<sup>2</sup>-hybridized carbon structures. One-dimensional CNTs are grown over metal nanoparticle catalysts,<sup>123</sup> while two-dimensional graphene is grown over metal surfaces such as ruthenium,<sup>124</sup> platinum,<sup>125</sup> iridium,<sup>126</sup> nickel,<sup>127</sup> or copper.<sup>128</sup> Lately, nickel and copper metal substrates are very popular due to their high availability and low cost as compared to other types of metal substrates.<sup>127–132</sup> It is significantly noteworthy to

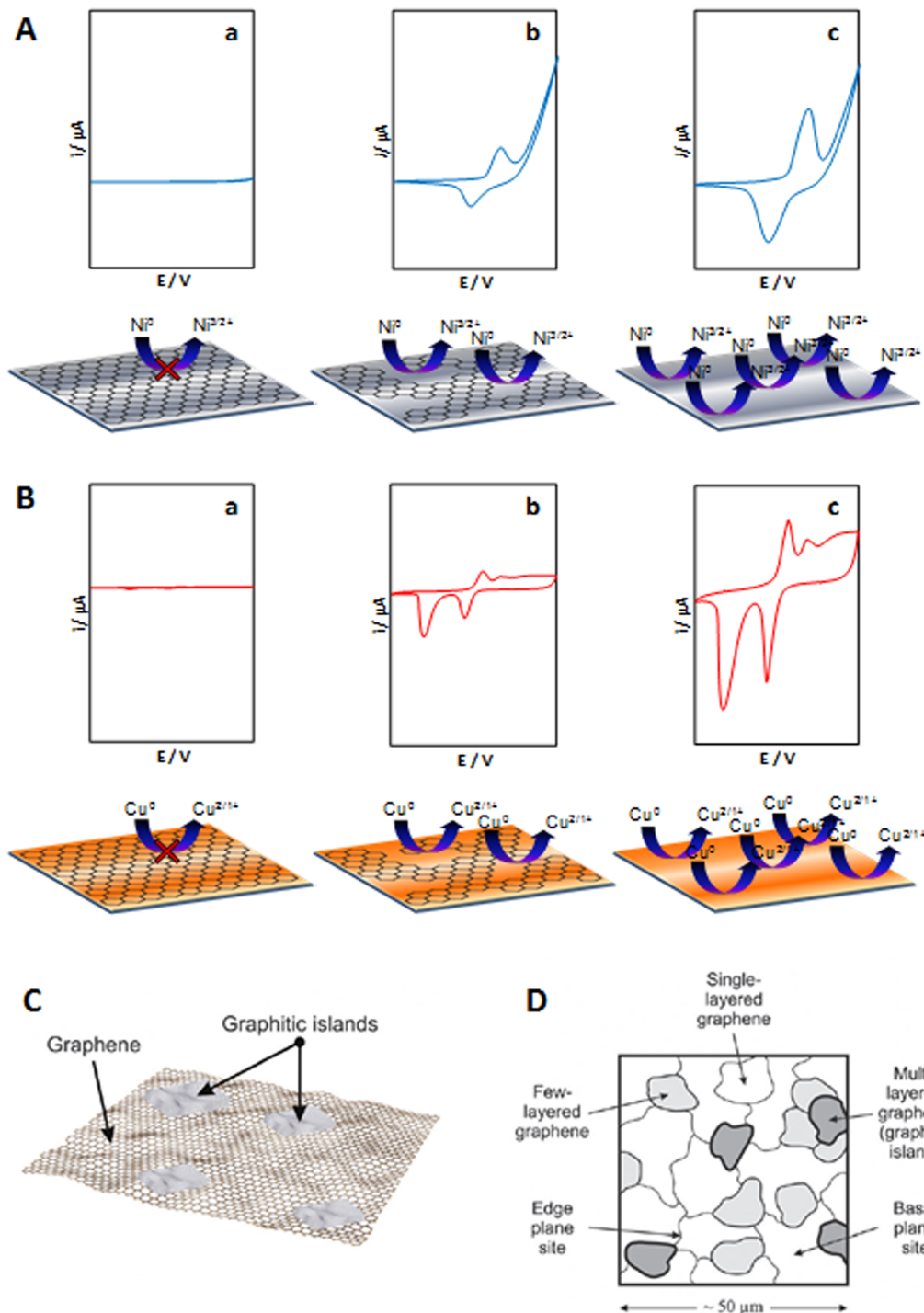


**Figure 3.** Electrochemistry of CVD graphene is influenced by the defects in its structure and electrochemically available Ni or Cu substrate. (A) Electrochemical redox signal of Ni generated in relation to the Ni metal surface coverage and (B) electrochemical redox signal of Cu generated in relation to the Cu foil surface coverage: (a) no signal is generated by a fully covered metal, (b) signal generated by the metal partially exposed by a defective graphene film, and (c) uncovered metal generates the maximum electrochemical signal. Reprinted with permission from ref 155. Copyright 2013 Royal Society of Chemistry. (C) Schematic representation of layered graphitic regions on a graphene film and (D) an underlying graphene surface with few and multilayered graphitic islands, indicating the basal and edge plane electron transfer sites. Reprinted with permission from ref 157. Copyright 2011 Royal Society of Chemistry.

mention that graphene grown on nickel substrate has been applied for flexible and transparent electrodes<sup>133</sup> while a 30-in. graphene surface has been produced on copper foil substrate and then transferred to a flexible transparent substrate through a roll-to-roll process.<sup>130</sup> The carbon feedstock is usually a gaseous species such as methane, ethane, or propane,<sup>134</sup>

although the use of a solid source has also been demonstrated.<sup>132</sup> It is important to highlight that graphene grown on Ni is highly polycrystalline, consisting of areas with different layers of graphene. On the other hand, Cu allows the formation of larger monocrystalline areas of mostly single layer graphene. This phenomenon is due to the fact that carbon has a

higher solubility in Ni than in Cu. Therefore, more carbon atoms are crystallized in an uncontrolled orientation during the cooling process of Ni substrate, resulting in a typical patchworklike pattern of graphene. As a lower amount of carbon atoms is dissolved in a Cu substrate, only single or double layer graphene is created during the cooling process. Moreover, the presence of surface oxygen on Cu substrate was found to accelerate graphene domain growth in a diffusion-limited growth kinetic and dendritic in nature.<sup>135</sup> Nevertheless, precise tunings of the deposition temperature, pressure, cooling time, and quality of metal substrates have improved the production technique to enable the growth of mostly single layer and large crystalline-sized graphene on the order of a millimeter.<sup>131,136,137</sup> Despite such improvements, pure single crystalline graphene has not yet been produced. The reason is that the crystallization of the carbon atoms starts from different nucleation sites during the cooling process and then crystals grow laterally with specific lattice orientations until the entire surface of the metal substrate is covered. The meeting points of these different islands of graphene are often the roots of several problems. Some discrepancies occur among the different orientations of the graphene islands to generate the so-called grain/domain boundaries. Such boundaries represent defects in CVD graphene and can result in the alteration of its mechanical,<sup>138</sup> electrochemical,<sup>139</sup> and electronic properties.<sup>140,141</sup>

Despite all the improved growth techniques of CVD graphene, the graphene film has limited or no use if it is not transferred to a different arbitrary surface and if the metal catalyst substrate is not removed. Therefore, the transfer process should be considered an integral part of the preparation steps for CVD graphene. The transfer of CVD graphene onto arbitrary substrates can be achieved using polymer-supported metal etching/transfer or mechanical exfoliation with special functionalized polymers.<sup>142</sup> It is important to note that the transfer process usually causes a significant degradation of the graphene quality due to the formation of wrinkles or structural damages from tearing and ripping.<sup>143,144</sup> This is the reason why improvements in the transfer process could be even more worthy than developing better CVD growth processes.<sup>142</sup>

The most common transfer method involves the etching of metal substrate while the graphene is supported by an inert polymer such as PMMA or PDMS.<sup>118,129</sup> Apart from that, several other transfer substrates such as PTFE, PVC, PC, CN/CA, PET, paper, and cotton cloth have been investigated and applied via a hot/cold lamination process.<sup>145</sup> Once the metal substrate is completely etched, the graphene is transferred to a desired substrate followed by the removal of the supporting inert polymer. This type of procedure is particularly delicate, because it can not only generate mechanical stress to cause structural damages and alterations but also contribute as an important source of contamination by metallic impurities, which can dramatically alter the electronic<sup>146,147</sup> and electrochemical properties<sup>148</sup> of the transferred graphene. It has been shown, for example, that the etching agents [FeCl<sub>3</sub>, Fe(NO<sub>3</sub>)<sub>3</sub>] usually adopted to dissolve copper and nickel metal substrates contaminate the transferred graphene with a significant amount of Fe impurities.<sup>148,149</sup> Our group has demonstrated that such Fe impurities altered the electrochemical behavior of CVD graphene toward the reduction of cumene hydroperoxide.<sup>148</sup> In addition, it is also important to consider that an incomplete etching process can contaminate CVD graphene with extremely redox active residuals, such as Ni or Cu metals.<sup>148,150–152</sup>

Recently, the transfer of graphene sheets has been assisted by the generation of bubbles. Rummeli and co-workers were able to separate PMMA–graphene from the growth substrates without etching by inducing O<sub>2</sub> bubble generation with a mixture of NH<sub>4</sub>OH, H<sub>2</sub>O<sub>2</sub>, and H<sub>2</sub>O.<sup>153</sup> Moreover, Loh and co-workers demonstrated a face-to-face transfer of wafer-scale graphene films that saw the integration of both growth and transfer steps on a single wafer. The novel approach relied on nascent gas bubbles and capillary bridges to provide high-quality graphene with low defects.<sup>154</sup>

In the event that CVD graphene is adopted as an electrode material without any transfer process, it is of crucial importance to consider the efficiency of the CVD process to form a continuous and homogeneous graphene film on the metal catalyst substrate. Any fractures or holes, even at the submicrometer level on the graphene film, can leave the metal catalyst exposed and available to interact with external agents. As such, the overall electrochemical properties of the CVD graphene layer may be wrongly evaluated, since the exposed metal catalyst substrate are redox active (Figure 3A,B).<sup>155,156</sup> In addition, CVD graphene can contain small graphitic islands that can dominate its electrochemistry toward simple inorganic or biologically active molecules (Figure 3C,D).<sup>157,158</sup>

**2.2.4. 3D Graphene.** One of the main issues of utilizing graphene for electrochemical purposes is that the individual isolated graphene sheets deposited on conducting surfaces tend to restack, which, in some instances, downplays its advantage of high surface area and decreases the availability of electroactive sites. However, this problem can be avoided by the construction of well-defined porous 3D graphene structures. Two synthesis approaches for 3D graphene have so far been attempted, mainly by depositing a graphene layer on Ni 3D foam by the CVD technique<sup>159,160</sup> or converting well-defined 3D pyrolyzed porous photoresist films fabricated by lithography to 3D graphene.<sup>161</sup> The latter technique enables the creation of 3D graphene with a pore size of ~500 nm, which is about 2 orders of magnitude lower than that of the former. Apart from that, 3D graphene shows faster heterogeneous electron transfer than 3D porous carbon with enhanced oxygen reduction activity.<sup>160,161</sup> Moreover, 3D graphene can act as a standalone sensing platform;<sup>162</sup> however, it often serves as 3D conducting support for catalytic particles, such as Pt or Pd nanoparticles or Ni/Co hydrogel for enhanced oxygen reduction capability,<sup>163,164</sup> or with transition metal dichalcogenides for improved electrochemical hydrogen evolution reaction.<sup>165</sup> 3D graphene prepared by the CVD technique can also take advantage of the underlying Ni layer to provide electrocatalytic sites for enzymeless glucose oxidation.<sup>166</sup>

### 2.3. Processability of Graphene Materials

The potential applications of graphene materials can easily be realized if processable graphene sheets are available in large quantities. Graphene obtained from the bottom-up and top-down methods are largely hydrophobic in nature. The high specific surface area of graphene promotes spontaneous irreversible agglomerations or restacking via van der Waals interaction. As a result of that, the obtained graphene will form a graphite-like material. A closer look into the interplay between graphene and its dispersing medium is important to overcome this challenge. In fact, studies based on molecular dynamic simulation and kinetic theory by Blankschtein and co-workers showed that solvation forces arising from the

restructuring of solvent molecules at the liquid/solid interface play a significant role in stabilizing graphene in suspensions. Solvents such as NMP, DMSO, DMF, and GBL are able to form an energy barrier for restacking between two graphene sheets.<sup>167</sup> Several of these solvents were used to obtain graphene via a solution-based exfoliation method, as discussed in subsection 2.1.2. Despite that, the limitation on the types of appropriate polar solvents is very narrow and restricts potential applications of graphene. Moreover, achieving high graphene dispersion stability in water is, in fact, greatly pursued. On the other hand, graphene oxide displays a relatively high dispersion stability in water due to the presence of oxygen-containing groups, and its stability in several types of organic solvents has been previously investigated.<sup>168</sup> Several approaches to obtain stable graphene dispersions in water focus on modifying the graphene materials, either by covalent or noncovalent modifications. Although covalent modifications offer a higher extent of dispersibility than the noncovalent approaches, they entail a major degradation to the electronic structure and charge transfer properties of graphene. One of the several noncovalent modifications is the attachment of small aromatic molecules containing hydrophilic groups via  $\pi-\pi$  interaction. All of these molecules contain polar functional groups to assist in maintaining strong repulsion forces among the graphene sheets. For example, methylene green,<sup>169</sup> pyrene-1-sulfonic acid sodium salt, 3,4,9,10-perylenetetracarboxylic diimide bisbenzenesulfonic acid,<sup>170</sup> *p*-phenyl-SO<sub>3</sub>H,<sup>171</sup> and 1-pyrenebutyrate<sup>172</sup> have been applied to improve the dispersion stability of graphene. Other approaches attempt to create nanocomposites by using polymers such as PMMA<sup>173</sup> or poly(sodium 4-styrenesulfonate).<sup>174</sup> Another alternative deals directly with the inherent carboxyl groups from chemically reduced GO. Common reducing agents such as hydrazine do not generally reduce the carboxyl groups, so these groups could be easily conferred with negative charges by tuning the pH with ammonia<sup>175</sup> or potassium hydroxide<sup>176</sup> to exert electrostatic repulsion between the graphene sheets. Recently, small flakes of solution-based exfoliated graphene have been shown to disperse well in water as a result of the reduction of flake size and enhanced edge effects.<sup>177</sup>

The deposition of graphene materials for electrochemistry applications is often performed by drop-casting of a graphene materials dispersed in organic solvents. Other methods include creating polymer composites or employing conjugation chemistry to adhere graphene sheets to electrode surfaces. In order to achieve a good and homogeneous coverage of graphene, usage of a well-dispersed solution of graphene is important. It is also crucial to note that the application of graphene solution dispersed via noncovalent approaches for electrochemical detection purposes should proceed with care, since the applied polymers or small aromatic molecules could possess inherent electrochemistry or interfere with the intended electrochemical detections (see subsection 3.3).

#### 2.4. Characterization Methods

Characterizations of graphene materials can be achieved using various techniques prior to usage in potential applications. Due to the variability of graphene materials prepared on the basis of different approaches, a complete characterization is always required to fully understand the types of graphene that one is dealing with and, more importantly, the specific structural and chemical properties. It is often necessary to combine several

different characterization techniques to obtain a clear idea of the graphene properties.

*Optical microscopy* (OM) is one of the first and surprisingly easiest techniques to identify graphene down to the thickness of a single layer. This was initially demonstrated in 2004 by Novoselov et al. to quickly identify sheets of single layer graphene among a large number of multilayer structures.<sup>12</sup> A trained eye can easily distinguish and identify single layer graphene on the basis of the interference of color changes caused by single or few layer graphene depositions on a thin SiO<sub>2</sub>/Si substrate. For a good visual contrast, the SiO<sub>2</sub> layer is usually close to 300 nm in thickness (purple/violet color).<sup>178</sup> Several other studies have been carried out to gain a better understanding of the optical phenomenon and to further improve the visualization.<sup>178–180</sup> Although the large availability of optical microscopes may have possibly facilitated the explosion of graphene research, this optical technique has many limitations. For example, optical microscopy can only explore micrometer-sized samples, cannot be adopted for large-scale industrial identifications, and, more importantly, cannot detect submicrometer/nanometer-sized structural defects.

*Scanning probe microscopy*, including scanning tunneling microscopy (STM) and atomic force microscopy (AFM), probably represent the best techniques available to identify the structure of graphene sheets and to determine the exact number of graphene layers. Due to the different interaction between the AFM tip and the substrate or graphene material as well as the presence of a thin layer of water on the graphene surface, a single layer graphene deposited on a silicon wafer is generally detected with steps of about 1 nm instead of the theoretical 0.34 nm.<sup>12</sup> Nevertheless, it is currently the most reliable technique to quantify the thickness of graphene sheets. STM can be used to visualize the carbon atoms in graphene structures, even in a nanometer-sized area. This allows the identification of defects such as adatoms, penta- or heptamember rings, and vacancies, which can cause altered electronic properties of the graphene.<sup>181</sup> The atomic resolution achieved by both AFM and STM can be very useful, but it requires expensive instrumentations and extremely long analysis time. This limits the usage of scanning probe microscopy to only academic and fundamental studies with no possibility of being applied for large-scale identification and quality monitoring.

*Electron microscopy*, such as scanning electron microscopy (SEM) and transmission electron microscopy (TEM), are powerful imaging tools to characterize graphene materials. High-resolution TEM (HRTEM) can reach atomic resolution with clear visualization of the carbon lattice.<sup>182</sup> SEM can be used for a fast identification of the graphene structure, in particular, CVD graphene, which will appear darker in contrast to the metal substrate it is grown on. It is important to note that both SEM and TEM utilize electron beams, which can be destructive at a certain energy level, resulting in almost unavoidable defects and damage on the graphene structure.<sup>183</sup> Graphene sheets have also been applied as a support material for other TEM investigations.<sup>184</sup>

*Raman spectroscopy* has emerged as one of the most convenient techniques for characterizing graphene materials in a nondestructive way to provide information on structural features, density of defects, and the number of graphene layers. It functions on the basis of analyzing the scattering of monochromatic light that interacts with molecular vibrations and phonons of a particular solid. It has been used extensively to characterize carbon materials that show significant and

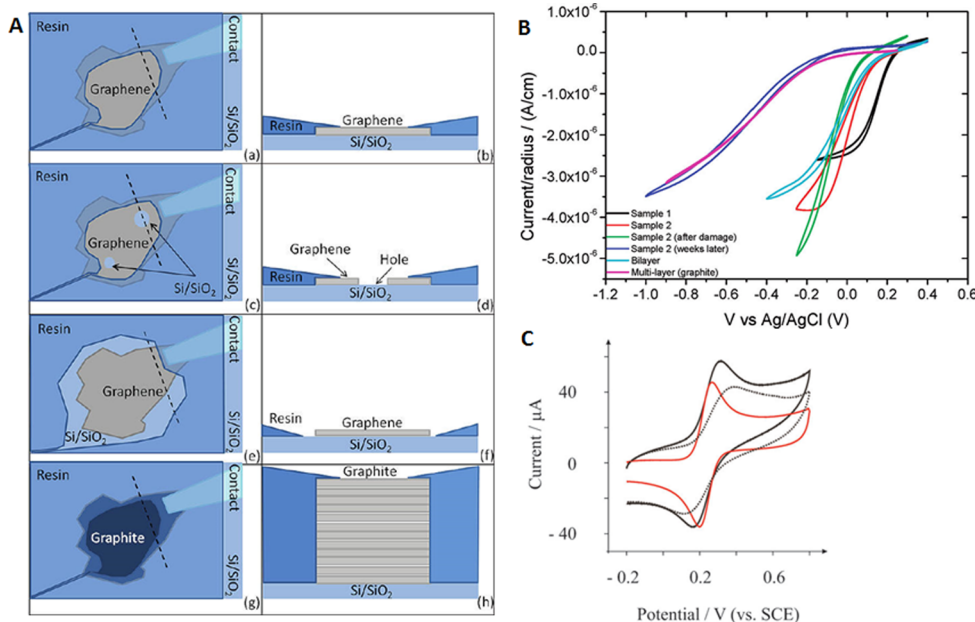


**Figure 4.** (A) Preparation of individual graphene flake measurements. On the left, top view of the samples; on the right, cross section along the black dashed line. Samples are classified as defect-free monolayers, with all the edges covered by the masking resin (a, b), defective monolayers with evident holes (c, d), monolayers with exposed edges (e, f), and multilayers (g, h). (B) Current (normalized to electrode radius) vs potential response for the graphene monolayer samples (samples 1 and 2), a bilayer sample and the multilayer. Reprinted with permission from ref 24. Copyright 2011 American Chemical Society. (C) Cyclic voltammetric profiles recorded in 1 mM potassium ferrocyanide/1 M KCl using bare basal plane (dotted line) and edge plane (red solid line) pyrolytic graphite electrodes and an 2 mg graphene (solid black line) modified basal plane pyrolytic graphite electrode. Scan rate: 100 mV s<sup>-1</sup>. Reprinted with permission from ref 26. Copyright 2010 Royal Society of Chemistry.

characteristic Raman features in the region of 800–3000 cm<sup>-1</sup>. Graphite and graphene materials are characterized by an intense band at about 1580 cm<sup>-1</sup> (G band) as a result of in-plane vibrations of sp<sup>2</sup>-bonded carbons. A D band at around 1360 cm<sup>-1</sup> is generated by the out-of-plane vibrations of sp<sup>2</sup> carbon atoms, but it is active only in the presence of defects (edges, sp<sup>3</sup> carbons, vacancies, adatoms, etc.). In addition, a weak D' peak at about 1620 cm<sup>-1</sup> is observed in the presence of disorders. An important band, denominated as 2D, is generated at about 2700 cm<sup>-1</sup> and is attributed to the second-order two-phonon mode. This band changes substantially in relation to the quality and number of graphene layers.<sup>185</sup> The intensity ratio of the G and 2D bands as well as their relative positions can be used to determine the number of graphene layers. A single graphene sheet generates a sharp 2D band, which is roughly four times more intense than the G band. Upon increasing the number of graphene layers up to five layers, the 2D band decreases in intensity, splits into multiple subpeaks, and shifts toward higher wavenumbers up to 5 cm<sup>-1</sup>.<sup>186</sup> The Raman spectrum of graphene consisting more than five layers is hardly distinguishable from that of graphite.<sup>185,187</sup> Recently, an elegant method to distinguish the type of disorder present in graphene has been proposed on the basis of analyzing the intensity ratio between the D and D' bands.<sup>188</sup> Besides Raman scattering, Rayleigh scattering has also been proposed to characterize graphene materials with a possibility to distinguish up to six layers of graphene sheets.<sup>189</sup>

X-ray photoelectron spectroscopy (XPS) is another common tool to characterize graphene materials. By irradiating a graphene sample with high-energy photons, electrons from the core levels can be extracted from the surface layer of the material. Subsequent analysis of the kinetic energies of the extracted electrons provides information on the atomic

compositions and oxidative states of the available elements in the material. For the application of graphene materials, important information such as C/O ratio and the types of oxygen functional groups present on the materials can be obtained. Graphene doped with heteroatoms such as nitrogen, sulfur, or boron can be characterized with XPS as well. It is the main characterization tool to evaluate the degree of oxidation of graphite during the preparation of GO and to monitor the efficiency of a particular reducing agent on GO.<sup>190</sup> Despite that, XPS has some limitations; for example, useful information can only be obtained from the top 20 atomic layers of a material. This means that for highly heterogeneous materials, the measured atomic compositions may not be a good representation of the entire mass of the materials. In addition, even a high-resolution analysis on a particular element can only provide a rough estimation of its oxidation states. This is due to the fact that small changes in oxidation states typically generate overlapping signals. Moreover, further deconvolution of the XPS signal is required to provide useful yet not absolute information, and the accuracy of the fittings is highly operator-dependent. In the case of homogeneous materials, XPS is a powerful characterization tool considering that it can provide chemical information in a relatively short time and only requires a thin millimeter-sized coverage of samples for analysis. However, the instrumentation is usually quite expensive, since an UHV condition is required for a meaningful analysis.

### 3. ELECTROCHEMISTRY AT GRAPHENE SURFACES

#### 3.1. Graphene and Heterogeneous Electron Transfer

The rate of heterogeneous electron transfer, that is, the transfer of electrons from/to graphene sheets to/from molecules, is correlated not only to the molecules in question but also to the amount of defects, functional groups, and impurities present on

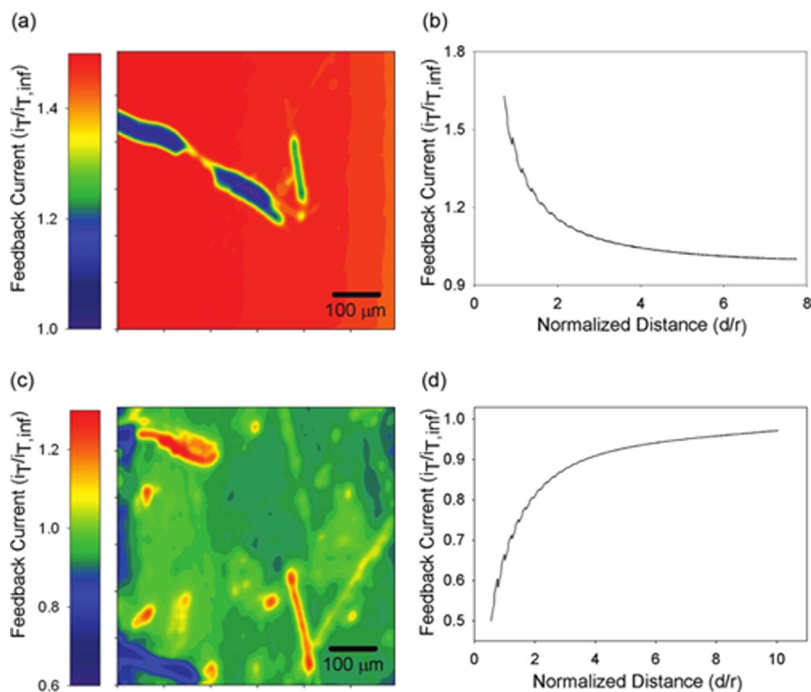


**Figure 5.** Role of the defects in CVD on its electrochemistry by scanning electrochemical microscopy. SECM images of monolayer graphene with different mediators. (a) Positive feedback SECM image showing graphene in red and exposed Si/SiO<sub>2</sub> in blue with 1 mM FeMeOH as mediator. The graphene electrode was biased at -0.2 V vs Ag/AgCl and the tip was biased at 0.5 V vs Ag/AgCl. (c) An intermediate-negative feedback SECM image showing the bulk graphene in green/blue and defects of higher activity in orange with 2 mM K<sub>3</sub>Fe(CN)<sub>6</sub> as the mediator. The graphene electrode was biased at 0.8 V vs Ag/AgCl and the tip was biased at -0.1 V vs Ag/AgCl. (d) Intermediate-negative feedback current profile as the tip approaches a pristine area of the graphene surface. The large features in the SECM images coincide with regions in which graphene was deliberately removed by scratching the surface with a glass tip. Reprinted with permission from ref 204. Copyright 2012 American Chemical Society.

the graphene sheets.<sup>191</sup> When describing the heterogeneous electron transfer (HET) on graphene, it is only sensible to start with the description of graphite, which is a highly ordered multilayer stack of graphene sheets. While doing so, we should still keep in mind that a multilayer structure may exhibit different electrochemistry compared to a single layer structure. Highly oriented pyrolytic graphite can be cut in two perpendicular directions to expose the basal plane or edge plane of the graphene sheets. It has been shown that the heterogeneous electron transfer rates of edge and basal planes of graphite are indistinguishable for certain compounds, such as ruthenium hexaammonium,<sup>192–194</sup> or are dramatically different, like in case of ferro/ferricyanide couple, Fe<sup>2+/3+</sup>, dopamine, ascorbic acid, and others.<sup>195–197</sup> The HET rate of ferro/ferricyanide at the edge plane is very fast, while the HET rate at the basal plane is often limited to near-zero under macroscopic voltammetry measurements.<sup>195</sup> Recent studies by electrochemical cell microscopy has however demonstrated a fast HET rate on the freshly cleaved basal plane of HOPG, but this activity faded rapidly over a short period of time.<sup>198</sup> In general, the basal plane is significantly less active than the edge plane of graphite. This is also true in the case of the edge plane in comparison to a folded basal plane of high curvature.<sup>199</sup> It was found that the presence of a higher amount of oxygen functional groups on graphite will result in a slower electron transfer rate as well.<sup>200</sup> Graphene behaves in many ways similarly to graphite. The exfoliation of graphite into smaller fragments, such as single and few layer graphene, increases the amount of basal plane per volume, but the amount of available edge plane remains the same. Therefore, the exfoliation of

graphite to graphene does not provide any advantages for compounds that are highly electrochemically active at the edge plane but inactive at the basal plane of graphene. This was clearly shown in the case of dopamine, ascorbic acid, uric acids, potassium ferrocyanide, and  $\beta$ -nicotinamide adenine dinucleotide, where the electrochemical responses on single layer, few layer, and multilayer graphene materials were practically indiscernible.<sup>201–203</sup> Instead, a higher loading of graphene materials on the electrode surfaces led to slower electron transfer rates due to the blockage of electroactive edges.<sup>203</sup> Detailed studies on mechanically exfoliated single layer graphene established the HET rate constant ( $k^0$ ) of the basal plane to be  $\sim 1.2 \times 10^{-3}$  cm s<sup>-1</sup> (Figure 4A,B).<sup>24</sup> This established HET rate was found to be independent of the amount of structural defects in the basal plane of the measured graphene,<sup>24</sup> which surprisingly contradicted the common wisdom of electrochemistry on graphite whereby a larger amount of defects in the basal plane usually leads to a faster HET rate.<sup>193</sup> Similar studies on CVD graphene containing chemically and mechanically induced defects, measured using the scanning electrochemical microscopy technique, indeed demonstrated that the  $k^0$  at sites with a structural defect were about 1 order of magnitude higher than that of the basal plane (Figure 5).<sup>204</sup> In that particular work, the defects were passivated by the electropolymerization of *o*-phenylenediamine.<sup>204</sup> Brownson and Banks, on the other hand, demonstrated the dominating role of graphitic islands present on the surface of CVD graphene as the active sites for fast electrochemistry (Figure 3C,D).<sup>157</sup> Similarly, reduced graphene materials prepared by the top-down oxidative method exhibited

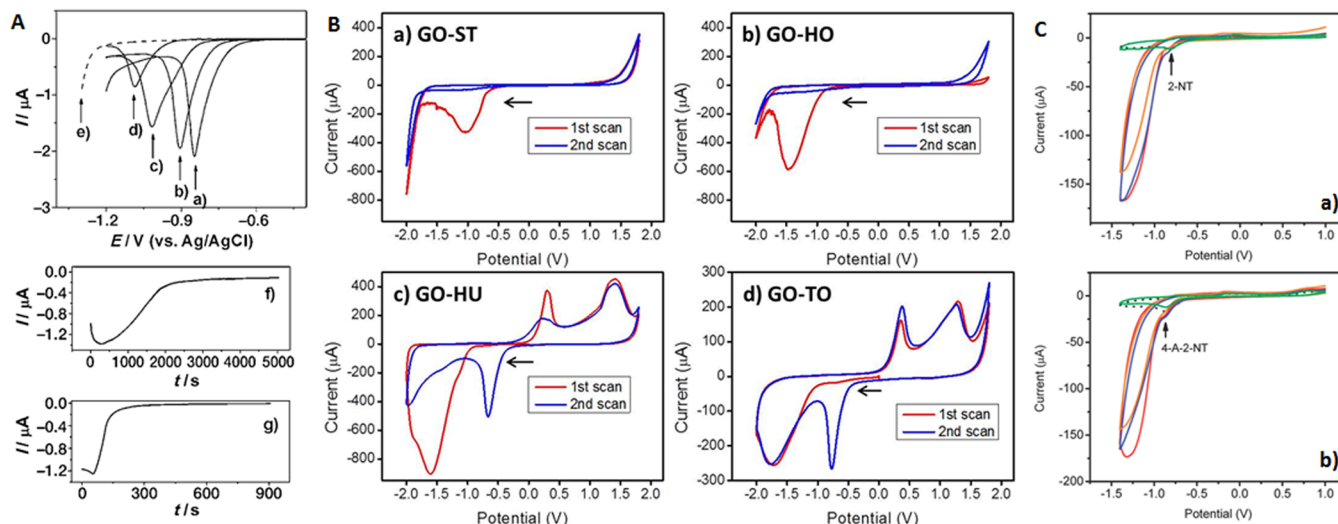


**Figure 6.** (A) (a–d) Linear sweep voltammograms of the GC electrode in contact with 7  $\mu\text{m}$ -thick GO films on quartz ( $54 \text{ cm}^2$ ) at pH values of 4.12 (a), 7.22 (b), 10.26 (c), and 12.11 (d). (e) Linear sweep voltammograms of the GC electrode suspended in PBS (1 M, pH 4.12). (f, g) Typical  $i$ – $t$  curves for the electrolysis of 7  $\mu\text{m}$ -thick GO films on quartz ( $5 \times 4 \text{ cm}^2$ , curve f) and on a GC electrode (3 mm diameter; curve g) with an applied potential of  $-0.90 \text{ V}$  in PBS (1 M, pH 4.12). Reprinted with permission from ref 65. Copyright 2009 John Wiley and Sons. (B) Inherent electrochemistry of graphene oxides depends on the preparation route. Cyclic voltammograms of graphene oxides prepared via the methods of (a) Staudenmaier (GO-ST), (b) Hofmann (GO-HO), (c) Hummers (GO-HU), and (d) Tour (GO-TO) scanned toward reducing potentials. Note that methods a and b are chlorate-based and c and d permanganate-based. Conditions: supporting electrolyte, 50 mM PBS at pH 7.2; scan rate, 100  $\text{mV s}^{-1}$ . Arrows indicate the direction of the first scans (red). All starting potentials are at 0.0 V and are with reference to the Ag/AgCl reference electrode. Reprinted with permission from ref 211. Copyright 2013 John Wiley and Sons. (C) Cyclic voltammograms of (a) 20 ppm 2-nitrotoluene and (b) 20 ppm 4-amino-2-nitrotoluene with different CMG-modified GC and bare GC electrodes. Bare GC, black dotted line; graphene oxide, red line; graphite oxide, blue line; chemically reduced graphene oxide, orange line; electrochemically reduced graphene oxide, green line. Conditions: scan rate of 0.1 V/s, 20 mM borate buffer (pH 9.3), buffer solution purged for 15 min with  $\text{N}_2$  before measurements, 20 ppm 2-nitrotoluene. Reprinted with permission from ref 212. Copyright 2011 American Chemical Society.

positive correlations between the density of defects in graphene sheets, as determined by Raman spectroscopy, and HET rates.<sup>66</sup> It was shown that the HET rate of ferricyanide at graphene is faster than that at the basal plane of HOPG but slower at the edge plane of HOPG (Figure 4C).<sup>26</sup> This is due to the fact that the edge plane of HOPG exhibits a very high density of electroactive edges (spacing between the layers in graphite is 3.35 Å). These results were independently confirmed.<sup>66</sup>

Graphene, especially when prepared from graphene oxide by the chemical, thermal, or electrochemical reduction of oxygen functional groups, can contain a large amount of oxygen functional groups.<sup>66</sup> It should be noted that the starting material, graphene oxide, typically exhibits a C/O ratio of  $\sim 2$  and a subsequent reduction process can improve this ratio anywhere from the range of  $\sim 3$  to  $\sim 15$ . It was also shown on the basis of a systematic study of graphene oxide and several reduced graphene materials that with increasing C/O ratio, the HET rate increases.<sup>66</sup> With a strong grasp of knowledge on the influence of oxygen functional groups toward the electrochemistry of graphene, thermally and chemically reduced graphene materials (i.e., graphene materials containing residual oxygen functional groups) can be electrochemically activated or deactivated. Such activation by electrochemical reduction and deactivation by electrochemical oxidation strongly influences the electrochemistry of compounds that are sensitive to the presence of oxygen functional groups, such as ascorbic acid or ferro/ferricyanide. On the other hand, compounds that are known to be electrochemically insensitive to the presence of oxygen functional groups, such as  $[\text{Ru}(\text{NH}_3)_6]^{2+/3+}$ , will not be affected.<sup>205</sup> Furthermore, this activation process can be

precisely tuned by the extent of electrochemical reduction performed on graphene oxide.<sup>69</sup> It is also of interest to note that thermally reduced graphene materials prepared using graphite oxide materials produced by different oxidative methods (those of Hummers, Hofmann, and Staudenmaier) exhibit very contrasting electrochemistry.<sup>206</sup> This is due to the fact that different oxidation methods will introduce a different amount of defects and oxygen functional groups to the graphene sheets. The properties of graphene materials prepared by different routes are summarized in Appendix 2.

### 3.2. Inherent Electrochemical Activity of Graphene-Related Materials

We have described in the previous sections that graphene oxide is a structurally and chemically complex material. It contains a large amount of carbon–oxygen bonds, thus creating a variety of oxygen functional groups, such as epoxide, peroxide, carbonyl (aldehyde, ketone and quinone), and carboxyl groups. In fact, the distribution of these oxygen functional groups differs on the basis of the preparation methods of graphene oxide (the Staudenmaier, Hofmann, or Hummers method) and the eventual reduction methods of graphene oxide.<sup>207</sup> Some of these oxygen functional groups are inherently electrochemically active, whereby they can be oxidized or reduced, at mild electrochemical potentials. These groups include quinones, hydroxyls, aldehydes, epoxides, and peroxides. At more extreme potentials and pH, it is also possible to reduce carboxyl groups (usually at potentials lower than  $-2 \text{ V}$ ).<sup>208</sup> Most of these groups reflected high cathodic peak currents (aldehyde, epoxide, and peroxide) or anodic peak currents (aldehyde and hydroxyl). It is important to mention that the electrochemical reduction of oxygen functional groups residing on the

surface of graphite demonstrates a distinct wave at ca.  $-1\text{ V}$  (vs  $\text{Hg}/\text{Hg}_2\text{SO}_4$ ), which was reported about 3 decades ago.<sup>209</sup> Dong and co-workers highlighted that it was possible to electrochemically reduce the oxygen functional groups of graphene oxide patterned on various conductive and insulating substrates at different pH with just a modest potential of ca.  $-1\text{ V}$  (vs  $\text{Ag}/\text{AgCl}$ ) (Figure 6A).<sup>65</sup> This discovery was subsequently applied by many other research groups as a “green” approach for the reduction of graphene oxide.<sup>68</sup> It should be noted that even though there is insufficient information on the types of oxygen functional groups that are reduced during this process, it is likely that epoxide, aldehyde, and peroxide groups are reduced at potentials of ca.  $-1\text{ V}$  while carboxyl groups are left unreduced. The stability of carboxyl groups toward electrochemical reduction at a potential of ca.  $-1\text{ V}$  was confirmed by high-resolution XPS analysis.<sup>210</sup> It is also interesting to note that different preparation methods of graphite oxide, such as those of Staudenmaier, Hofmann, Hummers, or Tour, demonstrate contrasting reduction potentials. Specifically, the Staudenmaier and Hofmann oxidation methods employ potassium chlorate as an oxidizing agent, while the Hummers and Tour methods apply potassium permanganate. While graphite oxide materials prepared by the Staudenmaier and Hofmann methods exhibit a single reduction wave with a peak potential at ca.  $-1.2\text{ V}$  (vs  $\text{Ag}/\text{AgCl}$ ), the Hummers method yields graphite oxide that shows three distinctive waves, reflecting the different oxygen functional groups that are reduced at very different potentials (ca.  $-1.2$ ,  $-1.4$ , and  $-1.8\text{ V}$  vs  $\text{Ag}/\text{AgCl}$ ).<sup>211</sup> On the other hand, graphite oxide prepared by the Tour method exhibits superposed waves at ca.  $-1.4$  and  $-1.8\text{ V}$  (Figure 6B).<sup>211</sup>

Apart from that, high-resolution XPS studies revealed that the Hummers and Tour synthetic procedures generated a higher content of carbonyl and carboxylic groups compared to the Staudenmaier and Hofmann methods. In addition, the oxygen functionalities of graphite oxide materials prepared by the two permanganate-based methods demonstrated reversible electrochemical behaviors. In fact, a cyclic voltammetry scan in the anodic direction revealed two anodic peak currents at about  $+0.3$  and  $+1.4\text{ V}$ . On the basis of pH study, the electrochemistry of the quinone–hydroquinone pair was suggested to be behind this unique electrochemical reversible character.<sup>211</sup>

It should be noted that the common reduction potential of the peroxide group is about  $-0.7\text{ V}$ , aldehyde about  $-1.0\text{ V}$ , epoxide about  $-1.5\text{ V}$ , and carboxyl group about  $-2.0\text{ V}$  (vs  $\text{Ag}/\text{AgCl}$ ).<sup>207</sup> This is not only true for graphite oxide but for graphene oxide as well.<sup>84</sup> Given that, the electrochemical reduction of graphene oxide can be used as a tool to prepare reduced graphene oxide for further applications, such as electrochemical biosensing devices, which will be described in the following section 4.

Moreover, the electrochemical reduction of solid-state graphene oxide can be used for the quantification of oxygen functional groups on graphene surfaces. Since the exact amount of transferred charge can be measured during the electrochemical reduction of solid-state graphene oxide material, the amount of electrochemically reducible oxygen functional groups can thus be quantified.<sup>82</sup> There were  $\sim 4.3$  electrochemically reducible oxygen functional groups on a graphene oxide material of  $1\text{ nm}^2$ . Interestingly, chemically reduced graphene oxide (using  $\text{NaBH}_4$ ) still contained  $\sim 2.5$  electrochemically reducible oxygen functional groups per  $1\text{ nm}^2$ , reflecting an incomplete chemical reduction. As an extension of

this quantification approach, the inherent electrochemistry of graphene oxide can also be used as an electroactive label for biosensing applications (see section 4).

Since the electrochemical reduction method can be easily controlled and monitored, it can be adopted to tune the electrochemical properties of graphene oxide films. In fact, it has been demonstrated that the C/O ratio of graphene oxide film can be tuned by applying different cathodic potentials for a fixed period of time, with direct consequences on the electrochemical properties.<sup>69</sup>

However, the susceptibility of graphene oxide to electrochemical reduction can be detrimental to certain applications, such as energy storage or sensing, which frequently incorporate graphene oxide or chemically reduced graphene oxide materials in the device setups. It has been shown that the analytical signals for the reduction of nitroaromatic compounds are completely hindered by a much larger current signal originating from the reduction of graphene oxide electrode materials itself (Figure 6C).<sup>212</sup> The inherent electrochemistry of graphene materials prepared by different routes is summarized in Appendix 2.

### 3.3. Influence of Dopants and Impurities on Graphene Electrochemistry

Doping of graphene with nonmetallic elements, such as nitrogen, sulfur, boron, or hydrogen, significantly changes its electronic structure and leads to potential catalysis or inhibition of redox reactions on its surface. The doping of graphene for important industrial/device applications, such as oxygen reduction reaction in fuel cells and capacitance in supercapacitors will be discussed in the respective subsections 5.1 and 5.2. Here, we wish to discuss the general influence of doping on graphene; dopants that are electron-withdrawing (i.e., halogens) or electron-donating (i.e., nitrogen) have important effects on the electrochemistry of the doped-graphene materials. N-doped graphene can be prepared by several ways, such as via the exfoliation of graphite oxide in  $\text{NH}_3$  atmosphere<sup>213</sup> or the exposure of reduced graphene to nitrogen plasma.<sup>214</sup> Such N-doped graphene generally exhibit a faster heterogeneous electron transfer rate toward ferro/ferricyanide redox probe<sup>213</sup> and promoted electrocatalytic reduction of hydrogen peroxide on its surface<sup>214</sup> compared to its undoped counterpart. On the other hand, halogen-doped graphene materials obtained via the exfoliation of graphite oxide in the corresponding halogen atmospheres exhibited decreasing HET rates toward ferro/ferricyanide redox probe with increasing size of the halogen atom.<sup>215</sup> Apart from that, the hydrogenation of graphene sheets toward graphane (which exhibits a large band gap)<sup>216</sup> provided interesting electrochemical properties. Specifically, graphane with a low hydrogen coverage ( $\sim 3$  atomic %) demonstrated a low HET rate toward ferro/ferricyanide redox probe<sup>217</sup> while graphane with higher coverage of hydrogen ( $\sim 19$  atomic %) showed a higher HET rate.<sup>218</sup>

Moreover, graphene materials contain a significant amount of impurities that can dramatically influence the electrochemical properties. These impurities can originate from the starting material used to fabricate the graphene materials, such as graphite and carbon nanotubes, or from the fabrication processes of these materials. The source of impurities in graphite and CNTs was previously discussed in subsection 2.1.6. These impurities are wide-ranging, from electrochemically inactive  $\text{SiO}_2$  to electrocatalytic transition metals, such as

Ni, Fe, and Co. These impurities remain in graphene despite strong oxidative treatment of graphite with concentrated sulfuric and nitric acids as well as consequent thermal or ultrasonication/chemical exfoliation/reduction treatments.<sup>97,102</sup> In fact, these metal-based impurities are responsible for numerous reports on the excellent electrocatalytic activity of graphene toward many analytes, such as cumene hydroperoxide, L-glutathione, sodium hydrogen sulfide, and hydrazine, which were erroneously ascribed to the graphene materials themselves. It has been demonstrated that the removal of such metallic impurities is highly challenging, as the impurities remain in the graphene materials even after treatment with Cl<sub>2</sub> gas at 1000 °C for 10 min.<sup>97</sup> Furthermore, ultrasonication treatments on graphene materials have strong influences on the availability of metallic impurities, whereby an extended ultrasonication time can result in the release of a higher amount of redox active impurities in the graphene dispersions.<sup>219</sup> Apart from just graphite source, graphene nanoribbons prepared from carbon nanotubes contain embedded residual metallic impurities originating from the synthesis of the nanotubes as well. These residual metallic impurities, which remain on the surface of the graphene nanoribbons, were found to be responsible for the observed electrocatalytic behaviors toward the oxidation of NaHS and hydrazine.<sup>108</sup> In the light of that, metallic impurities can be viewed as a kind of dopant and can be exploited for their electrocatalytic effects if the exact availabilities in graphene materials can be accurately quantified. For example, such impurities-containing graphene materials can be used as electrocatalytic surfaces for the detection of organic peroxides.<sup>220</sup>

Another type of major impurity is amorphous carbon. This type of impurity can also be present in carbon starting materials (such as carbon nanotubes<sup>221</sup>) and propagate throughout the entire preparation route to the final graphene material. Moreover, it can be formed as a side product when graphene sheets are digested under strong oxidative conditions as well. The presence of such amorphous carbon impurities in graphene was found to be responsible for the observed electrochemical activity of graphene toward NADH, acetaminophen, and hydroquinone.<sup>37</sup>

Apart from the aforementioned dopants and impurities, surfactant is also a cause for concern in the electrochemistry of graphene materials. Surfactants are often introduced into suspensions of graphene materials as stabilizers. Although surfactants are not inherently electroactive, they can significantly influence the voltammetric signals of a wide variety of compounds ranging from ferro/ferricyanide to NADH and other biomarkers.<sup>38,39</sup> The exact influences can be observed on both the anodic or cathodic directions, depending on the charge of the analytes of interest and the charge of the surfactants.<sup>222</sup> While voltammetric responses are often affected, electrochemical impedance signals are also susceptible to the presence of surfactants used for preparing colloidal suspensions of graphene.<sup>40</sup>

### 3.4. Spectroelectrochemistry of Graphene

Spectroelectrochemistry is a method which combines electrochemistry with *in situ* spectroscopy. Spectroelectrochemistry can be applied for three different kinds of applications with regard to graphene materials: (i) It allows the *in situ* determination of products (or intermediates) from electrochemical reactions occurring on graphene surfaces. (ii) Electrochemical methods can be utilized to dope graphene

materials with high precisions and to investigate the influences of such doping by *in situ* spectroscopic techniques (i.e., Raman spectroscopy). Specifically, hole doping can be achieved by applying anodic potentials and electrodoping by applying cathodic potentials. (iii) Electrochemical methods can be used to alter graphene surfaces (i.e., to reduce graphene oxide to graphene or vice versa) with *in situ* spectroscopic analysis to study the inherent structural changes on the surfaces of the modified graphene materials.

Given the high optical transparency of graphene films, they are ideal materials for spectroelectrochemical investigations of products from electrochemical reactions. Moreover, graphene is also an ideal candidate to replace common ITO transparent electrodes in spectroelectrochemical measurements, since the electrochemical window of graphene is very wide. The application of a transparent graphene-based spectroelectrochemical cell has been previously demonstrated with amphiphilic cyanine dye.<sup>223</sup>

The application of *in situ* Raman spectroelectrochemistry has led to the discovery of a very important feature in the Raman spectra of CVD graphene. The G and G' (also known as 2D) bands in Raman spectra are typically used to evaluate the quality of graphene, whether it is single, double, or triple layer, etc. Careful hole and electron doping by electrochemical methods have shown that the G' to G ratio depends very strongly on the extent of doping.<sup>224</sup> Moreover, Raman spectroscopy was applied in combination with electrochemical doping of graphene layers to investigate the individual layers of a double layer graphene. This was achieved by an ingenious fabrication design of the double layer graphene, whereby the first graphene layer was fabricated with only <sup>12</sup>C atoms while the second graphene layer was made up entirely of <sup>13</sup>C atoms. Since the Raman spectra of individual graphene layers were significantly shifted and dissimilar, it was possible to investigate the individual layers separately. Subsequent electrochemical doping and *in situ* Raman spectroscopy on the double layer CVD graphene revealed that the particular graphene layer that was in contact with the Si/SiO<sub>2</sub> substrate was strongly doped by the substrate, while the upper graphene layer did not exhibit any sign of doping by the Si/SiO<sub>2</sub> substrate.<sup>225,226</sup>

On another note, it is possible to electrochemically reduce graphene oxide to reduced graphene oxide by applying cathodic potentials, as previously described in subsection 3.2. The start of the electrochemical reduction is commonly observed at a cathodic potential of -0.7 V (vs Ag/AgCl electrode).<sup>65,69,82</sup> On the basis of the *in situ* Raman spectroscopy, structural changes were observed on graphene oxide subjected to a modest cathodic potential of -0.2 V (vs calomel reference electrode). The *in situ* Raman spectroscopy also indicated a strong increase in conductivity on the electrochemically reduced graphene material when compared with the graphene oxide precursor. Upon the reversal of the voltammetric scan from -1.0 V to the anodic region of up to 0 V, no structural changes were detected by Raman spectroscopy, which confirmed the chemical irreversibility of the electrochemical reduction of graphene oxide.<sup>227</sup> While the spectroelectrochemical study on the electrochemical reduction of graphene oxide provided concrete evidence of the reduction phenomenon, it has also led to the development of a more in-depth analysis that utilized *in situ* surface-enhanced infrared spectroscopy. It was found that the application of cathodic potentials below -0.8 V not only led to the reduction of various oxygen functional groups, such as epoxide, peroxide, and aldehyde, but also to the reduction of

water molecules and a corresponding increase of  $-\text{OH}$  groups on graphene surfaces.<sup>228</sup>

Although graphene is fairly stable in the anodic region, it can undergo oxidation to graphene oxide at a potential of +2 V (vs Ag/AgCl). While UV-vis *in situ* spectroelectrochemical measurements demonstrated that the electrolytes surrounding graphene appeared not to have any influence on the cyclic voltammetry behaviors, a higher amount of electrochemically generated graphene oxide was observed with increasing cation sizes of the electrolytes, from  $\text{Li}^+$  to  $\text{Na}^+$  and  $\text{K}^+$ .<sup>229</sup>

#### 4. GRAPHENE IN ELECTROCHEMICAL SENSING AND BIOSENSING

Graphene and graphene-related materials have been largely exploited to develop improved chemical and biological electrochemical sensors. This is not only due to the better and unique electrochemical properties of graphene materials, but also to the ease of functionalizing the graphene surfaces with specific elements of interest. Several strategies that have been applied to build analytical devices will be described in the following subsections according to the specific electrochemical detection technique adopted.

##### 4.1. Voltammetric and Amperometric Graphene Sensors and Biosensors

Voltammetry and amperometry methods are the most adopted transducing techniques in the development of sensing systems due to their simplicity, significant sensitivity achievable, and low-cost instrumentations. Voltammetry and amperometry belong to the group of potentiostatic techniques where the electrode potential is controlled and applied to drive an electron transfer reaction, resulting in a measured current. In amperometry, the current is monitored over time after the application of a fixed potential.<sup>230</sup> Besides cyclic voltammetry, other voltammetric techniques have been introduced mainly to improve the limit of detections in quantitative measurements. These techniques are based on pulse technologies where the current is measured after a potential pulse is applied. Depending on the excitation waveform, normal pulse voltammetry (NPV), square-wave voltammetry (SWV), and differential pulse voltammetry (DPV) are often applied. These techniques, together with amperometric techniques, are generally adopted in (bio)sensing systems for analytical purposes ranging from the direct detection of important biomarkers to immuno, DNA, and cell analysis for both environmental and clinical applications.

**4.1.1. Analysis of Biomarkers.** An enormous number of works are dedicated to the application of graphene and graphene-related materials for the analysis of important biomarkers, which are small molecules directly or indirectly relevant to clinical diagnosis. Novel electrochemical sensors built with graphene are generally tested for the detection of glucose,  $\beta$ -nicotinamide adenine dinucleotide and its reduced form ( $\text{NAD}^+/\text{NADH}$ ), hydrogen peroxide ( $\text{H}_2\text{O}_2$ ), dopamine (DA), ascorbic acid (AA), and uric acid (UA).

Glucose is without any doubt the most tested analyte. This is not only due to its importance in monitoring diabetic disease but also to the considerable usefulness of developing portable, point-of-care, and user-friendly devices for its detection. Glucose sensors based on graphene are generally built by immobilizing glucose oxidase enzyme (GOx) on a graphene electrode surface. This is done in a way that ensures both a biocompatible environment, which promotes the highest

enzyme activity, and also a good electrical contact between the graphene electrode and the active center of the enzyme, which generates a fast electrochemical response. Different composite materials have been previously proposed. Lin and co-workers proposed a biocomposite combining reduced graphene oxide (rGO), GOx, and chitosan to obtain a limit of detection (LOD) of 20  $\mu\text{M}$ .<sup>231</sup> Similar combinations have been presented using graphite oxide instead of rGO,<sup>232</sup> or introducing other nanostructured materials, such as AuNPs,<sup>233,234</sup> PdNPs,<sup>235,236</sup> AgNPs,<sup>237</sup> and PtNPs to enhance the electron transfer.<sup>238</sup> Recently, several glucose sensors employed electrochemically reduced GO (ERGO)<sup>239–241</sup> to immobilize GOx to obtain, in the best case, a LOD as low as 5  $\mu\text{M}$ .<sup>241</sup> Although the use of GOx allows for a high selectivity toward the detection of glucose, the performance of the resulting sensor ultimately depends on the stability of GOx, which is rather low. As such, several nonenzymatic sensors have been developed to replace GOx, specifically PtNi NPs,<sup>242</sup> Pt nanoflowers,<sup>243</sup> NiO NPs,<sup>244</sup> and  $\text{CuO}$ <sup>245</sup> and  $\text{Co}_3\text{O}_4$  nanowires,<sup>246</sup> among others. It is noteworthy to mention the remarkable result obtained by Dong et al., who developed a glucose sensor based on a 3D graphene foam modified with  $\text{Co}_3\text{O}_4$  nanowires to achieve a LOD as low as 25 nM.<sup>246</sup>

The detection of NADH has an enormous importance for the development of amperometric biosensing systems, since it is an electroactive cofactor that participates in all dehydrogenase reactions for the conversion of important substrates such as alcohol, lactate, and glucose. The redox reaction of NADH has been investigated using different graphene materials. Tang et al. adopted chemically reduced GO (CRGO), which showed a remarkable oxidation shift of about 30 mV as compared to graphite and bare GC electrodes.<sup>247</sup> A further improvement was obtained by functionalizing the graphene with methylene green.<sup>169</sup> Our group has studied the redox behavior of NADH at different graphene material surfaces<sup>66</sup> as well as at CVD multilayer graphene transferred onto flexible surfaces.<sup>119</sup> A graphene composite was proposed using ERGO and polythionine, which upon deposition onto a GC electrode provided a LOD of 0.1  $\mu\text{M}$  for NADH.<sup>248</sup> Similarly to NADH,  $\text{H}_2\text{O}_2$  is also particularly important for the development of biosensing systems, since it is an enzymatic product of oxidases, a substrate of peroxidases, and an important mediator in clinical as well as pharmaceutical analyses. The detection of  $\text{H}_2\text{O}_2$  can be achieved using horseradish peroxidase enzyme (HRP) immobilized onto graphene-based electrodes and nonenzymatic composites. Recently, Lu et al. prepared a composite using CRGO with self-assembled cyclodextrin (CD) to trap adamantine-tagged HRP enzyme molecules. The composite sensor was able to detect  $\text{H}_2\text{O}_2$  with a LOD of 0.1  $\mu\text{M}$ .<sup>249</sup> Nonenzymatic systems have been proposed lately using sulfonated graphene modified with AuNPs to achieve a LOD of 0.2  $\mu\text{M}$ ,<sup>250</sup> and also exfoliated GO modified with  $\text{Co}_3\text{O}_4$  NPs to reach a LOD of 0.3  $\mu\text{M}$ .<sup>251</sup> Other examples involve the use of AgNPs<sup>252</sup> or PtNPs<sup>253</sup> in combination with reduced GO to achieve, in the latter scenario, a LOD as low as 80 nM.<sup>253</sup>

Dopamine (DA) is a neurotransmitter found in serum samples at a concentration between 0.01 and 1  $\mu\text{M}$ . Its deficiency is correlated to Parkinson's disease, and therefore, a large volume of research works aimed at developing sensitive, rapid, and decentralized sensing devices for its detection have been carried out. Besides its low physiological concentration, which demands very sensitive detection systems, high concentrations of interfering substances such as ascorbic acid

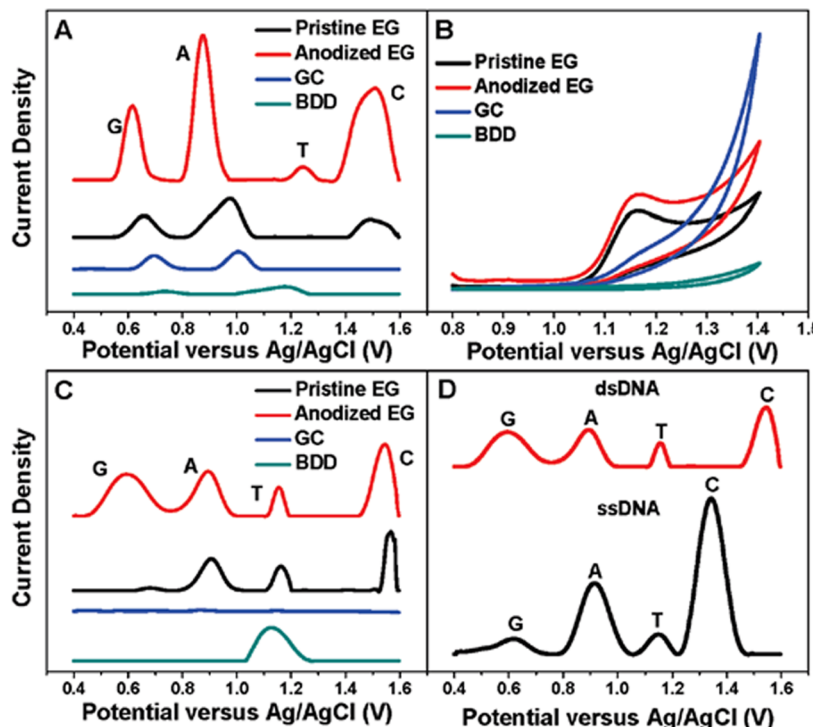


**Figure 7.** Activation of epitaxial graphene via anodization is necessary for DNA bases sensing. DPV profiles for pristine EG, anodized EG, GC, and BDD electrodes in (A) a 30  $\mu\text{M}$  equimolar mixture of G, A, T, and C; (B) 1.0 mM thymine; (C) 30  $\mu\text{g mL}^{-1}$  dsDNA; and (D) anodized EG in 30  $\mu\text{g mL}^{-1}$  dsDNA and 30  $\mu\text{g mL}^{-1}$  ssDNA. Supporting electrolyte: 10 mM KCl/10 mM PBS solution at pH 7. Reprinted with permission from ref 115. Copyright 2010 American Chemical Society.

(AA) and uric acid (UA) require the sensing platforms to be highly specific as well. Since these three substances are electroactive, they can be detected via voltammetric techniques by monitoring the respective electro-oxidation signals. Due to the overlapping oxidation potentials of the three substances, however, electrocatalytic systems are required to clearly distinguish and separate each generated signal. With a high density of edgelike sites and excellent electrocatalytic properties, graphene-based electrodes have demonstrated excellent performances in detecting DA, even in the presence of AA and UA. One of the first examples on the excellent electrocatalytic properties of graphene edges in detecting DA was shown by Shang and co-workers, who grew multilayer graphene nanoflakes by a microwave-plasma-enhanced CVD technique to obtain a very high density of exposed edgelike planes.<sup>254</sup> They were able to detect DA at a LOD of 0.17  $\mu\text{M}$  in the presence of 1 mM AA and 0.1 mM UA. Several other examples of graphene electrodes were tested using CRGO,<sup>255,256</sup> CRGO in combination with  $\beta$ -cyclodextrin,<sup>257</sup> PtNPs,<sup>258</sup> Zn/Al hydroxides,<sup>259</sup> PdNPs,<sup>260</sup> and  $\text{Fe}_3\text{O}_4$  NPs,<sup>261</sup> to name a few. Interestingly, an extremely low LOD was achieved using electrochemically reduced GO in combination with polyvinylpyrrolidone (PVP) polymer. The sensor was able to detect 0.2 nM DA in the presence of 1 mM AA.<sup>262</sup> A LOD of 20 nM was recently achieved using water-soluble sulfonated graphene.<sup>263</sup> Good performances were also demonstrated for graphene electrodes grown by CVD methods. Lim et al. synthesized few layer graphene by epitaxial growth on SiC and showed that an electrochemical anodization treatment to the graphene increased the density of defects. The resultant graphene enabled simultaneous detection of DNA bases and resolved signals from AA, DA, and UA (Figure 7).<sup>115</sup> Banks and co-workers also tested CVD graphene electrodes in comparison

to standard carbon electrodes such as glassy carbon (GC), edge-plane pyrolytic graphite electrode (EPPG), and basal-plane pyrolytic graphite electrode (BPPG).<sup>158</sup> They clearly show that the electrocatalytic properties of CVD graphene are due to the presence of graphitic islands across the graphene surfaces resembling edgelike sites.

**4.1.2. DNA Analysis.** Detection of nucleic acids can be performed by means of voltammetric techniques based on two different strategies: (i) direct electrochemical detection of DNA bases and polynucleotides and (ii) monitoring the hybridization event by means of electroactive labels. On the basis of the first strategy, due to the electroactive DNA bases, direct electrochemical signals can be recorded during the electrooxidation of the four bases, which occur at different potentials.<sup>264</sup> Graphene-based electrodes have been employed for sensitive and simultaneous detection of free DNA bases as well as for short DNA polynucleotides. The importance of exposed edgelike planes in graphene for the catalytic oxidation of the four DNA bases was demonstrated by our group by using a sensor modified with stacked graphene nanofibers. In comparison to a multiwalled CNT-based electrode, the SGNF sensor showed a sensitivity of up to 4 times higher due to the higher density of exposed edgelike sites.<sup>265</sup> Similar studies were performed to compare different graphene materials with the aim of selecting the optimal structural and chemical features of graphene materials for the electrochemical analysis of DNA bases.<sup>266,267</sup> CRGO-modified GC electrodes employed by Dong and co-workers demonstrated excellent capabilities to simultaneously detect all DNA bases. The group highlighted the possibility for a direct detection of a single-nucleotide polymorphism (SNP) in a short oligonucleotide.<sup>268</sup> Impressive results were obtained by Akhavan et al., who prepared a sensor consisting of graphene oxide nanowalls with a preferred vertical orientation deposited

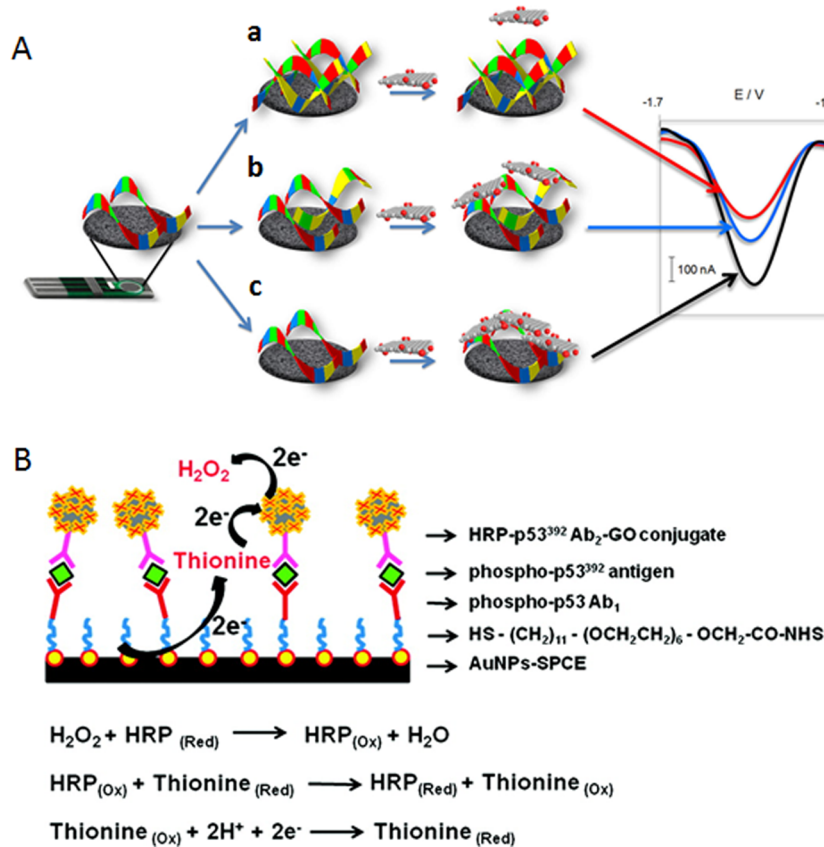


**Figure 8.** Graphene as a label for biosensing. (A) Graphene oxide nanoplatelets as inherently electroactive labels for single nucleotide polymorphism detection. The hybridization step was performed with a complementary target (a), one-mismatch target (b), and noncomplementary target (c). Reprinted with permission from ref 84. Copyright 2012 American Chemical Society. (B) Graphene as carrier of enzyme label for immunosensing using horseradish peroxidase–p53<sup>392</sup> Ab<sub>2</sub>–graphene oxide conjugate. Reprinted with permission from ref 285. Copyright 2011 American Chemical Society.

on a graphite electrode. This formed an extremely high density of active edge sites, which allowed the direct electrochemical detection of dsDNA oligonucleotides with a LOD as low as 9.4 zM.<sup>269</sup> Graphene oxide was also used to modify pencil graphite electrodes (PGE) to obtain enhanced analytical performances when monitoring hybridization events between DNA probe immobilized on the electrode surface and a target DNA strand.<sup>270</sup> Finally, our group also used a reduced graphene oxide platform to show how the peak potential and current for the oxidation of DNA bases may be influenced by the specific base sequence of an oligomer.<sup>271</sup>

Subsequently, according to the second strategy, which uses electroactive labels, typical sensing schemes involve the modification of the electrode surface with graphene materials, immobilization of ssDNA probe, hybridization with target DNA strand, and specific interaction with a signal carrier. For example, in the work of Yan and co-workers, an ERGO-modified GC electrode containing oligonucleotides carrying –SH groups was immobilized with ssDNA probes modified with AuNPs by exploiting Au–S interactions. Subsequently, target DNA strands labeled with biotins were allowed to hybridize. Carbon nanospheres modified with streptavidin and carrying HRP enzymes were then introduced and allowed to interact specifically with the biotin target DNA. DPV detection of 2,2'-diaminoazobenzene produced by the HRP enzyme after the introduction of *o*-phenylenediamine and hydrogen peroxide allowed the quantification of the target DNA down to 5 aM level.<sup>272</sup> Liu et al. recently prepared a reduced GO electrode

decorated with AuNPs by electrochemical coreduction of GO film and AuCl<sub>4</sub><sup>-</sup>. After the immobilization of DNA probes, a sandwich-type format was adopted to bind target DNA strands and secondary HRP-labeled oligonucleotides. A LOD of 3.4 fM was achieved.<sup>273</sup> Lin and co-workers used a similar electrode surface with graphene and AuNPs but employed 1,10-phenanthroline cobalt ([Co(phen)<sub>2</sub>(Cl)(H<sub>2</sub>O)]<sup>+</sup>) complex as an electroactive intercalator.<sup>274</sup> In a completely new approach, our group developed a biosensing platform in which graphene oxide nanoplatelets were used as an electroactive label for the detection of DNA hybridization and polymorphism. The differentiation of a single-base mismatch was achieved by exploiting the different affinity of the graphene nanoplatelets for single- and double-stranded DNA (Figure 8A).<sup>84</sup>

The advent of graphene offered new and exciting possibilities for the development of novel nanopore-based DNA sequencing devices. These devices involve the application of an electric field to drive negatively charged DNA molecules through a nanopore open membrane. A current signal can therefore be generated by each nucleotide base with intensities specific for each base. DNA sequencing could then be performed in a fast and precise fashion. However, single-base resolution can only be achieved with extremely thin membranes. As such, graphene has been considered the ideal material to this aim due to its atomic thickness and excellent electrical properties.<sup>275–278</sup> Proof-of-concept experiments have already been proposed using dsDNA molecules<sup>279,280</sup> and recently also with short single strand oligonucleotides.<sup>281</sup> While the prospect is good,

graphene nanopores are often plagued by severe clogging and attachment of DNA molecules. A recent attempt of tuning the hydrophobicity of graphene into a hydrophilic substrate by noncovalent functionalization has provided a workaround.<sup>282</sup>

**4.1.3. Protein Analysis.** Graphene and graphene-related materials have been used to modify electrode surfaces with the aim of enhancing electrochemical responses as well as increasing the electrode surface area to ease the loading of bioreceptors. A large number of specific biorecognition molecules, such as antibodies, coupled with fast electrochemical responses of graphene electrodes synergistically provide sensors with high sensitivities and good performances. A simple graphene/chitosan composite electrode was used by Xie et al. for the analysis of p53 tumor suppressor protein. The group employed a sandwich detection scheme with a secondary antibody labeled with HRP enzyme. A voltammetric signal was generated in the presence of thionine and  $\text{H}_2\text{O}_2$ , which was directly related to the p53 protein concentration. Using this sensor, a LOD of 0.1 ng/mL was calculated.<sup>283</sup> The same group also proposed a signal amplification strategy by using a carbon sphere to carry additional secondary antibody and HRP enzymes. This sensor was tested for the detection of  $\alpha$ -fetoprotein (AFP) and is capable of reaching a LOD of 0.02 ng/mL.<sup>284</sup> In other works, graphene sheets have been used to carry secondary antibodies and enzyme molecules in order to achieve signal amplification with sandwich-type immunosensors (Figure 8B).<sup>285,286</sup> N-doped graphene sheets have also been used to develop immunosensors for the analysis of AFP<sup>287</sup> and CA15-3<sup>288</sup> proteins.

In order to simplify the fabrication processes and analytical responses, voltammetric immunosensors that exploit the blocking effect generated by the antigens captured so that no secondary antibody and label are required have been proposed. Ma and co-workers recently prepared a GO electrode modified with thionine and AuNPs to immobilize carcinoembryonic antigen (CEA) antibody. The incubation with increasing concentrations of CEA saw a proportional decrease of voltammetric signals. The LOD of the sensor was calculated as 0.05 fg/mL of CEA.<sup>289</sup>

A different strategy that exploits the inherent electroactivity of GO nanosheets to directly monitor biospecific interactions was also proposed.<sup>83,290</sup> Moreover, the oxygen functional groups on the GO nanosheets platelets can be electrochemically reduced to generate a current signal. The formation of specific aptamer/thrombin<sup>83</sup> or avidin/biotin<sup>290</sup> complexes favor the partial detachment of these complexes from the electrode surface. Thus, current signal measured from the addition of GO nanosheets can then be correlated to the amount of complexes detached, which is in turn proportional to the concentration of the target analytes.

**4.1.4. Cell Analysis.** Voltammetric or amperometric techniques can be used for both the analysis of specific molecules released from stimulated cells as well as for the recognition and quantification of cells (cancer cells most commonly). Graphene is generally adopted in the modification of electrode surfaces to enhance the electrochemical signals and to provide a biocompatible interface that has good cell adhesion properties.

An amperometric sensor for the detection of  $\text{H}_2\text{O}_2$  released from human cells was proposed by Guo et al. in 2010. The group prepared a multilayer electrode biointerface by depositing reduced graphene oxide onto an ITO electrode, followed by the deposition of Prussian blue as  $\text{H}_2\text{O}_2$  catalyst

and finally laminin matrix protein to promote cell adhesion. Breast cancer cells were grown on the electrode surface and the sensor was able to detect  $\text{H}_2\text{O}_2$  with a LOD of 0.1  $\mu\text{M}$  upon stimulation.<sup>291</sup> In another work, laccase–ABTS mediators were immobilized onto reduced graphene oxide. The sensor, in this case, was adopted for the sensitive detection of oxygen released by erythrocytes with a LOD as low as 10  $\mu\text{M}$ .<sup>292</sup>

With regard to the quantification of cells, the main purpose is to develop an ultrasensitive electrochemical sensor for the quantification of cells that can be grown directly onto the sensing surface or specifically “picked” from a mixed sample. Recently, electrochemically reduced GO was used as an electrode modifier to immobilize anti-EpCAM antibodies. This biointerface was then used to detect Hep3B cancer cells, which specifically bind to the anti-EpCAM antibodies. A sandwich system was then generated using antibody-modified  $\text{SiO}_2$  nanoparticles carrying ZnTe or CdTe quantum dots. Square wave voltammetry was finally adopted to measure the amount of Zn and Cd after their dissolution, which is directly proportional to the number of cells attached. A LOD as low as 10 cells  $\text{mL}^{-1}$  was achieved (Figure 9).<sup>293</sup> Very recently, Castillo and co-workers prepared a sensor that consisted of immobilized peptide nanotubes–folic acid receptors (PNT–FA) on graphene-modified screen-printed electrodes. The group adopted a cyclic voltammetric technique to measure electrochemical signals from  $\text{K}_3[\text{Fe}(\text{CN})_6]$  probe in order to quantify the number of cells (HeLa) immobilized on the electrode surface. Cells captured on the electrode surface created an insulating layer, which reduced the intensity of the recorded electrochemical signals. With this simple setup, a LOD of 250 cells  $\text{mL}^{-1}$  was obtained.<sup>294</sup>

**4.1.5. Analysis of Heavy Metals.** Voltammetric techniques are particularly useful for the analysis of metal ions due to their high sensitivity and selectivity. Since heavy metals such as  $\text{Cd}^{2+}$ ,  $\text{Hg}^{2+}$ ,  $\text{Zn}^{2+}$ ,  $\text{Pb}^{2+}$ , and  $\text{Cu}^{2+}$  generate highly distinguishable signals, multiplex analysis can be accomplished. In order to lower the LODs, it is common to employ stripping methodologies that consist of a preliminary accumulation/reduction of the metal ions on the electrode surface by applying a fixed cathodic potential, followed by a voltammetric analysis (stripping) that scans the potential toward anodic potentials. Using the accumulation treatment, LODs as low as  $10^{-10}\text{ M}$  can be achieved.

Nanomaterials-based electrodes are capable of providing more sensitive electrode interfaces due to increased surface area, faster electron transfer, and faster mass transport rates.<sup>295</sup> Recently proposed graphene-based electrochemical sensors for the analysis of heavy metals achieved extremely good performances, surpassing those obtained using, for example, CNTs or metal nanoparticles.<sup>295</sup> In 2009, Li et al. proposed a Nafion–graphene composite electrode for the analysis of  $\text{Pb}^{2+}$  and  $\text{Cd}^{2+}$  using differential pulse anodic stripping voltammetry (DPASV). In their work, a LOD of 0.02  $\mu\text{g L}^{-1}$  was obtained for both  $\text{Pb}^{2+}$  and  $\text{Cd}^{2+}$ .<sup>296,297</sup> A nanocomposite consisting of reduced GO, poly(vinylpyrrolidone), chitosan, and AuNPs was proposed by Zhang and co-workers for the analysis of  $\text{Hg}^{2+}$  and the sensor had a LOD of 6 ppt.<sup>298</sup> In order to improve the entrapment and detection of heavy metal ions, elements such as bismuth<sup>299</sup> or mercury<sup>300</sup> and compounds like  $\text{AlOOH}$ <sup>301</sup> have been introduced in graphene composites due to their strong affinities for heavy metals. A self-assembled alkyl-functionalized GO was recently demonstrated for the sensitive detection of  $\text{Cu}^{2+}$ .<sup>302</sup> It is worth mentioning the study carried out by Banks

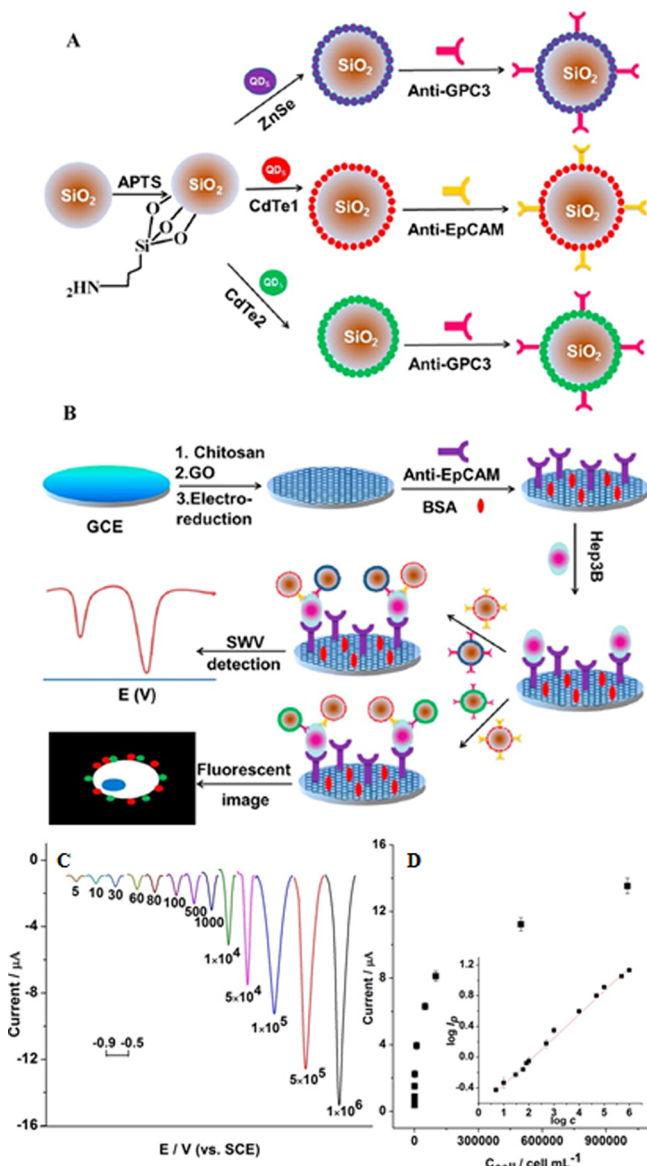


**Figure 9.** (A) Schematic of the preparation of Si/Zn/anti-GPC3, Si/Cd1/anti-EpCAM, and Si/Cd2/anti-GPC3 and (B) the fluorescent and electrochemical detection procedures of circulating tumor cells. (C) SWV of Si/Cd1/anti-EpCAM-Hep3B-anti-EpCAM/chitosan/electrochemically reduced GO/GCE at Hep3B cell concentration of 5, 10, 30, 60, 80, 100, 500, 1000,  $1 \times 10^4$ ,  $5 \times 10^4$ ,  $1 \times 10^5$ ,  $5 \times 10^5$ , and  $1 \times 10^6$  cells  $\text{mL}^{-1}$ . (D) Plot of peak current obtained by dissolved Si/Cd1/anti-EpCAM-Hep3B-anti-EpCAM/chitosan/electrochemically reduced GO/GCE vs Hep3B cell concentration in incubation solution. Inset in part D is the linear regression plot. Reprinted with permission from ref 293. Copyright 2013 American Chemical Society.

and co-workers on the use of surfactant-free and surfactant-stabilized commercial graphene for the analysis of heavy metals. The group showed that both types of graphene formulations brought no real advantage over the use of standard electrode interfaces such as glassy carbon electrode.<sup>38,303</sup> The same group also tested CVD graphene electrodes for the analysis of heavy metals. In this work, nickel-supported CVD graphene was used as received without removal of the underlying metal. The group noticed a detrimental effect from the underlying nickel supporting substrate during the cathodic accumulation step,

which then caused a poorer performance of the sensor for the analysis of  $\text{Pb}^{2+}$ .<sup>156</sup>

**4.1.6. Graphene in Security Applications.** Graphene-based electrodes were also used for detection purposes in security-related areas.<sup>304</sup> The detections of high-energy explosives and nerve agents (improvised ones, which are, in fact, potent pesticides)<sup>305</sup> were investigated on graphene-based electrodes. The electrochemical detection of nitroaromatic (high-energy) explosives is facilitated by the presence of  $-\text{NO}_2$  in the molecules. Up to six-electron reduction of each nitro groups on 2,4,6-trinitrotoluene (TNT) is facilitated on amorphous carbon, graphite, and graphene electrodes,<sup>306–308</sup> but not on boron-doped diamond electrodes<sup>309</sup> and related compound. Single layer, few layer, and multilayer graphene showed no major advantages for the electrochemical detection of TNT.<sup>310</sup> This was further extended to the use of thermally reduced graphene oxide materials fabricated from graphite oxide prepared by various methods, such as those of Hummers, Staudenmaier, and Hofmann. The Hofmann-method-based graphene exhibited the highest sensitivity for detecting TNT in seawater.<sup>311</sup> Moreover, the size dependency of the graphene sheets was also studied. Specifically, in comparison between graphene sheets prepared from stacked graphite nanofibers with dimensions of  $50 \times 50 \text{ nm}$  (graphene nanoplatelets) and graphene sheets prepared from multiwalled carbon nanotubes with dimensions of  $300 \text{ nm} \times 5 \mu\text{m}$  (graphene nanoribbons),<sup>95</sup> the graphene nanoribbons provided an order of magnitude higher sensitivity than graphene nanoplatelets toward the detection of TNT.<sup>312</sup> Although boron-doped graphene did not show any enhanced performance when compared to its nondoped counterpart, it performed much better than boron-doped diamond, which did not provide any analytical signal at all.<sup>309</sup> Hydrogenated graphene exhibited poorer performance for the electrochemical detection of TNT than its non-hydrogenated counterpart.<sup>313</sup>

Graphene surfaces decorated with metal/metal oxide nanoparticles are often applied for the detection of organophosphorous pesticide, such as methyl parathion. Methyl parathion contains an  $-\text{NO}_2$  group, and thus, similar to nitroaromatic explosives, it can be detected via direct electrochemical reduction. A second mode of detection of methyl parathion involves an indirect detection via the inhibition of acetylcholine esterase by the pesticide. The direct electrochemical reduction of methyl parathion was reported on chemically reduced graphene oxide/chitosan composite.<sup>314</sup> Moreover, nanoparticles such as Au,<sup>315</sup>  $\text{ZrO}_2$ ,<sup>316,317</sup> and  $\text{TiO}_2$ <sup>318</sup> doped on reduced graphene oxide sheets were reported to enhance the cathodic currents originating from the reduction of nitro group in methyl parathion. However, the mechanism behind the enhancement was not clear. Graphene sheets decorated with acetylcholinesterase, an enzyme which can be irreversibly inactivated by organophosphate pesticides, was also used as a sensitive platform for methyl parathion detection on both bare graphene and CdS NPs-decorated graphene electrode configurations.<sup>319,320</sup>

#### 4.2. Impedimetric Graphene Sensors and Biosensors: Toward Label-Free Detection

Electrochemical impedance spectroscopy (EIS) is especially suited for monitoring changes in the interfacial properties of an electrode surface.<sup>321</sup> The technique is particularly sensitive and can be advantageously exploited for sensing and biosensing protocols on graphene platforms.<sup>322</sup>

One of the biggest advantages of using EIS is that it does not require any additional signal-generating labels to detect changes on the surface interfaces or biorecognition events. This tremendously simplifies the analytical procedures since it can be carried out with minimal or no sample pretreatments. In addition, the technique is not destructive and does not cause any alteration to the analytes. In fact, EIS has been adopted in combination with graphene materials for DNA, protein, and cell analysis.

**4.2.1. DNA Analysis.** The analysis of DNA with impedimetric detection generally involves the measurement of impedance signals before and after hybridization events between DNA probes immobilized on an electrode platform and target DNA sequences present in a sample.<sup>323,324</sup> Such a biorecognition event changes the electrode interface and generates different impedance signals. In cases whereby significantly different impedance signals are recorded before and after the biorecognition events, the sensor is not only able to discriminate between complementary and noncomplementary DNA targets but also to detect the presence of single-nucleotide polymorphism (SNP). When building a DNA electrochemical sensor and, in particular, with impedimetric detection, the first and foremost aspect to consider is the immobilization of the DNA sequence probe on the electrode surface. Three possible strategies are usually adopted: (i) covalent immobilization, (ii) physical adsorption, and (iii) affinity immobilization. Recently, our group has performed a comparative study on the three methods to immobilize thrombin-specific aptamers onto graphene oxide films.<sup>325</sup> On the basis of EIS analyses, it was concluded that the physical adsorption and covalent immobilization techniques not only demonstrated similar performances, but were also superior to sensors prepared by the affinity immobilization through avidin/biotin linkages. Moreover, our group has also investigated the influence on the extent of covalent attachment points of DNA probes toward hybridizations with target DNA strands.<sup>326</sup> It was shown that a single covalent attachment point onto reduced graphene oxide films provided the most efficient hybridization and, therefore, a more sensitive analysis. Similarly, Dubuisson et al. obtained a better performance from an impedimetric sensor prepared on the basis of covalent immobilization of DNA probes onto epitaxial graphene (EG) compared to the physical adsorption.<sup>327</sup> Despite that, our group has shown that physically adsorbed DNA on different graphene platforms can be a simple and convenient strategy to provide excellent LOD in the picomolar (pM) range for the detection of a SNP correlated to Alzheimer's disease.<sup>328</sup> Other impedimetric investigations were performed using the adsorption strategy to immobilize single-stranded DNA onto different chemically modified graphene materials, such as graphene oxide, electrochemically reduced GO, thermally reduced GO,<sup>329</sup> and polyaniline–ERGO nanocomposites<sup>330</sup> as well as aminopropyltriethoxysilane (APTES)–ERGO composite.<sup>331</sup> Even though promising results were obtained from the physical adsorption strategy to immobilize sensing DNA probes, covalent attachment, which involved the formation of amide bonds between amino-terminated DNA probes and oxygen-containing groups disseminated all over the graphene materials, remained as the most widely employed method.<sup>332</sup> With this approach in mind, attempts have been proposed to increase the oxygen functionalities on graphene surfaces by introducing, for example, perylene tetracarboxylic acid (PTCA),<sup>333</sup> poly(xanthurenic acid),<sup>334</sup> or 1-aminopyr-

ene<sup>335</sup> or by adopting specific surface chemistry to increase the number of carboxylic groups on the graphene platform.<sup>336</sup> A slightly different immobilization strategy was also proposed by preparing AuNP-decorated graphene materials in which the AuNPs were used as anchors for the attachment of amino or sulfur-terminated DNA sensing probes.<sup>337,338</sup>

**4.2.2. Protein Analysis.** Impedimetric protein sensors exploit two possible recognition elements that are immobilized on the electrode surface: (i) antibodies, which are able to recognize and bind specific target antigens, and (ii) aptamers, which are small peptides or oligonucleotides that have conformations and structures capable of binding target molecules. The latter is a promising element for future developments of protein sensors due to the ease of production, well-known binding mechanism, and, more importantly, the possibility to synthesize specific binding properties toward any target protein/molecule in theory.<sup>339</sup>

Graphene and graphene-related materials are recently employed to improve the loading of biorecognition elements on electrode surfaces and to increase the number of signaling labels for a signal enhancement approach. One of the simplest strategies was proposed by Roy et al., who immobilized anti-IgG probes on the surface of GO-modified glassy carbon electrode (GCE) through EDC–NHS chemistry. The sensor reached a LOD in the nanomolar range for rabbit IgG used as a demonstrative molecule.<sup>340</sup>

Our group also tested different graphene materials for the fabrication of both an impedimetric immunosensor for the analysis of IgG molecule<sup>341</sup> and an impedimetric aptasensor for the analysis of thrombin.<sup>342</sup> We concluded that while thermally reduced graphene material showed the best performances for antibody-based biosensors, graphene oxide offered the most sensitive platform for aptamer-based sensors. In a different approach, graphene oxide was used as a signal carrier enhancer in a sandwich-type immunosensor.<sup>343</sup> This was achieved by first immobilizing anti-CEA antibodies on a AuNP-modified GC electrode. After incubation with the target CEA, the sandwich system was generated using GO-modified with both anti-CEA antibodies and HRP enzymes. The final impedimetric detection was performed after the immersion of the sensor into a precipitating solution consisting of 4-chloro-1-naphthol in ethanol and H<sub>2</sub>O<sub>2</sub>. HRP present in the sandwich system will thus generate insoluble benzo-4-chlorohexadienone upon contact with the precipitating solution to result in large alterations in the impedance of the electrode.<sup>343</sup> The first example of impedimetric aptasensor fabricated using single-layer CVD graphene was demonstrated recently by Gutes et al. After a galvanic deposition of AuNPs onto the CVD graphene, the group etched away the copper substrate, transferred the graphene onto a GC electrode and immobilized a peptide specific to decabromodiphenyl ether. Subsequent impedimetric detection provided a sensitive analysis of DBDE in the range of 5–100 ppt.<sup>344</sup>

**4.2.3. Cell Analysis.** The high sensitivity of EIS provides a good detection technique to monitor changes occurring on electrode surfaces. This is important in order to recognize and quantify cells adhered on electrode surfaces as well as to monitor changes in cell behaviors in response to specific external stimuli. The use of graphene to enhance the sensitivity of the technique by improving electrical conductivity and creating a surface more favorable for cell adhesion and growth has only recently been demonstrated. This shows that research on the development of sensitive impedimetric cytosensors with

integrated graphene and graphene-based composite materials is only at its very early stage. One of the first example was proposed in 2011 by Feng et al., who prepared a composite with chemically reduced GO and 3,4,9,10-perylenetetracarboxylic acid. After deposition of the composite material on an electrode, the numerous carboxylic groups available on the material were used to link a specific aptamer with a high affinity toward nucleolin, which is an overexpressed protein of breast and cervical carcinoma cells. The sensor showed a LOD of about 1000 cells per mL.<sup>345</sup> Similar approaches were recently developed thereafter. Chemically reduced GO/carboxymethyl chitosan composite was prepared as a starting film which was then enriched with folic acid (FA). FA can be used to bind certain cancer cells bearing folate receptors on the cell membrane. This sensor reached a LOD of around 500 cells per mL.<sup>346</sup> A lower detection limit of about 30 cells per mL was obtained by He and co-workers, who simply combined negatively charged GO and positively charged poly-L-lysine to create a surface with enhanced cell adhesion properties.<sup>347</sup>

#### 4.3. Potentiometric Graphene Sensors and Biosensors

Potentiometric devices operate by measuring the potential difference between two electrodes, whereby one of it functions as a reference electrode with fixed potential while the other as an indicator electrode that changes its potential in response to analyte concentration. An ion selective electrode (ISE) is one of the most widely used potentiometric sensors characterized by the presence of an ion selective membrane, which allows the exchange of only one ion (the target ion) between an inner solution and the sample solution with ideally no interference from other ions present. In such a setup, electrochemical equilibrium is attained and a potential difference is generated between the two separated phases based on the Nernst equation.<sup>348</sup> If the inner solution has a constant potential, the potential across the membrane measured by the device is only correlated to the amount of target analyte ion.<sup>348</sup> Different types of membranes have been used, ranging from classical solid glass or single crystal membranes to liquid membranes embedded in polymeric matrices (PVC). The original concept of an ISE, as described above, consists of an electrode immersed in an inner solution separated from the sample solution by a selective membrane. Such conventional liquid-contact ISEs are mechanically fragile, suffer from possible leakage of filling solution, and can be difficult to miniaturize. A new generation of ISEs based on a solid-contact incorporates solid transducers between the conductive electrode surface and the selective membrane. Fabrication of this new type of ISE is tremendously simplified with the possibility of preparing miniaturized devices.<sup>349</sup>

The first few materials proposed as solid transducers were conducting polymers that have both ion exchange and redox capabilities to ensure a stable ion-to-electron response. However, the conducting polymers normally suffer from side redox reactions with interfering species and have high sensitivities to light and O<sub>2</sub> and CO<sub>2</sub> gases, which may alter their performances over time. Therefore, novel materials have emerged to replace these conducting polymers. In particular, nanostructured carbon materials have demonstrated excellent performance without the long-standing problems encountered by conducting polymers. Fullerenes,<sup>350</sup> microporous carbon,<sup>351</sup> and carbon nanotubes<sup>352,353</sup> have been previously applied and graphene is currently proposed as a novel high-performance material for all-solid-state ISE.

One of the first applications of graphene for solid-state ISE was demonstrated in 2011 by Ping et al., who modified a GC electrode surface with chemically reduced GO to function as a transducer for potassium ion detection with a PVC-based selective membrane. The sensor showed better performances than sensors based on conducting polymers.<sup>354</sup> The same group also adopted electrochemically reduced GO to modify a screen-printed electrode to detect Ca<sup>2+</sup> ions.<sup>355</sup> Michalska and co-workers developed a potentiometric sensor that employed functionalized graphene as a transducer and selective film for Zn<sup>2+</sup> ions.<sup>356</sup> Investigations on the transduction mechanism of reduced graphene material were performed by Rius and co-workers using cyclic voltammetry and EIS before testing the potentiometric sensor performances for Ca<sup>2+</sup> ion detection at different thicknesses of reduced graphene material.<sup>357</sup> Apart from that, a comparison between the usage of CNTs and graphene on a disposable solid-state electrode system was recently demonstrated with the analysis of Na<sup>+</sup> ions.<sup>358</sup>

### 5. GRAPHENE IN ENERGY SYSTEMS

#### 5.1. Graphene for Capacitors and Supercapacitors

The capacitance of classical carbon materials, such as carbon black, graphite, and carbon nanotubes is closely related to the amount of sp<sup>3</sup> defects in the sp<sup>2</sup> lattice.<sup>359</sup> It was found that the capacitance of the materials increased with the amount of active areas, specifically sp<sup>2</sup> edge planes and defects.<sup>360</sup> As such, a material with a higher amount of active areas should theoretically have a significantly higher capacitance. The theoretical surface area of graphene is 2630 m<sup>2</sup> g<sup>-1</sup>, which is about 100 times more than that of graphite powder (~10 m<sup>2</sup> g<sup>-1</sup>)<sup>361</sup> and double that of single-walled carbon nanotubes. When the capacitance of a single sheet of monolayer graphene was measured, however, it was found that the charge that could be simultaneously stored on both sides of the sheet was much lower than the charge that can be stored on just one side. It was suggested that such an observation was due to the fact that the capacitance of single layer graphene displayed quantum behaviors.<sup>362</sup> In addition to this issue, graphene-fabricated electrodes from well-defined and flat graphene sheets tend to stack and exhibit very similar capacitance to graphitic structures, on the order of tens of farads per gram.<sup>363</sup> The preparation method of graphene, that is, whether the graphene is prepared by chemical, electrochemical, or thermal reduction of graphene oxide, significantly influences the capacitance of the final graphene material.<sup>364–366</sup> In fact, the current trend indicated that graphene materials carrying a lower amount of oxygen functionalities provided a higher capacitance.<sup>364–366</sup> With regard to the restacking issue of these graphene materials, there were many attempts to space out the graphene sheets with nanoparticles (i.e., Au)<sup>367</sup> or carbon nanotubes.<sup>368–374</sup> In some cases, a dramatic increase of capacitance was reported for CNT/graphene hybrid materials, even just by simple mixing and drying of these two carbon materials;<sup>368–373</sup> in other instances, however, such CNT/graphene hybrid materials exhibited weight-specific capacitance corresponding to the average capacitances of the individual carbon components.<sup>374</sup> The aggregates of defective graphene were known to have a weight capacitance of ~100 F/g.<sup>375</sup> A highly wrinkled cross-linked graphene oxide surface can reach a specific capacitance of 211 F/g.<sup>376</sup> Another type of graphene material obtained from the exfoliation of graphene with strong base (KOH), a procedure similar to the fabrication of activated amorphous

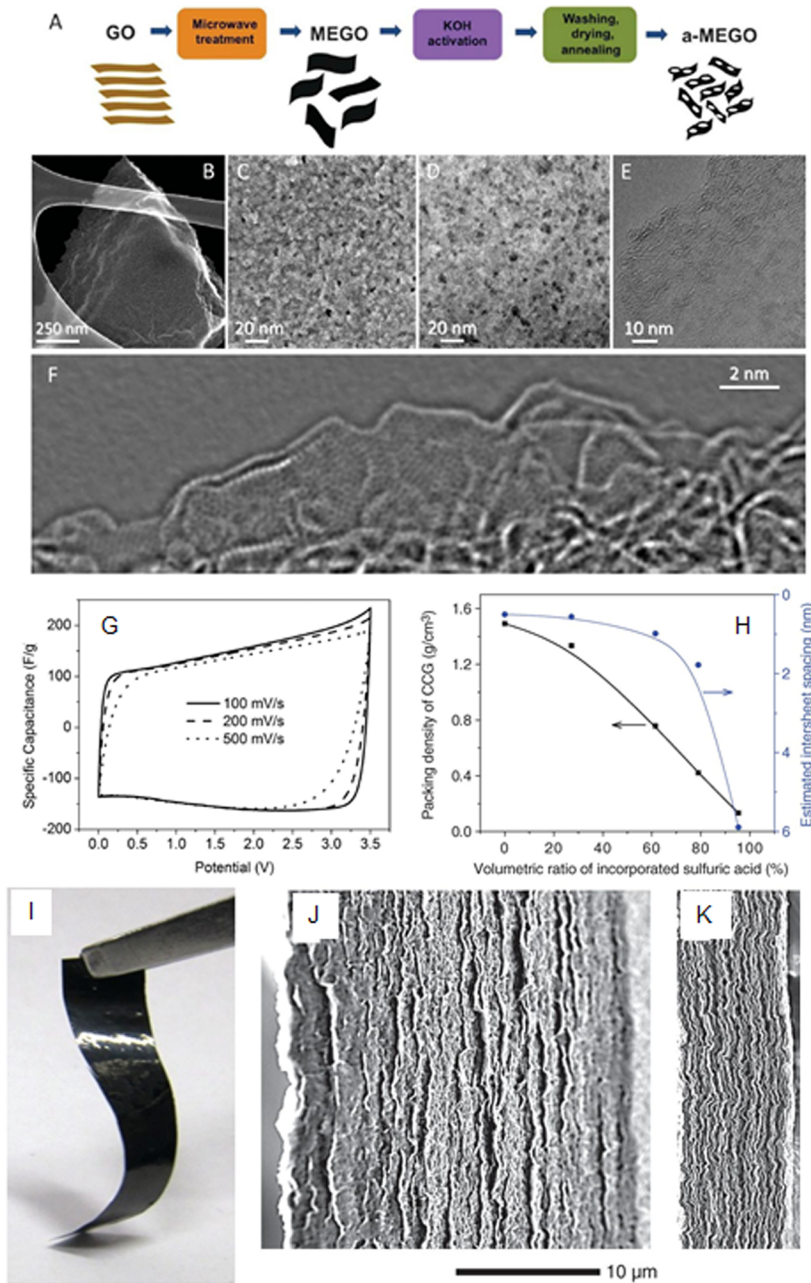


**Figure 10.** Graphene-based supercapacitors. (A) Schematic showing the microwave exfoliation/reduction of GO and the following chemical activation of microwave-exfoliated graphite oxide (MEGO) with KOH that creates pores while high electrical conductivity is retained. (B) Low magnification SEM image of a 3D a-MEGO piece (“a” stands for KOH activation). (C) High-resolution SEM image of a different sample region that demonstrates the porous morphology. (D) ADF-STEM image of the same area as in part C), acquired simultaneously. As seen, a-MEGO contains micro- and mesopores with a distribution of sizes between ~1 and ~10 nm. (E) High-resolution phase contrast electron micrograph of the thin edge of an a-MEGO chunk, taken at 80 kV. There is a variation in focus across the image because of the sloped nature of the sample and changes in sample thickness. The image shows the presence of a dense network of nanometer scale pores surrounded by highly curved, predominantly single-layer carbon. (F) Exit wave reconstructed HR-TEM image from the edge of a-MEGO. The in-plane carbon atoms are clearly resolved, and a variety of *n*-membered carbon rings can be seen. Substantial curvature of the single-carbon sheets is visible, with the in-plane crystallinity being preserved. (G) Supercapacitor performance of a-MEGO (SSA  $\sim$  2400  $\text{m}^2/\text{g}$ ) in the BMIM BF<sub>4</sub>/AN electrolyte. CV curves for different scan rates. Rectangular shapes indicate the capacitive behavior. Reprinted with permission from ref 378. Copyright 2011 The American Association for the Advancement of Science. (H) The relation between the volumetric ratio of incorporated electrolyte and the packing density as well as the estimated intersheet spacing. (I) A photograph showing the flexibility of the film. SEM images of cross sections of the obtained EM-CCG films containing (J) 78.9 vol % and (K) 27.2 vol % of H<sub>2</sub>SO<sub>4</sub>, respectively, corresponding to  $\rho = 0.42$  and 1.33 g/cm<sup>3</sup>. Reprinted with permission from ref 381. Copyright 2013 The American Association for the Advancement of Science.

carbon, is capable of having an increased active surface area beyond the theoretical 2630  $\text{m}^2/\text{g}$ .<sup>377</sup> The resulting KOH-activated graphene exhibited a capacitance of  $\sim$ 165 F/g (Figure 10A–G).<sup>378</sup>

Moreover, the presence of pores smaller than 0.7 nm in the KOH-activated graphene was determined as the major contributor to the enhanced capacitance.<sup>379</sup> In other

works, the density of energy storage was increased by the close packing of graphene sheets, with reported weight capacitances of >200 F/g, either using laser scribbled graphene<sup>380</sup> or liquid mediation of closely packed graphene sheets and corrugates (Figure 10H–K).<sup>381</sup> It should also be noted here that the observed capacitance of graphene can be significantly influenced by the presence of surfactants used to stabilize the graphene dispersions.<sup>382</sup>

Further efforts to increase the capacitances of graphene materials were carried out by doping graphene with various heteroatoms, such as nitrogen, sulfur, or boron. Despite a large number of research articles published on the increased capacitance of N-doped (n-dopant; the N atom is an electron donor) graphene materials, little is known about the mechanism.<sup>383–386</sup> The effect was suggested to arise from a quantum capacitance effect. Quantum capacitance is closely related to the modification of the electronic structure of graphene.<sup>387</sup> Interestingly, boron (p-dopant) doping on graphene, which leads to the introduction of electron deficient atoms to the graphene structure, also provides an increased capacitance for graphene.<sup>388</sup> As for sulfur-doped graphene, a proposed mechanism suggested that the increased capacitance was a result of sulfur species located in small micropores. These sulfur species affected the charge on the graphene surface and decreased the surface affinity to adsorb water. This resulted in a specific electrosorption of electrolyte ions and increased the capacitance of the sulfur-doped graphene.<sup>389</sup> Electrical charge can be stored in graphene capacitors at the electrode/electrolyte interface based on electrochemical double layer (EDCL) capacitance, as was described above. Apart from that, there are other techniques used to enhance the capacitance of these graphene materials. Pseudocapacitance, which functions according to a redox electrochemical reaction of groups or materials available on graphene surfaces, is usually utilized, as it dramatically increased the amount of stored electrical charge. There are generally two major directions to achieve this: (i) utilization of metal oxide nanoparticles (i.e.,  $\text{NiO}_x$ ,  $\text{Mn}_x\text{O}_y$ ) supported by conductive graphene sheets or (ii) utilization of conducting polymer/graphene composites. Chen et al. deposited  $\text{MnO}_2$  nanoparticles on graphene sheets via direct synthesis with  $\text{KMnO}_4$  and  $\text{MnCl}_2$ ; such  $\text{MnO}_2$ -doped graphene material exhibited a capacitance of ~200 F/g.<sup>390</sup> Another approach, which immersed activated graphene in a solution of  $\text{KMnO}_4$  to deposit  $\text{MnO}_2$  on its surface, resulted in a capacitance of ~250 F/g.<sup>391</sup> The same method was applied to deposit  $\text{MnO}_2$  on 3D graphene, leading to a weight-specific capacitance of 389 F/g.<sup>392</sup> Moreover, the application of polymer brushes to stabilize  $\text{MnO}_2$  nanoparticles on graphene oxide surfaces provided a hybrid material with a capacitance of 372 F/g.<sup>393</sup> The role of oxidation levels on the underlying graphene in  $\text{MnO}_2$ /graphene composites indicated that with an increased oxidation level of graphene, the capacitance of the composite significantly decreased.<sup>394</sup>  $\text{V}_2\text{O}_5$  nanowire decorated graphene oxide material prepared by a solvothermal method exhibited a capacitance of 80 F/g.<sup>395</sup>  $\text{Ni}(\text{OH})_2$  nanoparticle decorated graphene oxide obtained via the decomposition of  $\text{Ni}(\text{CH}_3\text{COO})_2$  at 80 °C with consequent hydrothermal treatment gave well-defined  $\beta\text{-Ni}(\text{OH})_2$ . Such composites exhibited a very large capacitance of 1335 F/g.<sup>396</sup>  $\text{Ni}(\text{OH})_2$  nanoparticles on graphene oxide composites prepared via the hydrolysis of  $\text{Ni}(\text{Ac})_2$  exhibited a capacitance of 1828 F/g.<sup>397</sup>  $\alpha\text{-Fe}_2\text{O}_3$  nanotube/reduced graphene oxide composites demonstrated good stability and a capacitance of ~200 F/g.<sup>398</sup> Apart

from that, conducting polymer/graphene composites also showed highly enhanced pseudocapacitance, with polyaniline/graphene oxide composite demonstrating a capacitance of 480 F/g.<sup>399</sup>

## 5.2. Oxygen Reduction Reaction on Graphene

Oxygen reduction reaction (ORR) is an important reaction in fuel cells and Zn/air batteries. Although ORR is conventionally catalyzed by Pt/C, the high cost and limited availability of platinum prompted an immediate search for alternative catalyst systems. In fact, graphene has been utilized in two different directions for ORR: (i) as a conductive support with high surface area for metal/metal oxide electrocatalysts and (ii) applied directly as electrocatalysts for nonmetal heteroatom-doped graphene for metal-free oxygen reduction catalysis on its surface. The combinations of transition-metal-based catalyst nanoparticles on heteroatom-doped graphene are most often reported.

Manganese oxide nanoparticles are usually utilized as electrocatalysts for the oxygen reduction reaction on graphene sheets. Kim and co-workers fabricated  $\text{Mn}_3\text{O}_4$  nanoparticles on reduced graphene oxide using ionic liquid as anchor for  $\text{Mn}_3\text{O}_4$  nanoparticles. The group observed an anodic shift of ~100 mV for ORR on the manganese oxide-doped graphene material when compared to unmodified graphene.<sup>400</sup> Qiao and co-workers fabricated a hybrid nitrogen-doped graphene/ $\text{Mn}_3\text{O}_4$  for an enhanced ORR performance, whereby the group observed an anodic shift of ~30 mV for the onset reduction peak of oxygen at the  $\text{Mn}_3\text{O}_4$ -modified N-doped graphene material when compared to the precursor N-doped graphene.<sup>401</sup> In a similar manner, Cheng et al. deployed  $\text{MnO}_2$ -nanoparticle-modified reduced graphene.<sup>402</sup> A hybrid of spinel manganese–cobalt oxide decorated on graphene oxide exhibited an anodic shift of ~60 mV for ORR when compared to nondecorated graphene (Figure 11).<sup>403</sup> Apart from that, graphene was doped with different precious metals, such as Pt, Pd, Ag, Ru, and Rh, under inert ( $\text{N}_2$ ) and reducing ( $\text{H}_2$ ) atmospheres. It was found that the doped graphene materials prepared under  $\text{H}_2$  reducing atmosphere provided the best performance for ORR, with Pd-doped graphene exhibiting an anodic shift of 20 mV when compared to an undoped graphene surface.<sup>404</sup> In a similar manner, graphene doped with Fe, Mn, Co, and Ni was prepared in  $\text{N}_2$  and  $\text{H}_2$  atmospheres to enhance the ORR performances.<sup>405</sup> Fe-based composite prepared on N-doped graphene demonstrated a significant electrocatalysis for ORR with an anodic shift of its onset potential by 200 mV.<sup>406</sup> In a different work, CNT–graphene composite was fabricated from incompletely unzipped carbon nanotubes. The Fe-based residual impurities from CNTs growth as well as nitrogen impurities found in these sheets led to enhanced ORR performance on these materials.<sup>407</sup>

Heteroatom doping of graphene is a popular route toward the so-called metal-free ORR catalyst. Various dopants such as N, S, B, and P have been used. Regardless of the dopant type (n or p dopant), electrocatalytic effects toward the ORR are always observed. This suggests that the mechanism of ORR on these metal-free doped graphene materials is not well-understood. N-doped graphene was fabricated by the pyrolysis of graphene oxide with nitrogen-containing cationic surfactants; the resulting N-doped graphene showed a better performance than similarly prepared carbon nitrides in the absence of graphene.<sup>408</sup> Another research group pyrolyzed polyaniline on graphene oxide to obtain N-doped graphene for ORR.<sup>409</sup> In a

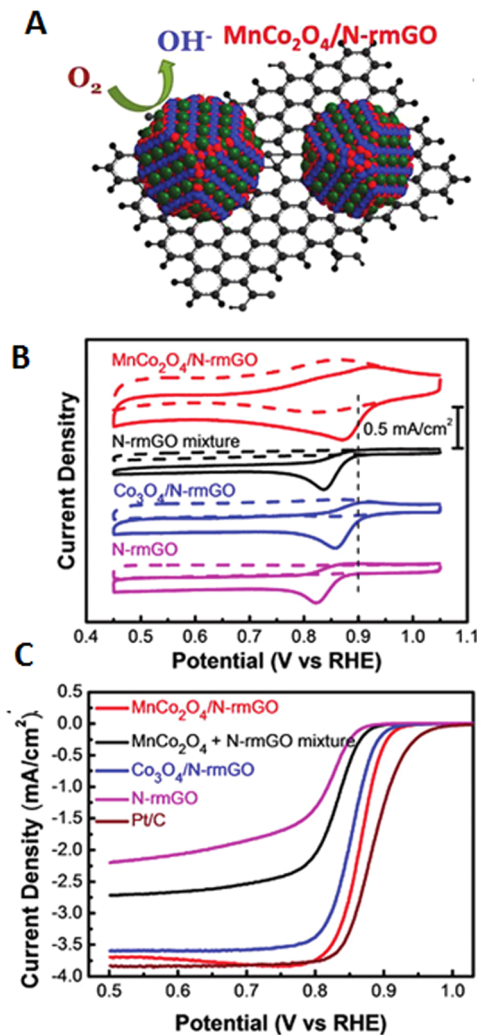


**Figure 11.** Oxygen reduction reaction on graphene decorated with nanoparticles. (A) Schematics of manganese–cobalt spinel  $\text{MnCo}_2\text{O}_4$ -decorated nitrogen-doped graphene hybrid for electrocatalytic oxygen reduction reaction. (B) CV curves of  $\text{MnCo}_2\text{O}_4/\text{N-rmGO}$  hybrid,  $\text{MnCo}_2\text{O}_4+\text{N-rmGO}$  mixture,  $\text{Co}_3\text{O}_4/\text{N-rmGO}$  hybrid, and N-rmGO on glassy carbon electrodes in  $\text{O}_2$ -saturated (solid line) or  $\text{N}_2$ -saturated (dash line) 1 M KOH. The peak position of Pt/C is shown as a dashed line for comparison. (C) Rotating-disk electrode voltammograms of  $\text{MnCo}_2\text{O}_4/\text{N-rmGO}$  hybrid,  $\text{MnCo}_2\text{O}_4+\text{N-rmGO}$  mixture,  $\text{Co}_3\text{O}_4/\text{N-rmGO}$  hybrid, N-rmGO, and Pt/C in  $\text{O}_2$ -saturated 1 M KOH at a sweep rate of 5 mV/s at 1600 rpm. Reprinted with permission from ref 403. Copyright 2012 American Chemical Society.

similar manner, S-doped graphene was synthesized using graphene oxide and benzene disulfide as starting materials before carbonization in an inert atmosphere at temperatures of  $\sim 1000^\circ\text{C}$ .<sup>410</sup> Direct incorporation of sulfur into the graphene lattice was carried out by exfoliating various graphite oxide materials (prepared by the Hofmann, Hummers, or Staudenmaier method) in  $\text{H}_2\text{S}$ ,  $\text{CS}_2$ , or  $\text{SO}_2$  atmospheres at different (600 and  $1000^\circ\text{C}$ ) temperatures.<sup>411</sup> It was found that the major differences in the sulfur contents in these graphene lattices were due to the different kinds of graphite oxide used (Hummers graphite oxide being the most favorable, with  $\sim 7$  atomic % of sulfur in graphene), while the types of atmospheres and temperatures played only a minor role. Such S-doped graphene materials were consequently used for ORR.<sup>411</sup> Another sulfur-doping approach ball-milled graphite with

elemental sulfur using stainless steel balls to create edge-sulfurized graphene nanoplatelets to function as electrocatalyst for ORR.<sup>412</sup> Apart from that, a codoped S/N-doped graphene material was prepared by coheating graphene oxide mixed with melamine (N-source) and benzyl disulfide (S-source) at  $900^\circ\text{C}$ . The resulting S/N-doped graphene exhibited a more positive onset potential for ORR than individual N- or S-doped graphene materials.<sup>413</sup> Another group exploited a similar procedure of doping graphene with sulfur and nitrogen, but using graphene oxide and ammonium thiocyanate as precursors.<sup>414</sup> Doping of graphene with electron-withdrawing atom, such as boron, was reported by heating graphite oxide with  $\text{B}_2\text{O}_3$  at  $1200^\circ\text{C}$ , and the incorporation of  $\text{B}_2\text{O}_3$  via vaporization was suggested. However, one should note that  $\text{B}_2\text{O}_3$  sublimes at  $\sim 1500^\circ\text{C}$ . Nevertheless, the ORR electrocatalysis was reported on such B-doped graphene.<sup>415</sup> B/N- and P/N-doped graphene materials were prepared with N-doped graphene using boric or phosphoric acid solution as sources of boron and phosphorus. The preparation involved mixing graphene oxide with the acids, which were subsequently left to evaporate. It is unlikely that, in this case, phosphorus or boron is incorporated into the graphene lattice.<sup>213,416,417</sup> In a different work, B/N-doped graphene was prepared by annealing graphene oxide in  $\text{NH}_3$  atmosphere with consequent heating to  $900^\circ\text{C}$  in the presence of  $\text{H}_3\text{BO}_3$ . A synergic effect of B/N-doped graphene toward ORR was reported.<sup>418</sup>

### 5.3. Graphene-Based Solar Cells

The high optical transparency and electrical conductivity together with electrocatalytic properties toward certain redox processes make graphene an ideal material to be exploited in photovoltaics.<sup>419,420</sup> Several different applications of graphene were proposed with the aim of obtaining highly efficient solar cells.<sup>421</sup> Dye-sensitized solar cells (DSSCs) represent a significant breakthrough in the field of solar energy conversion devices, due to their low production cost, simplified fabrication process, and excellent conversion efficiency.<sup>422</sup> In general, DSSCs are made up of four elements, which consist of a dye-sensitized  $\text{TiO}_2$  semiconductor, a transparent conducting electrode, a layer of electrolyte containing the redox mediator, and a counter electrode.<sup>423</sup> Thin films of reduced GO (rGO) were proposed by Müllen and co-workers to replace indium–tin oxide (ITO) as material for the fabrication of transparent conductive electrode.<sup>424</sup> Despite a power conversion efficiency (PCE) of 0.26%, which was lower compared to fluorinated tin oxide (FTO) devices (0.84%), this work pioneered the use of graphene as a transparent conductive electrode. Subsequent work employing CVD-grown graphene in combination with poly(3,4-ethylenedioxythiophene) (PEDOT) as transparent cathode in catalyst-free solar cells demonstrated its superior performance over the corresponding ITO/Pt-based electrode.<sup>425</sup>

Another important application of graphene in DSSCs involves its usage as a catalytic counter electrode. Typical catalysts include platinized FTO or ITO electrodes, in which Pt catalyzes the reduction of the oxidized redox shuttle ( $\text{I}_3^-$ ,  $\text{Co}^{3+}$ ,  $\text{T}_2$ ) to facilitate dye regeneration.<sup>421</sup> Graphene nanoplatelets (GNPs) adopted by Kavan and co-workers as transparent catalyst electrode (Pt-free) in DSSCs systems with  $\text{Co}^{3+}/\text{Co}^{2+}$  redox mediator<sup>426,427</sup> demonstrated superior performance compared to platinized FTO-based devices (Figure 12A). Similarly, the same group investigated the usage of GNPs in combination with  $\text{I}_3^-/\text{I}^-$  redox shuttle with promising results

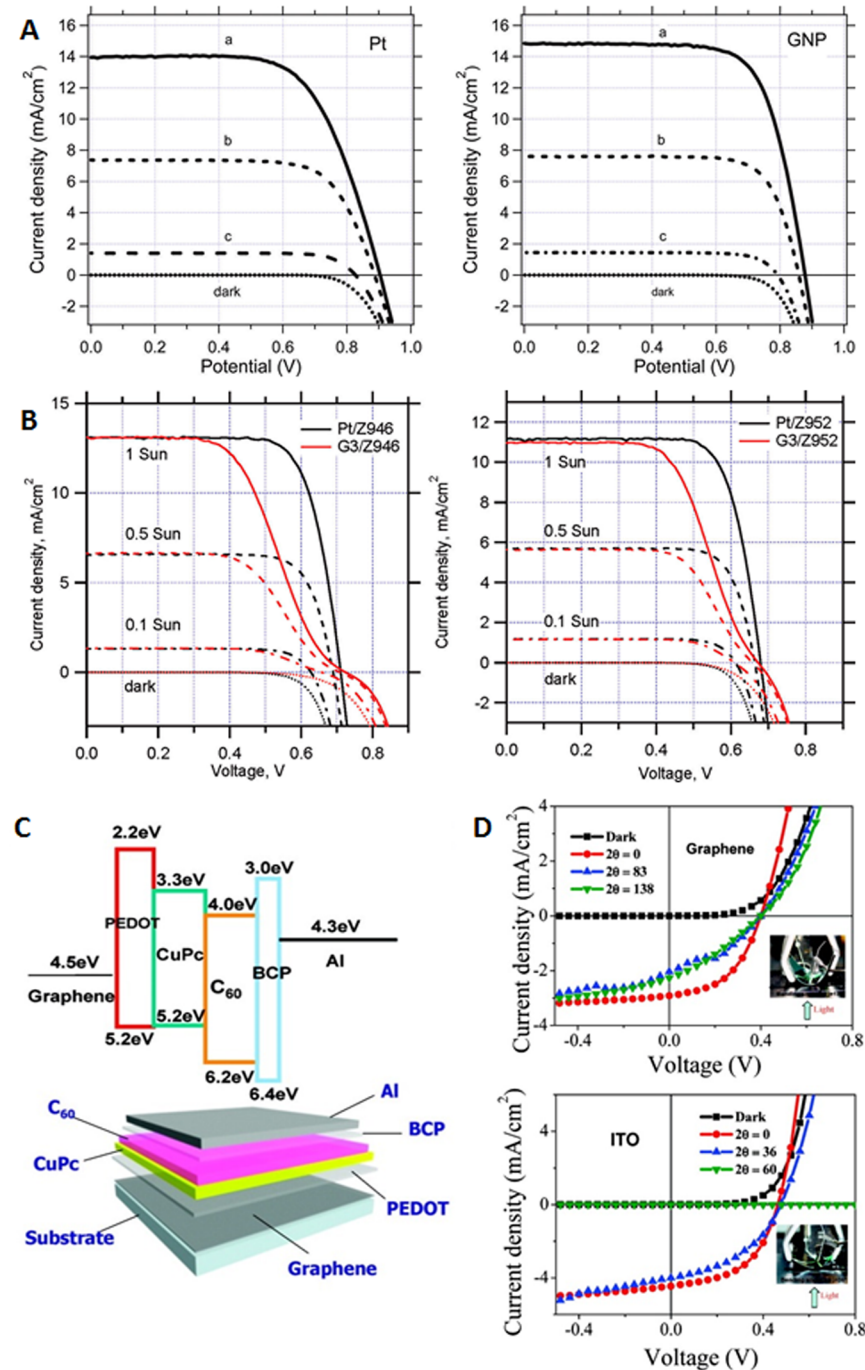


**Figure 12.** (A) Current–voltage characteristics of DSSC with Y-123-sensitized  $\text{TiO}_2$  photoanode and acetonitrile solution of  $\text{Co}(\text{bpy})_3^{3+/2+}$  with Pt-FTO (left) and graphene-FTO (right) counterelectrode. The illumination intensity is 1 sun (curves a), 0.51 sun (curves b), 0.095 sun (curves c), and 0 sun (curves dark). Reprinted with permission from ref 427. Copyright 2011 American Chemical Society. (B) Current–voltage characteristics of a dye-sensitized solar cell with the platinized FTO (black lines) or G3 cathode (red lines) under various light intensities: (left chart) Z946 electrolyte and (right chart) Z952 electrolyte. Reprinted with permission from ref 428. Copyright 2011 American Chemical Society. (C) Schematic representation of the energy level alignment (top) and construction of the heterojunction organic solar cell fabricated with graphene as anodic electrode: CVD graphene/PEDOT/CuPc/ $\text{C}_{60}$ /BCP/Al. (D) Current density vs voltage characteristics of CVD graphene (top) or ITO (bottom) photovoltaic cells under 100  $\text{mW}/\text{cm}^2$  AM1.5G spectral illumination for different bending angles. Insets show the experimental setup employed in the experiments. Reprinted with permission from ref 439. Copyright 2010 American Chemical Society.

(Figure 12B).<sup>428</sup> Chemically reduced GO in combination with GNPs demonstrated similar performance to Pt-FTO thanks to the improved adhesion of graphene materials to FTO electrode as well as to the high density of defects (active sites), which accelerated the redox process of  $\text{Co}(\text{bpy})_3^{3+/2+}$  mediator.<sup>429</sup>

Dye molecules in DSSCs can be replaced by inorganic quantum dots (QDs) such as CdS, CdSe, ZnS, and PbS, which possess high extension coefficients, various band gaps, and, more importantly, good stability. Similar to DSSCs, graphene can be used to enhance the electron transfer between the QD and  $\text{TiO}_2$  semiconductor in quantum dot solar cells

(QDSCs).<sup>430</sup> Li and co-workers proposed a multilayer graphene/CdS QDs film for QDSCs which demonstrated enhanced performance (IPCE > 16%) to similar devices prepared with SWCNTs and other carbon materials.<sup>431</sup> A similar layered electrode using graphene nanosheets and CdS QDs achieved remarkable performance due to improved and more uniform QD dispersion on the graphene sheets.<sup>432</sup> Moreover, graphene applied as a transparent front electrode in CdTe-based QDSCs obtained a PCE of 4.1%, which is superior to typical devices with a transparent ITO front electrode.<sup>433</sup> Recently, a Mo-based catalyst supported on electrically conductive CNT-rGO hybrid composite was adopted as a Pt-free catalytic electrode in QDSCs.<sup>434</sup> Apart from that, an interesting work by Lin et al. compared the performances of CVD-grown graphene, boron-doped graphene, and chemically reduced graphene as back-electrode in a CdTe QD solar cell. The group concluded that the boron-doped graphene, which has the lowest charge transfer resistance, offered the best performance with a PCE of almost 8%.<sup>435</sup> On another note, a slightly different photovoltaic scheme involves the use of organic conducting polymers (organic photovoltaic, OPV) to absorb light for the generation of electrons and holes, which are then transferred to an external electrode to produce currents. The most common transparent electrode in OPV cells is ITO. However, due to its high production cost, lack of flexibility, and scarce stability in acidic or alkaline ambiances, research efforts have focused on finding alternative materials for transparent electrode in OPV cells. In this case, graphene offers excellent opportunities. Reduced GO was spin-coated onto quartz by Chen and co-workers and tested as a transparent anode for OPV cells. The performance of the device was inferior to that of an ITO-based electrode but inevitably highlighted the potential of graphene in such applications.<sup>436,437</sup> Moreover, Yin et al. deposited rGO onto a flexible PET to fabricate a transparent electrode for a flexible OPV cell. The group highlighted the fact that the overall energy conversion efficiency was dependent on the compromise between transparency and sheet resistance.<sup>438</sup> Zhou and co-workers demonstrated an improved sheet resistance with CVD-grown graphene transferred onto PET substrates for flexible OPV cells, which obtained a performance comparable to that of an ITO-based device (Figure 12C,D).<sup>439</sup> Graphene modified with Al-TiO<sub>2</sub> was also applied as a transparent cathode in an OPV cell to achieve an energy conversion of 2.58%, which is almost 75% of the performance measured with an ITO-based device.<sup>440</sup> Another important application of graphene for organic solar cells is seen from the usage of GO and functionalized GO materials as transparent hole and electron extraction layers.<sup>441</sup> Li et al. demonstrated a pioneering work by replacing the commonly used PEDOT:PSS hole transport layer with GO and obtained a comparable performance with an energy conversion of about 3.5%.<sup>442</sup> Recently, the hole transport layer in an OPV cell made up of moderately reduced GO obtained by thermal treatment showed superior stability and better performance (PCE 3.98%) than a similar device prepared with PEDOT:PSS (PCE 3.85%).<sup>443</sup> Apart from that, due to the metallic character and zero band gap of graphene, it has also been successfully employed in metal/semiconductor Schottky junction solar cells.<sup>444</sup> The high transparency and flexibility of graphene can bring significant advantages to classical metal film/semiconductor systems or ITO/semiconductor systems.<sup>444</sup> A pioneering work by Li et al., who deposited graphene sheets onto n-type-doped Si, achieved a conversion efficiency of about

1.65% and provided important information on the performance of a solar cell in relation to the junction formation, passivation, etc.<sup>445</sup> Improvements were attained by using a Si pillar array instead of planar Si<sup>446</sup> and also by using doped graphene instead of pristine graphene for a remarkable energy conversion of 8.6%.<sup>447</sup> In order to avoid complicated transfer procedures of depositing CVD-grown graphene onto Si, Zhang and co-workers have recently developed a method to directly grow nanocrystalline graphene onto Si/SiO<sub>2</sub> using conventional photolithography and Si techniques. An efficient Schottky junction solar cell was obtained with a photovoltage responsivity of 300 V W<sup>-1</sup> at a light power of 0.2 V.<sup>448</sup> The usage of graphene oxide and reduced graphene oxide as Schottky junction with silicon has been investigated with detailed comparison of experimental and theoretical data as well as in-depth discussion on the factors influencing the deviation in performance between experimental and theoretical works.<sup>449</sup>

#### 5.4. Graphene-Based Lithium Ion Batteries

Lithium ion batteries (LIBs), in contrast to supercapacitors, are efficient, affordable, and high-energy-density electrochemical energy storage devices.<sup>450,451</sup> Since the first debut of commercial LIBs from Sony Corp. in 1991, they have been widely applied as the main power source for modern technologies ranging from consumer electronics to household power tools to passenger aircrafts. In order to improve the performance of LIBs, current research has focused on increasing the storage capacity of lithium in the anode and cathode of LIBs.<sup>452,453</sup> Given the high conductivity, surface area, and aspect ratio of graphene, it can act as a suitable material for the fabrication of anode and cathode.<sup>20,454</sup> The conventional graphitic anode of LIBs forms a graphite intercalation compound in the presence of lithium. In view of the stacked layered structure of graphite, lithium can only be stored within the sp<sup>2</sup> carbon hexadrons with a maximum theoretical capacity of 372 mAh g<sup>-1</sup> (LiC<sub>6</sub>).<sup>455</sup> As graphene can theoretically accommodate Li ions on both sides of the sheet, it can achieve a maximum capacity of 740 mAh g<sup>-1</sup> (LiC<sub>3</sub>).<sup>456</sup> Further theoretical study based on a Li<sub>2</sub> covalent molecule model identified that the most saturated lithium storage state can be achieved in disordered carbon with a capacity of 1116 mAh g<sup>-1</sup> (LiC<sub>2</sub>).<sup>457</sup>

Efforts to improve the performance of LIBs anode with graphene have realized innovative materials consisting of (a) solely graphene materials, (b) CNT- and C<sub>60</sub>-doped graphene, (c) porous/3D graphene, and (d) heteroatom-, metalloid-, metal-, metal oxide- or metal sulfide-doped graphene. While the performance of LIBs benefits from material with a large interlayer *d*-spacing (~4.0 Å),<sup>458</sup> active defects such as vacancies and edges on graphene materials can enhance lithium storage capability as well. This was highlighted from the higher reversible capacities of thermally reduced and electron beam irradiated graphene (Raman  $I_D/I_G$ : 1.51) at 1013–1054 mAh g<sup>-1</sup> in comparison to hydrazine-reduced graphene (Raman  $I_D/I_G$ : 0.74) at 330 mAh g<sup>-1</sup> under a current density of 50 mA g<sup>-1</sup>.<sup>459</sup> Another thermally reduced graphene applied as anode materials provided a reversible specific capacity of 1264 mAh g<sup>-1</sup> in the first cycle and subsequently 848 mAh g<sup>-1</sup> after 40 cycles at a current density of 100 mA g<sup>-1</sup>.<sup>460</sup> Further attempts to increase the interlayer spacing and surface area of graphene led to the introduction of CNT and C<sub>60</sub> as spacers between the graphene layers (*d*-spacing 4.0 and 4.2 Å), in which the

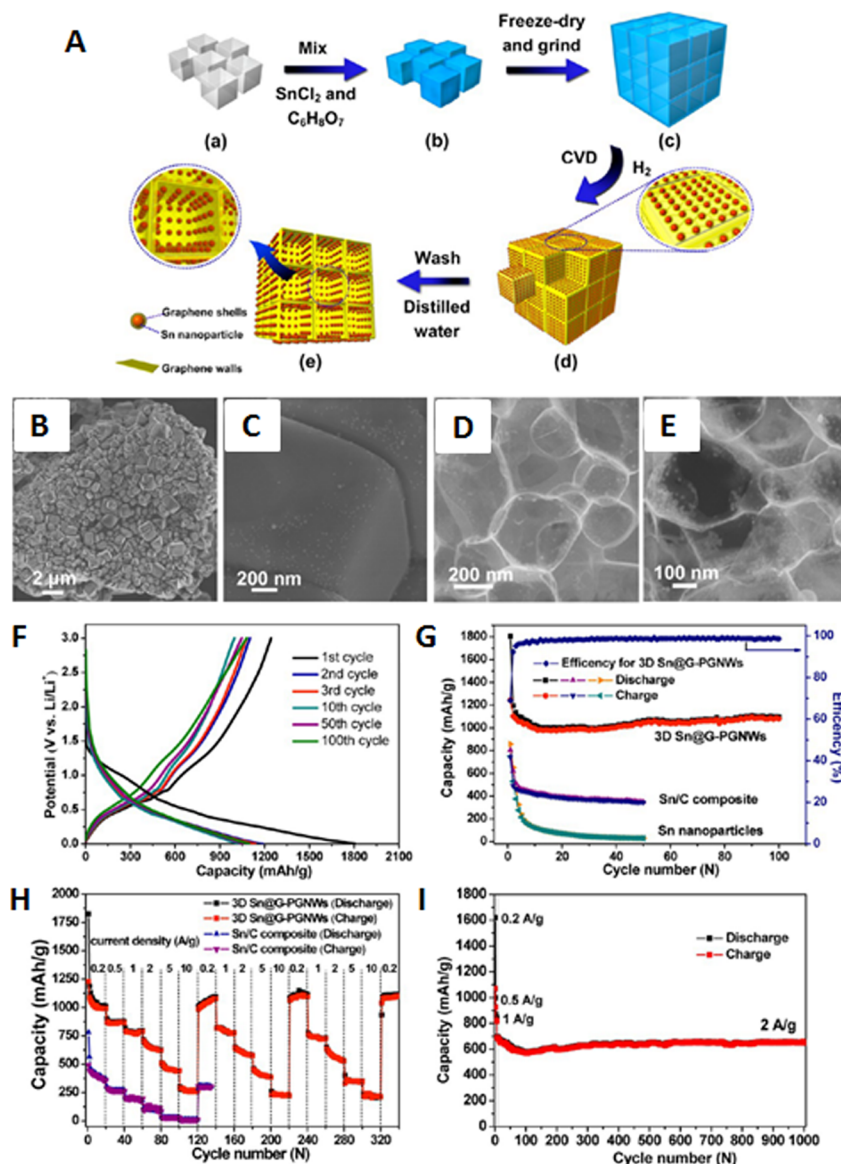


**Figure 13.** (A) Schematic illustration of the in situ CVD process for the one-step synthesis of 3D Sn@G-PGNWs using 3D NaCl self-assembly as a template. (B, C) SEM images of the CVD-synthesized products before eliminating NaCl. (D, E) SEM images of 3D Sn@G-PGNWs. (F) Voltage profiles of the 3D Sn@G-PGNW electrode at a current density of  $0.2 \text{ A g}^{-1}$ . (G) Cycle performance of the 3D Sn@G-PGNWs, Sn/C composite, and commercial Sn nanoparticles at a current density of  $0.2 \text{ A g}^{-1}$ . (H) Rate cycle performance of the electrodes of 3D Sn@G-PGNWs and Sn/C composite at charge/discharge rates from 0.2 to 10 C ( $1 \text{ C} = 1 \text{ A/g}$ ) for 340 cycles. (I) Cycle performance of the 3D Sn@G-PGNW electrode at current densities of 0.2, 0.5, and  $1 \text{ A g}^{-1}$  for the initial six cycles and then  $2 \text{ A g}^{-1}$  for the subsequent 1000 cycles. Reprinted with permission from ref 473. Copyright 2014 American Chemical Society.

presence of the spacers provided 135 and 145% improvements in specific capacity, respectively.<sup>461</sup> Despite the high specific capacity and excellent cycling performance of graphene-based LIBs, the lack of stable voltage plateaus on the charge/discharge curves may suggest their inability to provide a stable voltage output. Furthermore, porous or 3D-graphene-based anodes can create a high density of cross-plane ion diffusion channels, which promote a high rate of lithium ion transport and storage capability for ultrafast charge/discharge function. For example, photothermally reduced graphene anode with a porous framework supplied a steady capacity of  $156 \text{ mAh g}^{-1}$  over 1000 charge/discharge cycles at a current density of  $14.8 \text{ A g}^{-1}$ , providing a stable power density of  $10 \text{ kW kg}^{-1}$ .<sup>462</sup> Apart from that, doping of graphene with heteroatoms such as boron, nitrogen, and phosphorus is able to provide highly disordered

graphene to develop ultrafast charge/discharge LIBs.<sup>463–466</sup> Graphene doped with boron (0.88 atomic %) and nitrogen (3.06 atomic %) demonstrated capacities up to 1549 and  $1043 \text{ mAh g}^{-1}$ , respectively, at a current density of  $50 \text{ mA g}^{-1}$ .<sup>464</sup> Even at a high current density of  $25 \text{ A g}^{-1}$ , the electrodes retained capacities as high as 235 and  $199 \text{ mAh g}^{-1}$ , respectively.

Apart from that, the addition of graphene into metalloids, metals, and metal oxides improves their performances as anode materials by buffering the volume and structural changes that occur over the course of charge/discharge cycles. Although materials such as silicon, germanium, and tin have high theoretical capacities of 3579, 992, and  $1624 \text{ mAh g}^{-1}$ , respectively, they are hampered by a drastic volume change of up to 300% and formation of solid electrolyte interphase

(SEI) during cycling.<sup>454,467</sup> Si/graphene composite prepared from thermally reduced graphene and SiNP demonstrated a high reversible capacity of 1100 mAh g<sup>-1</sup> at a current density of 8 A g<sup>-1</sup> and approximately 3200 mAh g<sup>-1</sup> at 1 A g<sup>-1</sup>.<sup>468</sup> The observed capacity loss of 0.34% (at 8 A g<sup>-1</sup>) and 0.14% (at 1 A g<sup>-1</sup>) per cycle for 150 cycles was due to the formation of SEI and reaction of lithium with residual O- and H-containing groups in graphene. Moreover, a composite of porous silicon nanowire and graphene showed only small changes in specific charge capacity from 2347 to 2041 mAh g<sup>-1</sup> after 20 cycles.<sup>469</sup> The good performance was attributed to the porous structure of Si nanowire and the high conductivity of graphene. Apart from that, carbon-coated GeNP/reduced graphene composite demonstrated a reversible capacity of 940 mAh g<sup>-1</sup> at a current density of 50 mA g<sup>-1</sup> after 50 cycles, while carbon-coated GeNP showed only 490 mAh g<sup>-1</sup> under similar conditions.<sup>470</sup> The carbon coating acted as a buffer in minimizing volume change and facilitated the formation of a stable SEI while the presence of reduced graphene improved the overall dispersibility and conductivity of the composite. On the other hand, Sn/graphene composite with 3D architecture showed an impressive initial discharging capacity of 1250 mAh g<sup>-1</sup> and reversible charging capacity of 810 mAh g<sup>-1</sup> at a current density of 55 mA g<sup>-1</sup>, but it quickly degraded due to the formation of SEI.<sup>471</sup> Nevertheless, the presence of graphene withheld the volume change and thus provided a steady capacity of 508 mAh g<sup>-1</sup>, even after 100 cycles. Another work on graphene/Sn/graphene sandwich hybrid gave a specific capacity of 800 mAh g<sup>-1</sup> in the first 10 cycles and above 590 mAh g<sup>-1</sup> after 60 cycles at a current density of 50 mA g<sup>-1</sup>.<sup>472</sup> Utilizing NaCl particles as a template, the 3D hybrid of Sn/graphene (3D Sn@G-PGNW) was produced (Figure 13A–E).<sup>473</sup> The 3D hybrid provided higher reversible capacity and cycling stability in comparison to Sn/amorphous carbon (Sn/C) composite and Sn nanoparticles (Figure 13F–H). Moreover, a capacity of 682 mAh g<sup>-1</sup> at a current density of 2 A g<sup>-1</sup> was achieved, even after 1000 cycles, and with only 3.7% capacity loss (Figure 13I). On top of these, the incorporation of graphene into anode materials made up of metal oxides served to be vital as well. Typical metal oxide/graphene hybrids that have been investigated so far include SnO<sub>2</sub>, Co<sub>3</sub>O<sub>4</sub>, TiO<sub>2</sub>, NiO, and Fe<sub>3</sub>O<sub>4</sub>.<sup>454</sup> A composites of MoS<sub>2</sub>/graphene has also showed good cycling stability over 100 cycles with a reversible capacity of 1100 mAh g<sup>-1</sup> at a current density of 100 mA g<sup>-1</sup>.<sup>474</sup> Moreover, MoS<sub>2</sub>/3D graphene hybrid demonstrated a reversible capacity of 877 mAh g<sup>-1</sup> at a current density of 100 mA g<sup>-1</sup> after 50 charge/discharge cycles.<sup>475</sup>

While research on graphene for LIBs concentrated mostly on the anode, the high conductivity of graphene is also useful for the enhancement of LIBs cathode.<sup>476</sup> Common cathode materials for LIBs, such as LiCoO<sub>2</sub> (theoretical capacity of 170 mAh g<sup>-1</sup>), LiMn<sub>2</sub>O<sub>4</sub>, LiFePO<sub>4</sub>, and Li<sub>3</sub>V<sub>2</sub>(PO<sub>4</sub>)<sub>3</sub>, typically suffer from low electronic conductivities and impaired rate capability. As such, conducting additives (e.g., carbon black and acetylene black) are often introduced into cathode materials to improve the electrical conductivity and hinder the agglomeration of active electrode components. The availability of graphene has thus prompted its application as conducting additive in LIBs cathodes. For example, LiFePO<sub>4</sub>–graphene composite consisting of 1.5 wt % graphene demonstrated an initial discharge capacity of 160 mAh g<sup>-1</sup> at 0.2 C (LiFePO<sub>4</sub> delivered an initial capacity of 113 mAh g<sup>-1</sup>) and maintained at 109 mAh g<sup>-1</sup>, even at a higher rate of 10 C.<sup>477</sup> While the high

conductivity and structure of graphene is crucial to the rate capability and cyclability of LIBs cathodes, the preparation/mixing of the cathode materials proved to be equally important.

## 6. CONCLUSION AND FUTURE PERSPECTIVES

Graphene and its related materials exhibit a rather more interesting electrochemistry than it may first appear if we were to observe the definition of graphene by the IUPAC. This is due to the fact that a vast majority of graphene-related materials greatly differ from the IUPAC definition, being that these materials are structurally different; they contain defects, several layers, adatoms, and various oxygen functional groups. In addition, graphene often contains impurities, either metallic or carbonaceous, which directly influence the electrochemical behavior of the graphene materials. These impurities originate either from the starting material (graphite) or from the production processes. The most important lesson learnt from the preparation of graphene in the past decade is that the difference in synthetic method for graphene preparation strongly influences its structure and subsequent electrochemistry. Graphene oxide shows inherent solid-state electrochemistry, which originates from the presence of electroactive oxygen functional groups on its structure. This inherent electrochemistry differs based on the preparation method of graphene oxide, either by using chlorate or permanganate oxidants. Graphene oxide fabricated using chlorate oxidant shows a chemically irreversible reduction wave, while the usage of permanganate oxidant provided graphene oxide that exhibits chemically reversible electrochemical behavior in both the cathodic and anodic regions. Such inherent electrochemistry of graphene oxide was utilized in the application of graphene oxide nanoplatelets as labels for biomolecule recognition.

Doping of graphene with heteroatoms is a popular way to enhance its electrochemical performance. Graphene has been doped with both nonmetallic heteroatoms (B, N, S, and P) and transition metals (Pd, Pt, Rh, Ag, Fe, Ni, Co, and Mn). These doped graphene materials were shown to electrocatalyze the oxygen reduction reaction, which is very important for fuel cells and Zn/air battery technologies. Doping of graphene with nitrogen and boron was also reported to enhance the capacitance of graphene. Additional study has been extended to the hydrogenation of graphene, resulting in its partial conversion to graphane. On another note, spectroelectrochemistry is a very useful tool to study graphene. It provides additional insight into the mechanism of electrochemical reduction and oxidation of graphene to graphene oxide. It is also able to provide Raman analyses for doped graphene materials. Moreover, it has been shown that silicon substrate can electronically dope the layer of graphene to which it is attached.

Graphene-based materials have been utilized in a wide variety of electrochemical sensors, including voltammetric, amperometric, potentiometric, and electrochemical impedance spectroscopy. Many new approaches were tested, e.g., using graphene as platforms for biosensing, as carrier of electroactive labels (enzymes), or as a label. The application of heteroatom-doped graphene materials for fuel cells provides hope for the fabrication of metal-free catalyst. Even though the electrochemical application of graphene is growing, it is equally important to gain deeper insights into the factors behind the electrochemical properties of these graphene materials. Even though much of its electrochemistry and potential applications have been reported, many more questions remained unan-

swered. There is definitely huge room for improvement and discovery in graphene research.

## APPENDIX 1: IUPAC DEFINITIONS OF GRAPHITE, GRAPHENE, AND AMORPHOUS CARBON

**Graphite:** An allotropic form of the element carbon consisting of layers of hexagonally arranged carbon atoms in a planar condensed ring system of graphene layers. The layers are stacked parallel to each other in a three-dimensional crystalline long-range order. There are two allotropic forms with different stacking arrangements, hexagonal and rhombohedral. The chemical bonds within the layers are covalent with  $sp^2$  hybridization and with a C–C distance of 141.7 pm. The weak bonds between the layers are metallic with strength comparable to van der Waals bonding only.

**Note:** The term graphite is also used often but incorrectly to describe graphite materials, i.e., materials consisting of graphitic carbon made from carbon materials by processing to temperatures greater than 2500 K, even though no perfect graphite structure is present.

**Graphene layer:** A single carbon layer of the graphite structure, describing its nature by analogy to a polycyclic aromatic hydrocarbon of quasi-infinite size.

**Note:** Previously, descriptions such as graphite layers, carbon layers, or carbon sheets have been used for the term graphene. Because graphite designates that modification of the chemical element carbon in which planar sheets of carbon atoms, each atom bound to three neighbors in a honeycomb-like structure, are stacked in a three-dimensional regular order, it is not correct to use for a single layer a term which includes the term graphite, which would imply a three-dimensional structure. The term graphene should be used only when the reactions, structural relations, or other properties of individual layers are discussed.

**Amorphous carbon:** A carbon material without long-range crystalline order. Short-range order exists, but with deviations of the interatomic distances and/or interbonding angles with respect to the graphite lattice as well as to the diamond lattice.

(Definitions are from ref 7.)

## APPENDIX 2: OVERVIEW OF THE ELECTROCHEMISTRY OF GRAPHENE, GRAPHITE, AND GRAPHENE-RELATED MATERIALS

**Graphite:** It shows, in general, a very fast HET rate at the edges of the basal plane and a slow HET rate at the pristine basal plane. Defects in the basal plane lead to a higher HET rate, while surface oxygen-containing groups usually result in a lower HET rate. Graphite exhibits no inherent electrochemistry; it is very stable and has a large potential window. Graphene, in general, follows these trends. However, as graphene-related materials are very diverse, there are significant specifics.

**Pristine graphene:** The HET rate at pristine graphene is, in general, similar to that of graphite. However, this depends on the types of electrochemical probes used. It has been observed that, with increasing number of layers from monolayer to few layer graphene, the HET rate constant ( $k^0$ ) for ferro/ferricyanide does not change or slightly decreases while the  $k^0$  for  $\text{IrCl}_6^{2-}$  increases. Electrochemistry at folded edges shows a slower HET rate than at opened edges of graphene. Pristine graphene does not exhibit inherent electrochemistry.

**Graphene oxide and reduced graphene oxide:** Graphene oxide (GO) shows poor conductivity and very low/small  $k^0$

value. With the removal of oxygen-containing groups via chemical, electrochemical, or thermal reduction, the HET rate increases. The electrochemical reduction of graphene oxide can be applied for precise tuning of HET rates. Reduced graphene materials are highly defective and thus lead to overall higher HET rates. GO and chemically reduced GO exhibit significant inherent electrochemistry in only cathodic or in both cathodic and anodic regions, depending on whether they are prepared by chlorate or permanganate routes.

**CVD graphene:** Chemical vapor deposition of graphene is typically performed on Ni or Cu substrates. The electrochemistry of CVD graphene is directly related to the number of exposed defects/edges. It can be influenced (enhanced) by adatoms and graphitic islands on the CVD graphene. Similarly to graphite, the basal plane shows low HET kinetics to most electrochemical probes, while the defects/edges provide electrochemically active sites. CVD graphene does not exhibit inherent electrochemistry itself; however, since its growth coverage is usually only 95–98% of the Ni/Cu substrates, inherent electrochemistry can be observed from exposed underlying Ni/Cu metals. In a similar manner, this exposed underlying metal can act as an electrocatalyst.

**3D graphene:** It is typically grown on Ni/Cu substrates by the CVD method and thus its electrochemistry is closely related to CVD graphene. Alternatively, it can be prepared by the graphitization of 3D carbon, which results in a multilayer (graphitic) nature with a large number of defects that facilitate fast HET rates toward numerous electroactive compounds.

## AUTHOR INFORMATION

### Corresponding Author

\*E-mail: pumera@ntu.edu.sg; pumera.research@outlook.com.

### Notes

The authors declare no competing financial interest.

### Biographies



Adriano Ambrosi received his Ph.D. degree from Dublin City University (Dublin, Ireland) in 2007. As a postdoctoral researcher, he firstly worked for two years at ICN (Barcelona, Spain) and then, in 2009, at the National Institute for Materials Science (Tsukuba, Japan). In 2010, he joined the research group of Prof. Martin Pumera at Nanyang Technological University (Singapore), where he currently works as a Senior Research Fellow. His research interests include the application of nanomaterials to electrochemical biosensors, synthesis and fundamental electrochemical studies of graphene and other 2D materials for biosensing and energy storage devices, and synthetic nanomotors.



Chun Kiang Chua obtained his B.Sc. and Ph.D. in Chemistry & Biological Chemistry from the Nanyang Technological University, Singapore, in 2010 and 2013, respectively. He pursued his doctoral research with Prof. Martin Pumera on the synthesis and electrochemistry of graphene materials obtained by the top-down approach. He is currently a Postdoctoral Research Fellow in Prof. Pumera's group. His research interests revolve around the electrochemistry and organic chemistry modifications of carbon nanomaterials.



Alessandra Bonanni received her Ph.D. from Universitat Autònoma de Barcelona, (Barcelona, Spain). She then moved to Japan as a Postdoctoral Research Associate at the National Institute for Materials Science in Tsukuba, Japan. Currently, she is a Lecturer at Nanyang Technological University (NTU), Singapore. Her research interest is focused on the use of novel nanomaterials for the development of electrochemical devices for food analysis and biomedical applications.



Martin Pumera has been a faculty member at Nanyang Technological University (Singapore) since 2010. He received his Ph.D. at Charles University (Prague, Czech Republic), in 2001. After two postdoctoral stays (in the United States and Spain), he joined the National Institute

for Materials Science (Tsukuba, Japan) in 2006 for a tenure-track arrangement, and in 2008, he accepted a tenured position there. In 2009, Prof. Pumera received an ERC-StG award. Prof. Pumera has broad interests in nanomaterials and microsystems, in the specific areas of electrochemistry and synthetic chemistry of carbon nanomaterials, nanomotors, nanotoxicity, and energy storage devices. He is Associate Editor of *Science and Technology of Advanced Materials* and on the Editorial Board of *Chemistry—A European Journal*, *Electrochemistry Communications*, *Electrophoresis*, *Electroanalysis*, *The Chemical Records*, *ChemElectroChem*, and eight other journals. He has published over 270 peer-reviewed articles and has an h-index of 44.

## ACKNOWLEDGMENTS

M.P. acknowledges a Tier 2 grant (MOE2013-T2-1-056; ARC 35/13) from the Ministry of Education, Singapore.

## REFERENCES

- (1) von Starck, A.; Mühlbauer, A.; Kramer, C. *Handbook of Thermoprocessing Technologies: Fundamentals, Processes, Components, Safety*; Vulkan-Verlag: Essen, Germany, 2005; p 275.
- (2) CRC Handbook of Chemistry and Physics, 94th ed.; CRC Press: Boca Raton, FL, pp 121–123.
- (3) CRC Handbook of Chemistry and Physics, 94th ed.; CRC Press: Boca Raton, FL, p 46.
- (4) Lincoln Vogel, F. *J. Mater. Sci.* **1977**, *12*, 982.
- (5) CRC Handbook of Chemistry and Physics, 94th ed.; CRC Press: Boca Raton, FL, pp 41–43.
- (6) CRC Handbook of Chemistry and Physics, 94th ed.; CRC Press: Boca Raton, FL, pp 209–210.
- (7) Fitzer, E.; Kochling, K. H.; Boehm, H. P.; Marsh, H. *Pure Appl. Chem.* **1995**, *67*, 473.
- (8) Tiberj, A.; Huntzinger, J.-R.; Camassel, J.; Hiebel, F.; Mahmood, A.; Mallet, P.; Naud, C.; Veullien, J.-Y. *Nanoscale Res. Lett.* **2011**, *6*, 1.
- (9) Lenski, D. R.; Fuhrer, M. S. *J. Appl. Phys.* **2011**, *110*, 013720.
- (10) Morgan, A. E.; Somorjai, G. A. *Surf. Sci.* **1968**, *12*, 405.
- (11) [http://www.nobelprize.org/nobel\\_prizes/physics/laureates/2010](http://www.nobelprize.org/nobel_prizes/physics/laureates/2010).
- (12) Novoselov, K. S.; Geim, A. K.; Morozov, S. V.; Jiang, D.; Zhang, Y.; Dubonos, S. V.; Grigorieva, I. V.; Firsov, A. A. *Science* **2004**, *306*, 666.
- (13) Dreyer, D. R.; Ruoff, R. S.; Bielawski, C. W. *Angew. Chem., Int. Ed.* **2010**, *49*, 9336.
- (14) Boehm, H.-P. *Angew. Chem., Int. Ed.* **2010**, *49*, 9332.
- (15) Novoselov, K.; Jiang, D.; Schedin, F.; Booth, T.; Khotkevich, V.; Morozov, S.; Geim, A. *Proc. Natl. Acad. Sci. U. S. A.* **2005**, *102*, 10451.
- (16) Wu, J. S.; Pisula, W.; Mullen, K. *Chem. Rev.* **2007**, *107*, 718.
- (17) Guinea, F.; Katsnelson, M. I.; Geim, A. K. *Nat. Phys.* **2009**, *6*, 30.
- (18) Lee, C.; Wei, X.; Kysar, J. W.; Hone, J. *Science* **2008**, *321*, 385.
- (19) Balandin, A. A.; Ghosh, S.; Bao, W. Z.; Calizo, I.; Teweldebrhan, D.; Miao, F.; Lau, C. N. *Nano Lett.* **2008**, *8*, 902.
- (20) Geim, A.; Novoselov, K. *Nat. Mater.* **2007**, *6*, 183.
- (21) Geim, A. K. *Science* **2009**, *324*, 1530.
- (22) Banks, C.; Moore, R.; Davies, T.; Compton, R. *Chem. Commun.* **2004**, 1804.
- (23) Li, W.; Tan, C.; Lowe, M.; Abruna, H.; Ralph, D. *ACS Nano* **2011**, *5*, 2264.
- (24) Valota, A. T.; Kinloch, I. A.; Novoselov, K. S.; Casiraghi, C.; Eckmann, A.; Hill, E. W.; Dryfe, R. A. W. *ACS Nano* **2011**, *5*, 8809.
- (25) Banks, C.; Davies, T.; Wildgoose, G.; Compton, R. *Chem. Commun.* **2005**, 829.
- (26) Kampouris, D. K.; Banks, C. E. *Chem. Commun.* **2010**, *46*, 8986.
- (27) Hernandez, Y.; Nicolosi, V.; Lotya, M.; Blighe, F. M.; Sun, Z. Y.; De, S.; McGovern, I. T.; Holland, B.; Byrne, M.; Gun'ko, Y. K.; Boland, J. J.; Niraj, P.; Duesberg, G.; Krishnamurthy, S.; Goodhue, R.; Hutchison, J.; Scardaci, V.; Ferrari, A. C.; Coleman, J. N. *Nat. Nanotechnol.* **2008**, *3*, 563.

- (28) Hernandez, Y.; Lotya, M.; Rickard, D.; Bergin, S. D.; Coleman, J. N. *Langmuir* **2010**, *26*, 3208.
- (29) Blake, P.; Brimicombe, P. D.; Nair, R. R.; Booth, T. J.; Jiang, D.; Schedin, F.; Ponomarenko, L. A.; Morozov, S. V.; Gleeson, H. F.; Hill, E. W.; Geim, A. K.; Novoselov, K. S. *Nano Lett.* **2008**, *8*, 1704.
- (30) Li, X.; Zhang, G.; Bai, X.; Sun, X.; Wang, X.; Wang, E.; Dai, H. *Nat. Nanotechnol.* **2008**, *3*, 538.
- (31) Lotya, M.; Hernandez, Y.; King, P. J.; Smith, R. J.; Nicolosi, V.; Karlsson, L. S.; Blighe, F. M.; De, S.; Wang, Z. M.; McGovern, I. T.; Duesberg, G. S.; Coleman, J. N. *J. Am. Chem. Soc.* **2009**, *131*, 3611.
- (32) Lotya, M.; King, P.; Khan, U.; De, S.; Coleman, J. *ACS Nano* **2010**, *4*, 3155.
- (33) Englert, J. M.; Rohrl, J.; Schmidt, C. D.; Graupner, R.; Hundhausen, M.; Hauke, F.; Hirsch, A. *Adv. Mater.* **2009**, *21*, 4265.
- (34) Valles, C.; Drummond, C.; Saadaoui, H.; Furtado, C. A.; He, M.; Roubeau, O.; Ortolani, L.; Monthioux, M.; Penicaud, A. *J. Am. Chem. Soc.* **2008**, *130*, 15802.
- (35) Behabtu, N.; Lomeda, J.; Green, M.; Higginbotham, A.; Sinitskii, A.; Kosynkin, D.; Tsentalovich, D.; Parra-Vasquez, A.; Schmidt, J.; Kesselman, E.; Cohen, Y.; Talmon, Y.; Tour, J.; Pasquali, M. *Nat. Nanotechnol.* **2010**, *5*, 406.
- (36) Green, A.; Hersam, M. *Nano Lett.* **2009**, *9*, 4031.
- (37) Wang, L.; Ambrosi, A.; Pumera, M. *Chem.-Asian J.* **2013**, *8*, 1200.
- (38) Brownson, D. A. C.; Banks, C. E. *Electrochem. Commun.* **2011**, *13*, 111.
- (39) Brownson, D. A. C.; Metters, J. P.; Kampouris, D. K.; Banks, C. E. *Electroanalysis* **2011**, *23*, 894.
- (40) Bonanni, A.; Pumera, M. *Electrochem. Commun.* **2012**, *16*, 19.
- (41) Jnouï, A.; Metrot, A.; Storck, A. *Electrochim. Acta* **1982**, *27*, 1247.
- (42) Takada, Y.; Fujii, R. *Tanso* **1985**, *1985*, 110.
- (43) Noel, M.; Santhanam, R.; Flora, M. F. *J. Appl. Electrochem.* **1994**, *24*, 455.
- (44) Takenaka, H.; Kawaguchi, M.; Lerner, M.; Bartlett, N. *J. Chem. Soc. Chem. Commun.* **1987**, 1431.
- (45) Inagaki, M.; Iwashita, N.; Wang, Z. D.; Maeda, Y. *Synth. Met.* **1988**, *26*, 41.
- (46) Low, C. T. J.; Walsh, F. C.; Chakrabarti, M. H.; Hashim, M. A.; Hussain, M. A. *Carbon* **2013**, *54*, 1.
- (47) Su, C.-Y.; Lu, A.-Y.; Xu, Y.; Chen, F.-R.; Khlobystov, A. N.; Li, L.-J. *ACS Nano* **2011**, *5*, 2332.
- (48) Wang, G.; Wang, B.; Park, J.; Wang, Y.; Sun, B.; Yao, J. *Carbon* **2009**, *47*, 3242.
- (49) Alanyalioglu, M.; Jose Segura, J.; Oro-Sole, J.; Casan-Pastor, N. *Carbon* **2012**, *50*, 142.
- (50) Morales, G. M.; Schifani, P.; Ellis, G.; Ballesteros, C.; Martinez, G.; Barbero, C.; Salavagione, H. J. *Carbon* **2011**, *49*, 2809.
- (51) Wang, J.; Manga, K. K.; Bao, Q.; Loh, K. P. *J. Am. Chem. Soc.* **2011**, *133*, 8888.
- (52) Zhong, Y. L.; Swager, T. M. *J. Am. Chem. Soc.* **2012**, *134*, 17896.
- (53) Brodie, B. C. *Philos. Trans. R. Soc. Lon.* **1859**, *149*, 249.
- (54) Staudenmaier, L. *Ber. Dtsch. Chem. Ges.* **1898**, *31*, 1481.
- (55) Hofmann, U.; König, E. Z. *Anorg. Allg. Chem.* **1937**, *234*, 311.
- (56) Hummers, W. S.; Offeman, R. E. *J. Am. Chem. Soc.* **1958**, *80*, 1339.
- (57) Marcano, D.; Kosynkin, D.; Berlin, J.; Sinitskii, A.; Sun, Z.; Slesarev, A.; Alemany, L.; Lu, W.; Tour, J. *ACS Nano* **2010**, *4*, 4806.
- (58) Dreyer, D. R.; Park, S.; Bielawski, C. W.; Ruoff, R. S. *Chem. Soc. Rev.* **2010**, *39*, 228.
- (59) Zhu, Y. W.; Murali, S.; Cai, W. W.; Li, X. S.; Suk, J. W.; Potts, J. R.; Ruoff, R. S. *Adv. Mater.* **2010**, *22*, 3906.
- (60) Schniepp, H. C.; Li, J. L.; McAllister, M. J.; Sai, H.; Herrera-Alonso, M.; Adamson, D. H.; Prud'homme, R. K.; Car, R.; Saville, D. A.; Aksay, I. A. *J. Phys. Chem. B* **2006**, *110*, 8535.
- (61) McAllister, M. J.; Li, J. L.; Adamson, D. H.; Schniepp, H. C.; Abdala, A. A.; Liu, J.; Herrera-Alonso, M.; Milius, D. L.; Car, R.; Prud'homme, R. K.; Aksay, I. A. *Chem. Mater.* **2007**, *19*, 4396.
- (62) Sofer, Z.; Simek, P.; Pumera, M. *Phys. Chem. Chem. Phys.* **2013**, *15*, 9257.
- (63) Chee, S. Y.; Poh, H. L.; Chua, C. K.; Sanek, F.; Sofer, Z.; Pumera, M. *Phys. Chem. Chem. Phys.* **2012**, *14*, 12794.
- (64) Kotov, N. A.; Dekany, I.; Fendler, J. H. *Adv. Mater.* **1996**, *8*, 637.
- (65) Zhou, M.; Wang, Y.; Zhai, Y.; Zhai, J.; Ren, W.; Wang, F.; Dong, S. *Chem.—Eur. J.* **2009**, *15*, 6116.
- (66) Ambrosi, A.; Bonanni, A.; Sofer, Z.; Cross, J. S.; Pumera, M. *Chem.—Eur. J.* **2011**, *17*, 10763.
- (67) Sung Jin, A.; Yanwu, Z.; Sun Hwa, L.; Meryl, D. S.; Tryggvi, E.; Sungjin, P.; Aruna, V.; Jinho, A.; Rodney, S. R. *J. Phys. Chem. Lett.* **2010**, *1*, 1259.
- (68) Guo, H.-L.; Wang, X.-F.; Qian, Q.-Y.; Wang, F.-B.; Xia, X.-H. *ACS Nano* **2009**, *3*, 2653.
- (69) Ambrosi, A.; Pumera, M. *Chem.—Eur. J.* **2013**, *19*, 4748.
- (70) Stankovich, S.; Dikin, D. A.; Piner, R. D.; Kohlhaas, K. A.; Kleinhammes, A.; Jia, Y.; Wu, Y.; Nguyen, S. T.; Ruoff, R. S. *Carbon* **2007**, *45*, 1558.
- (71) Gao, W.; Alemany, L. B.; Ci, L. J.; Ajayan, P. M. *Nat. Chem.* **2009**, *1*, 403.
- (72) Ambrosi, A.; Chua, C. K.; Bonanni, A.; Pumera, M. *Chem. Mater.* **2012**, *24*, 2292.
- (73) Wang, G. X.; Yang, J.; Park, J.; Gou, X. L.; Wang, B.; Liu, H.; Yao, J. *J. Phys. Chem. C* **2008**, *112*, 8192.
- (74) Zhou, X.; Zhang, J.; Wu, H.; Yang, H.; Zhang, J.; Guo, S. *J. Phys. Chem. C* **2011**, *115*, 11957.
- (75) Gao, J.; Liu, F.; Liu, Y.; Ma, N.; Wang, Z.; Zhang, X. *Chem. Mater.* **2010**, *22*, 2213.
- (76) Zhu, C.; Guo, S.; Fang, Y.; Dong, S. *ACS Nano* **2010**, *4*, 2429.
- (77) Thakur, S.; Karak, N. *Carbon* **2012**, *50*, 5331.
- (78) Kuila, T.; Bose, S.; Khanra, P.; Mishra, A. K.; Kim, N. H.; Lee, J. H. *Carbon* **2012**, *50*, 914.
- (79) Akhavan, O.; Ghaderi, E. *Carbon* **2012**, *50*, 1853.
- (80) Cote, L. J.; Cruz-Silva, R.; Huang, J. X. *J. Am. Chem. Soc.* **2009**, *131*, 11027.
- (81) Strong, V.; Dubin, S.; El-Kady, M. F.; Lech, A.; Wang, Y.; Weiller, B. H.; Kaner, R. B. *ACS Nano* **2012**, *6*, 1395.
- (82) Chng, E. L. K.; Pumera, M. *Chem.—Asian J.* **2011**, *6*, 2899.
- (83) Loo, A. H.; Bonanni, A.; Pumera, M. *Nanoscale* **2013**, *5*, 4758.
- (84) Bonanni, A.; Chua, C. K.; Zhao, G. J.; Sofer, Z.; Pumera, M. *ACS Nano* **2012**, *6*, 8546.
- (85) Luo, J.; Cote, L.; Tung, V.; Tan, A.; Goins, P.; Wu, J.; Huang, J. *J. Am. Chem. Soc.* **2010**, *132*, 17667.
- (86) Chen, L.; Hernandez, Y.; Feng, X.; Müllen, K. *Angew. Chem., Int. Ed.* **2012**, *51*, 7640.
- (87) Jiao, L.; Zhang, L.; Wang, X.; Diankov, G.; Dai, H. *Nature* **2009**, *458*, 877.
- (88) Kosynkin, D. V.; Higginbotham, A. L.; Sinitskii, A.; Lomeda, J. R.; Dimiev, A.; Price, B. K.; Tour, J. M. *Nature* **2009**, *458*, 872.
- (89) Higginbotham, A.; Kosynkin, D.; Sinitskii, A.; Sun, Z.; Tour, J. *ACS Nano* **2010**, *4*, 2059.
- (90) Kosynkin, D. V.; Lu, W.; Sinitskii, A.; Pera, G.; Sun, Z. Z.; Tour, J. M. *ACS Nano* **2011**, *5*, 968.
- (91) Cano-Márquez, A.; Rodríguez-Macías, F.; Campos-Delgado, J.; Espinosa-González, C.; Tristán-López, F.; Ramírez-González, D.; Cullen, D.; Smith, D.; Terrones, M.; Vega-Cantú, Y. *Nano Lett.* **2009**, *9*, 1527.
- (92) Elías, A. L.; Botello-Méndez, A. s. R.; Meneses-Rodríguez, D.; Jehová González, V.; Ramírez-González, D.; Ci, L.; Muñoz-Sandoval, E.; Ajayan, P. M.; Terrones, H.; Terrones, M. *Nano Lett.* **2009**, *10*, 366.
- (93) Kang, Y. R.; Li, Y. L.; Deng, M. Y. *J. Mater. Chem.* **2012**, *22*, 16283.
- (94) Wong, C. H. A.; Pumera, M. *Phys. Chem. Chem. Phys.* **2013**, *15*, 7755.
- (95) Chua, C. K.; Sofer, Z.; Pumera, M. *Chem.-Asian J.* **2012**, *7*, 2367.
- (96) Pierson, H. O. *Handbook of Carbon, Graphite, Diamond, And Fullerenes: Properties, Processing, And Applications*; Noyes Publications: Devon, UK, 1993.

- (97) Ambrosi, A.; Chua, C. K.; Khezri, B.; Sofer, Z.; Webster, R. D.; Pumera, M. *Proc. Natl. Acad. Sci. U. S. A.* **2012**, *109*, 12899.
- (98) <http://www.superiorgraphite.com/brands-metalpure.php#synthetic>.
- (99) <http://www.cocangraphite.com/EN/Product/SupeRecarb/>.
- (100) <http://www.famousminerals.net/high-purity-synthetic-graphite.html>.
- (101) Marsh, H.; Heintz, E. A.; Rodríguez-Reinoso, F. *Introduction to Carbon Technologies*; Universidad de Alicante: Alicante, Spain, 1997.
- (102) Ambrosi, A.; Chee, S. Y.; Khezri, B.; Webster, R. D.; Sofer, Z.; Pumera, M. *Angew. Chem., Int. Ed.* **2012**, *S1*, 500.
- (103) Shelimov, K. B.; Esenaliev, R. O.; Rinzler, A. G.; Huffman, C. B.; Smalley, R. E. *Chem. Phys. Lett.* **1998**, *282*, 429.
- (104) Hou, P.-X.; Liu, C.; Cheng, H.-M. *Carbon* **2008**, *46*, 2003.
- (105) Rinaldi, A.; Frank, B.; Su, D. S.; Hamid, S. B. A.; Schlogl, R. *Chem. Mater.* **2011**, *23*, 926.
- (106) Wang, Y. H.; Shan, H. W.; Hauge, R. H.; Pasquali, M.; Smalley, R. E. *J. Phys. Chem. B* **2007**, *111*, 1249.
- (107) Pumera, M.; Ambrosi, A.; Chng, E. L. K. *Chem. Sci.* **2012**, *3*, 3347.
- (108) Wong, C. H. A.; Chua, C. K.; Khezri, B.; Webster, R. D.; Pumera, M. *Angew. Chem., Int. Ed.* **2013**, *S2*, 8685.
- (109) Yang, X. Y.; Dou, X.; Rouhanipour, A.; Zhi, L. J.; Rader, H. J.; Müllen, K. *J. Am. Chem. Soc.* **2008**, *130*, 4216.
- (110) Cai, J. M.; Ruffieux, P.; Jaafar, R.; Bieri, M.; Braun, T.; Blankenburg, S.; Muoth, M.; Seitsonen, A. P.; Saleh, M.; Feng, X. L.; Müllen, K.; Fasel, R. *Nature* **2010**, *466*, 470.
- (111) Berger, C.; Song, Z. M.; Li, T. B.; Li, X. B.; Ogbazghi, A. Y.; Feng, R.; Dai, Z. T.; Marchenkova, A. N.; Conrad, E. H.; First, P. N.; de Heer, W. A. *J. Phys. Chem. B* **2004**, *108*, 19912.
- (112) Berger, C.; Song, Z.; Li, X.; Wu, X.; Brown, N.; Naud, C.; Mayou, D.; Li, T.; Hass, J.; Marchenkova, A. N.; Conrad, E. H.; First, P. N.; de Heer, W. A. *Science* **2006**, *312*, 1191.
- (113) Emtsev, K. V.; Bostwick, A.; Horn, K.; Jobst, J.; Kellogg, G. L.; Ley, L.; McChesney, J. L.; Ohta, T.; Reshanov, S. A.; Roehrl, J.; Rotenberg, E.; Schmid, A. K.; Waldmann, D.; Weber, H. B.; Seyller, T. *Nat. Mater.* **2009**, *8*, 203.
- (114) de Heer, W. A.; Berger, C.; Wu, X. S.; First, P. N.; Conrad, E. H.; Li, X. B.; Li, T. B.; Sprinkle, M.; Hass, J.; Sadowski, M. L.; Potemski, M.; Martinez, G. *Solid State Commun.* **2007**, *143*, 92.
- (115) Lim, C. X.; Hoh, H. Y.; Ang, P. K.; Loh, K. P. *Anal. Chem.* **2010**, *82*, 7387.
- (116) Novoselov, K.; Fal'ko, V.; Colombo, L.; Gellert, P.; Schwab, M.; Kim, K. *Nature* **2012**, *490*, 192.
- (117) Farmer, D.; Chiu, H.-Y.; Lin, Y.-M.; Jenkins, K.; Xia, F.; Avouris, P. *Nano Lett.* **2009**, *9*, 4474.
- (118) Li, X.; Zhu, Y.; Cai, W.; Borysiak, M.; Han, B.; Chen, D.; Piner, R.; Colombo, L.; Ruoff, R. *Nano Lett.* **2009**, *9*, 4359.
- (119) Ambrosi, A.; Pumera, M. *J. Phys. Chem. C* **2013**, *117*, 2053.
- (120) Chen, S.; Brown, L.; Levendorf, M.; Cai, W.; Ju, S.-Y.; Edgeworth, J.; Li, X.; Magnuson, C. W.; Velamakanni, A.; Piner, R. D.; Kang, J.; Park, J.; Ruoff, R. S. *ACS Nano* **2011**, *S*, 1321.
- (121) Prasai, D.; Tuberquia, J. C.; Harl, R. R.; Jennings, G. K.; Bolotin, K. I. *ACS Nano* **2012**, *6*, 1102.
- (122) Rafiee, J.; Mi, X.; Gullapalli, H.; Thomas, A. V.; Yavari, F.; Shi, Y.; Ajayan, P. M.; Koratkar, N. A. *Nat. Mater.* **2012**, *11*, 217.
- (123) Yudasaka, M.; Kikuchi, R.; Matsui, T.; Ohki, Y.; Yoshimura, S.; Ota, E. *Appl. Phys. Lett.* **1995**, *67*, 2477.
- (124) Sutter, P. W.; Flege, J.-I.; Sutter, E. A. *Nat. Mater.* **2008**, *7*, 406.
- (125) Roumen, V.; Alexander, M.; Roumen, H. P.; Raymond, K.; Myrjam, M.; Annick, V.; Chris Van, H. *Nanotechnology* **2010**, *21*, 095602.
- (126) Coraux, J.; N'Diaye, A. T.; Busse, C.; Michely, T. *Nano Lett.* **2008**, *8*, 565.
- (127) Reina, A.; Jia, X.; Ho, J.; Nezich, D.; Son, H.; Bulovic, V.; Dresselhaus, M. S.; Kong, J. *Nano Lett.* **2009**, *9*, 30.
- (128) Li, X.; Cai, W.; An, J.; Kim, S.; Nah, J.; Yang, D.; Piner, R.; Velamakanni, A.; Jung, I.; Tutuc, E.; Banerjee, S. K.; Colombo, L.; Ruoff, R. S. *Science* **2009**, *324*, 1312.
- (129) Kim, K. S.; Zhao, Y.; Jang, H.; Lee, S. Y.; Kim, J. M.; Kim, K. S.; Ahn, J.-H.; Kim, P.; Choi, J.-Y.; Hong, B. H. *Nature* **2009**, *457*, 706.
- (130) Bae, S.; Kim, H.; Lee, Y.; Xu, X.; Park, J.-S.; Zheng, Y.; Balakrishnan, J.; Lei, T.; Kim, H. R.; Song, Y. I.; Kim, Y.-J.; Kim, K. S.; Ozilmez, B.; Ahn, J.-H.; Hong, B. H.; Iijima, S. *Nat. Nanotechnol.* **2010**, *S*, 574.
- (131) Li, X.; Magnuson, C. W.; Venugopal, A.; Tromp, R. M.; Hannon, J. B.; Vogel, E. M.; Colombo, L.; Ruoff, R. S. *J. Am. Chem. Soc.* **2011**, *133*, 2816.
- (132) Sun, Z.; Yan, Z.; Yao, J.; Beitler, E.; Zhu, Y.; Tour, J. M. *Nature* **2010**, *468*, 549.
- (133) Kim, R.-H.; Bae, M.-H.; Kim, D. G.; Cheng, H.; Kim, B. H.; Kim, D.-H.; Li, M.; Wu, J.; Du, F.; Kim, H.-S.; Kim, S.; Estrada, D.; Hong, S. W.; Huang, Y.; Pop, E.; Rogers, J. A. *Nano Lett.* **2011**, *11*, 3881.
- (134) Wassei, J. K.; Mecklenburg, M.; Torres, J. A.; Fowler, J. D.; Regan, B. C.; Kaner, R. B.; Weiller, B. H. *Small* **2012**, *8*, 1415.
- (135) Hao, Y.; Bharathi, M. S.; Wang, L.; Liu, Y.; Chen, H.; Nie, S.; Wang, X.; Chou, H.; Tan, C.; Fallahazad, B.; Ramanarayanan, H.; Magnuson, C. W.; Tutuc, E.; Yakobson, B. I.; McCarty, K. F.; Zhang, Y.-W.; Kim, P.; Hone, J.; Colombo, L.; Ruoff, R. S. *Science* **2013**, *342*, 720.
- (136) Tao, L.; Lee, J.; Chou, H.; Holt, M.; Ruoff, R. S.; Akinwande, D. *ACS Nano* **2012**, *6*, 2319.
- (137) Gong, Y.; Zhang, X.; Liu, G.; Wu, L.; Geng, X.; Long, M.; Cao, X.; Guo, Y.; Li, W.; Xu, J.; Sun, M.; Lu, L.; Liu, L. *Adv. Funct. Mater.* **2012**, *22*, 3153.
- (138) Huang, P. Y.; Ruiz-Vargas, C. S.; van der Zande, A. M.; Whitney, W. S.; Levendorf, M. P.; Kevek, J. W.; Garg, S.; Alden, J. S.; Hustedt, C. J.; Zhu, Y.; Park, J.; McEuen, P. L.; Muller, D. A. *Nature* **2011**, *469*, 389.
- (139) Brownson, D. A. C.; Banks, C. E. *Phys. Chem. Chem. Phys.* **2012**, *14*, 8264.
- (140) Jauregui, L. A.; Cao, H.; Wu, W.; Yu, Q.; Chen, Y. P. *Solid State Commun.* **2011**, *151*, 1100.
- (141) Yazyev, O. V.; Louie, S. G. *Nat. Mater.* **2010**, *9*, 806.
- (142) Kang, J.; Shin, D.; Bae, S.; Hong, B. *Nanoscale* **2012**, *4*, 5527.
- (143) Seul Ki, H.; Seung Min, S.; Onejae, S.; Byung Jin, C. J. *Electrochem. Soc.* **2012**, *159*, K107.
- (144) Liang, X.; Sperling, B. A.; Calizo, I.; Cheng, G.; Hacker, C. A.; Zhang, Q.; Obeng, Y.; Yan, K.; Peng, H.; Li, Q.; Zhu, X.; Yuan, H.; Walker, A. R. H.; Liu, Z.; Peng, L.-m.; Richter, C. A. *ACS Nano* **2011**, *S*, 9144.
- (145) Martins, L. G. P.; Song, Y.; Zeng, T.; Dresselhaus, M. S.; Kong, J.; Araujo, P. T. *Proc. Natl. Acad. Sci. U. S. A.* **2013**, *110*, 17762-7.
- (146) Krasheninnikov, A. V.; Nieminen, R. M. *Theor. Chem. Acc.* **2011**, *129*, 625.
- (147) Hu, F. M.; Ma, T. X.; Lin, H. Q.; Gubernatis, J. E. *Phys. Rev. B* **2011**, *84*, 075414.
- (148) Ambrosi, A.; Pumera, M. *Nanoscale* **2014**, *6*, 472.
- (149) Aleman, B.; Regan, W.; Aloni, S.; Altoe, V.; Alem, N.; Girit, C.; Geng, B. S.; Maserati, L.; Crommie, M.; Wang, F.; Zettl, A. *ACS Nano* **2010**, *4*, 4762.
- (150) Batchelor-McAuley, C.; Wildgoose, G. G.; Compton, R. G.; Shao, L. D.; Green, M. L. H. *Sens. Actuators B Chem.* **2008**, *132*, 356.
- (151) Dai, X.; Wildgoose, G. G.; Compton, R. G. *Analyst* **2006**, *131*, 901.
- (152) Chng, E. L. K.; Pumera, M. *Chem.—Asian J.* **2011**, *6*, 2304.
- (153) Gorantla, S.; Bachmatiuk, A.; Hwang, J.; Alsalmi, H. A.; Kwak, J. Y.; Seyller, T.; Eckert, J.; Spencer, M. G.; Rummeli, M. H. *Nanoscale* **2014**, *6*, 889.
- (154) Gao, L.; Ni, G.-X.; Liu, Y.; Liu, B.; Castro Neto, A. H.; Loh, K. P. *Nature* **2014**, *505*, 190.
- (155) Ambrosi, A.; Bonanni, A.; Sofer, Z.; Pumera, M. *Nanoscale* **2013**, *S*, 2379.
- (156) Brownson, D. A. C.; Banks, C. E. *RSC Adv.* **2012**, *2*, 5385.
- (157) Brownson, D. A. C.; Banks, C. E. *Phys. Chem. Chem. Phys.* **2011**, *13*, 15825.

- (158) Brownson, D. A. C.; Gomez-Mingot, M.; Banks, C. E. *Phys. Chem. Chem. Phys.* **2011**, *13*, 20284.
- (159) Chen, Z. P.; Ren, W. C.; Gao, L. B.; Liu, B. L.; Pei, S. F.; Cheng, H. M. *Nat. Mater.* **2011**, *10*, 424.
- (160) Brownson, D. A. C.; Figueiredo-Filho, L. C. S.; Ji, X.; Gomez-Mingot, M.; Iniesta, J.; Fatibello-Filho, O.; Kampouris, D. K.; Banks, C. E. *J. Mater. Chem. A* **2013**, *1*, 5962.
- (161) Xiao, X. Y.; Beechem, T. E.; Brumbach, M. T.; Lambert, T. N.; Davis, D. J.; Michael, J. R.; Washburn, C. M.; Wang, J.; Brozik, S. M.; Wheeler, D. R.; Burckel, D. B.; Polksky, R. *ACS Nano* **2012**, *6*, 3573.
- (162) Dong, X.; Wang, X.; Wang, L.; Song, H.; Zhang, H.; Huang, W.; Chen, P. *ACS Appl. Mater. Interfaces* **2012**, *4*, 3129.
- (163) Sattayasamitsathit, S.; Gu, Y. E.; Kaufmann, K.; Jia, W. Z.; Xiao, X. Y.; Rodriguez, M.; Minteer, S.; Cha, J.; Burckel, D. B.; Wang, C. M.; Polksky, R.; Wang, J. *J. Mater. Chem. A* **2013**, *1*, 1639.
- (164) Chen, S.; Duan, J. J.; Jaroniec, M.; Qiao, S. Z. *Angew. Chem., Int. Ed.* **2013**, *52*, 13567.
- (165) Chang, Y. H.; Lin, C. T.; Chen, T. Y.; Hsu, C. L.; Lee, Y. H.; Zhang, W. J.; Wei, K. H.; Li, L. *J. Adv. Mater.* **2013**, *25*, 756.
- (166) Xiao, X. Y.; Michael, J. R.; Beechem, T.; McDonald, A.; Rodriguez, M.; Brtunbach, M. T.; Lambert, T. N.; Washburn, C. M.; Wang, J.; Brozik, S. M.; Wheeler, D. R.; Burckel, D. B.; Polksky, R. *J. Mater. Chem.* **2012**, *22*, 23749.
- (167) Shih, C.-J.; Lin, S.; Strano, M. S.; Blankschtein, D. *J. Am. Chem. Soc.* **2010**, *132*, 14638.
- (168) Paredes, J. I.; Villar-Rodil, S.; Martinez-Alonso, A.; Tascon, J. M. D. *Langmuir* **2008**, *24*, 10560.
- (169) Liu, H.; Gao, J.; Xue, M.; Zhu, N.; Zhang, M.; Cao, T. *Langmuir* **2009**, *25*, 12006.
- (170) Su, Q.; Pang, S.; Alijani, V.; Li, C.; Feng, X.; Mullen, K. *Adv. Mater.* **2009**, *21*, 3191.
- (171) Si, Y.; Samulski, E. T. *Nano Lett.* **2008**, *8*, 1679.
- (172) Xu, Y.; Bai, H.; Lu, G.; Li, C.; Shi, G. *J. Am. Chem. Soc.* **2008**, *130*, 5856.
- (173) Ramanathan, T.; Abdala, A. A.; Stankovich, S.; Dikin, D. A.; Herrera Alonso, M.; Piner, R. D.; Adamson, D. H.; Schniepp, H. C.; Chen, X.; Ruoff, R. S.; Nguyen, S. T.; Aksay, I. A.; Prud'Homme, R. K.; Brinson, L. C. *Nat. Nanotechnol.* **2008**, *3*, 327.
- (174) Stankovich, S.; Piner, R. D.; Chen, X. Q.; Wu, N. Q.; Nguyen, S. T.; Ruoff, R. S. *J. Mater. Chem.* **2006**, *16*, 155.
- (175) Li, D.; Muller, M. B.; Gilje, S.; Kaner, R. B.; Wallace, G. G. *Nat. Nanotechnol.* **2008**, *3*, 101.
- (176) Park, S.; An, J.; Piner, R. D.; Jung, I.; Yang, D.; Velamakanni, A.; Nguyen, S. T.; Ruoff, R. S. *Chem. Mater.* **2008**, *20*, 6592.
- (177) Yi, M.; Shen, Z.; Liang, S.; Liu, L.; Zhang, X.; Ma, S. *Chem. Commun.* **2013**, *49*, 11059.
- (178) Blake, P.; Hill, E. W.; Neto, A. H. C.; Novoselov, K. S.; Jiang, D.; Yang, R.; Booth, T. J.; Geim, A. K. *Appl. Phys. Lett.* **2007**, *91*, 063124.
- (179) Roddaro, S.; Pingue, P.; Piazza, V.; Pellegrini, V.; Beltram, F. *Nano Lett.* **2007**, *7*, 2707.
- (180) Jung, I.; Pelton, M.; Piner, R.; Dikin, D. A.; Stankovich, S.; Watcharotone, S.; Hausner, M.; Ruoff, R. S. *Nano Lett.* **2007**, *7*, 3569.
- (181) Stolyarova, E.; Rim, K. T.; Ryu, S.; Maultzsch, J.; Kim, P.; Brus, L. E.; Heinz, T. F.; Hybertsen, M. S.; Flynn, G. W. *Proc. Natl. Acad. Sci. U. S. A.* **2007**, *104*, 9209.
- (182) Meyer, J.; Kisielowski, C.; Erni, R.; Rossell, M.; Crommie, M.; Zettl, A. *Nano Lett.* **2008**, *8*, 3582.
- (183) Liu, G. X.; Teweldebrhan, D.; Balandin, A. A. *IEEE Trans. Nanotechnol.* **2011**, *10*, 865.
- (184) Nair, R. R.; Blake, P.; Blake, J. R.; Zan, R.; Anissimova, S.; Bangert, U.; Golovanov, A. P.; Morozov, S. V.; Geim, A. K.; Novoselov, K. S.; Latychevskaia, T. *Appl. Phys. Lett.* **2010**, *97*, 153102.
- (185) Malard, L. M.; Pimenta, M. A.; Dresselhaus, G.; Dresselhaus, M. S. *Phys. Rep.* **2009**, *473*, 51.
- (186) Ferrari, A.; Meyer, J.; Scardaci, V.; Casiraghi, C.; Lazzeri, M.; Mauri, F.; Piscanec, S.; Jiang, D.; Novoselov, K.; Roth, S.; Geim, A. *Phys. Rev. Lett.* **2006**, *97*, 187401.
- (187) Cancado, L. G.; Takai, K.; Enoki, T.; Endo, M.; Kim, Y. A.; Mizusaki, H.; Speziali, N. L.; Jorio, A.; Pimenta, M. A. *Carbon* **2008**, *46*, 272.
- (188) Eckmann, A.; Felten, A.; Mishchenko, A.; Britnell, L.; Krupke, R.; Novoselov, K. S.; Casiraghi, C. *Nano Lett.* **2012**, *12*, 3925.
- (189) Casiraghi, C.; Hartschuh, A.; Lidorikis, E.; Qian, H.; Harutyunyan, H.; Gokus, T.; Novoselov, K.; Ferrari, A. *Nano Lett.* **2007**, *7*, 2711.
- (190) Luo, D.; Zhang, G.; Liu, J.; Sun, X. *J. Phys. Chem. C* **2011**, *115*, 11327.
- (191) Pumera, M. *Chem. Soc. Rev.* **2010**, *39*, 4146.
- (192) Rice, R. J.; McCreery, R. L. *Anal. Chem.* **1989**, *61*, 1637.
- (193) Bowling, R. J.; Packard, R. T.; McCreery, R. L. *J. Am. Chem. Soc.* **1989**, *111*, 1217.
- (194) Chen, P. H.; McCreery, R. L. *Anal. Chem.* **1996**, *68*, 3958.
- (195) Davies, T. J.; Hyde, M. E.; Compton, R. G. *Angew. Chem., Int. Ed.* **2005**, *44*, 5121.
- (196) Ambrosi, A.; Sasaki, T.; Pumera, M. *Chem.—Asian J.* **2010**, *5*, 266.
- (197) Pumera, M.; Scipioni, R.; Iwai, H.; Ohno, T.; Miyahara, Y.; Boero, M. *Chem.—Eur. J.* **2009**, *15*, 10851.
- (198) Lai, S. C. S.; Patel, A. N.; McKelvey, K.; Unwin, P. R. *Angew. Chem., Int. Ed.* **2012**, *51*, 5405.
- (199) Ambrosi, A.; Bonanni, A.; Pumera, M. *Nanoscale* **2011**, *3*, 2256.
- (200) Ji, X. B.; Banks, C. E.; Crossley, A.; Compton, R. G. *ChemPhysChem* **2006**, *7*, 1337.
- (201) Goh, M. S.; Pumera, M. *Chem.—Asian J.* **2010**, *5*, 2355.
- (202) Goh, M. S.; Pumera, M. *Anal. Chem.* **2010**, *82*, 8367.
- (203) Brownson, D. A. C.; Munro, L. J.; Kampouris, D. K.; Banks, C. E. *RSC Adv.* **2011**, *1*, 978.
- (204) Tan, C.; Rodríguez-López, J.; Parks, J. J.; Ritzert, N. L.; Ralph, D. C.; Abrúñia, H. D. *ACS Nano* **2012**, *6*, 3070.
- (205) Moo, J. G. S.; Ambrosi, A.; Bonanni, A.; Pumera, M. *Chem.—Asian J.* **2012**, *7*, 759.
- (206) Poh, H. L.; Sanek, F.; Ambrosi, A.; Zhao, G. J.; Sofer, Z.; Pumera, M. *Nanoscale* **2012**, *4*, 3515.
- (207) Chua, C. K.; Sofer, Z.; Pumera, M. *Chem.—Eur. J.* **2012**, *18*, 13453.
- (208) Grimshaw, J. In *Electrochemical Reactions and Mechanisms in Organic Chemistry*; Grimshaw, J., Ed.; Elsevier Science B.V.: Amsterdam, 2000.
- (209) Jürgen, O. B.; Heinz, P. F. *Angew. Chem., Int. Ed. Engl.* **1983**, *22*, 950.
- (210) Bonanni, A.; Ambrosi, A.; Pumera, M. *Chem.—Eur. J.* **2012**, *18*, 1668.
- (211) Eng, A. Y. S.; Ambrosi, A.; Chua, C. K.; Šanek, F.; Sofer, Z.; Pumera, M. *Chem.—Eur. J.* **2013**, *19*, 12673.
- (212) Toh, H. S.; Ambrosi, A.; Chua, C. K.; Pumera, M. *J. Phys. Chem. C* **2011**, *115*, 17647.
- (213) Poh, H. L.; Simek, P.; Sofer, Z.; Tomandl, I.; Pumera, M. *J. Mater. Chem. A* **2013**, *1*, 13146.
- (214) Wang, Y.; Shao, Y.; Matson, D. W.; Li, J.; Lin, Y. *ACS Nano* **2010**, *4*, 1790.
- (215) Poh, H. L.; Simek, P.; Sofer, Z.; Pumera, M. *Chem.—Eur. J.* **2013**, *19*, 2655.
- (216) Pumera, M.; Wong, C. H. A. *Chem. Soc. Rev.* **2013**, *42*, 5987.
- (217) Poh, H. L.; Sofer, Z.; Pumera, M. *Electrochim. Commun.* **2012**, *25*, 58.
- (218) Eng, A. Y. S.; Sofer, Z.; Simek, P.; Kosina, J.; Pumera, M. *Chem.—Eur. J.* **2013**, *19*, 15583.
- (219) Toh, R. J.; Pumera, M. *Faraday Discuss.* **2013**, *164*, 275.
- (220) Chee, S. Y.; Pumera, M. *Analyst* **2012**, *137*, 2039.
- (221) Ambrosi, A.; Pumera, M. *J. Phys. Chem. C* **2011**, *115*, 25281.
- (222) Wong, C. H. A.; Pumera, M. *Electrochim. Commun.* **2012**, *22*, 105.
- (223) Weber, C.; Eisele, D.; Rabe, J.; Liang, Y.; Feng, X.; Zhi, L.; Müllen, K.; Lyon, J.; Williams, R.; Vanden Bout, D.; Stevenson, K. *Small* **2010**, *6*, 184.

- (224) Kalbac, M.; Reina-Cecco, A.; Farhat, H.; Kong, J.; Kavan, L.; Dresselhaus, M. S. *ACS Nano* **2010**, *4*, 6055.
- (225) Kalbac, M.; Farhat, H.; Kong, J.; Janda, P.; Kavan, L.; Dresselhaus, M. S. *Nano Lett.* **2011**, *11*, 1957.
- (226) Kalbac, M.; Kong, J.; Kavan, L.; Dresselhaus, M. S. *Phys. Status Solidi B* **2012**, *249*, 2500.
- (227) Ramesha, G. K.; Sampath, S. *J. Phys. Chem. C* **2009**, *113*, 7985.
- (228) Viinikanoja, A.; Wang, Z.; Kauppila, J.; Kvarnstrom, C. *Phys. Chem. Chem. Phys.* **2012**, *14*, 14003.
- (229) Walker, E. K.; Vanden Bout, D. A.; Stevenson, K. J. *Anal. Chem.* **2012**, *84*, 8190.
- (230) Wang, J. *Analytical Electrochemistry*; John Wiley & Sons, Inc.: Hoboken, NJ, 2006.
- (231) Kang, X.; Wang, J.; Wu, H.; Aksay, I. A.; Liu, J.; Lin, Y. *Biosens. Bioelectron.* **2009**, *25*, 901.
- (232) Qiu, J.-D.; Huang, J.; Liang, R.-P. *Sens. Actuators B Chem.* **2011**, *160*, 287.
- (233) Chen, Y.; Li, Y.; Sun, D.; Tian, D. B.; Zhang, J. R.; Zhu, J. J. *Mater. Chem.* **2011**, *21*, 7604.
- (234) Zheng, J. B.; He, Y. P.; Sheng, Q. L.; Zhang, H. F. *J. Mater. Chem.* **2011**, *21*, 12873.
- (235) Lu, L.-M.; Li, H.-B.; Qu, F.; Zhang, X.-B.; Shen, G.-L.; Yu, R.-Q. *Bioelectron.* **2011**, *26*, 3500.
- (236) Zeng, Q.; Cheng, J.-S.; Liu, X.-F.; Bai, H.-T.; Jiang, J.-H. *Biosens. Bioelectron.* **2011**, *26*, 3456.
- (237) Lu, W. B.; Luo, Y. L.; Chang, G. H.; Sun, X. P. *Biosens. Bioelectron.* **2011**, *26*, 4791.
- (238) Wu, H.; Wang, J.; Kang, X. H.; Wang, C. M.; Wang, D. H.; Liu, J.; Aksay, I. A.; Lin, Y. H. *Talanta* **2009**, *80*, 403.
- (239) Liang, B.; Fang, L.; Yang, G.; Hu, Y. C.; Guo, X. S.; Ye, X. S. *Biosens. Bioelectron.* **2013**, *43*, 131.
- (240) Unnikrishnan, B.; Palanisamy, S.; Chen, S. M. *Biosens. Bioelectron.* **2013**, *39*, 70.
- (241) Mani, V.; Devadas, B.; Chen, S. M. *Biosens. Bioelectron.* **2013**, *41*, 309.
- (242) Gao, H. C.; Xiao, F.; Ching, C. B.; Duan, H. W. *ACS Appl. Mater. Interfaces* **2011**, *3*, 3049.
- (243) Wu, G. H.; Song, X. H.; Wu, Y. F.; Chen, X. M.; Luo, F.; Chen, X. *Talanta* **2013**, *105*, 379.
- (244) Zhu, X. H.; Jiao, Q. F.; Zhang, C. Y.; Zuo, X. X.; Xiao, X.; Liang, Y.; Nan, J. M. *Microchim. Acta* **2013**, *180*, 477.
- (245) Yu, H. Y.; Xu, M. Q.; Yu, S. H.; Zhao, G. C. *Int. J. Electrochem. Sci.* **2013**, *8*, 8050.
- (246) Dong, X. C.; Xu, H.; Wang, X. W.; Huang, Y. X.; Chan-Park, M. B.; Zhang, H.; Wang, L. H.; Huang, W.; Chen, P. *ACS Nano* **2012**, *6*, 3206.
- (247) Tang, L.; Wang, Y.; Li, Y.; Feng, H.; Lu, J.; Li, J. *Adv. Funct. Mater.* **2009**, *19*, 2782.
- (248) Li, Z.; Huang, Y.; Chen, L.; Qin, X.; Huang, Z.; Zhou, Y.; Meng, Y.; Li, J.; Huang, S.; Liu, Y.; Wang, W.; Xie, Q.; Yao, S. *Sens. Actuators B* **2013**, *181*, 280.
- (249) Lu, L. M.; Qiu, X. L.; Zhang, X. B.; Shen, G. L.; Tan, W. H.; Yu, R. Q. *Biosens. Bioelectron.* **2013**, *45*, 102.
- (250) Li, S. J.; Shi, Y. F.; Liu, L.; Song, L. X.; Pang, H.; Du, J. M. *Electrochim. Acta* **2012**, *85*, 628.
- (251) Ensaifi, A. A.; Jafari-Asl, M.; Rezaei, B. *Talanta* **2013**, *103*, 322.
- (252) Qin, X.; Luo, Y.; Lu, W.; Chang, G.; Asiri, A. M.; Al-Youbi, A. O.; Sun, X. *Electrochim. Acta* **2012**, *79*, 46.
- (253) Guo, S.; Wen, D.; Zhai, Y.; Dong, S.; Wang, E. *ACS Nano* **2010**, *4*, 3959.
- (254) Shang, N. G.; Papakonstantinou, P.; McMullan, M.; Chu, M.; Stamboulis, A.; Potenza, A.; Dhesi, S. S.; Marchetto, H. *Adv. Funct. Mater.* **2008**, *18*, 3506.
- (255) Kim, Y.-R.; Bong, S.; Kang, Y.-J.; Yang, Y.; Mahajan, R. K.; Kim, J. S.; Kim, H. *Biosens. Bioelectron.* **2010**, *25*, 2366.
- (256) Han, D.; Han, T.; Shan, C.; Ivaska, A.; Niu, L. *Electroanalysis* **2010**, *22*, 2001.
- (257) Tan, L.; Zhou, K.-G.; Zhang, Y.-H.; Wang, H.-X.; Wang, X.-D.; Guo, Y.-F.; Zhang, H.-L. *Electrochim. Commun.* **2010**, *12*, 557.
- (258) Sun, C.-L.; Lee, H.-H.; Yang, J.-M.; Wu, C.-C. *Biosens. Bioelectron.* **2011**, *26*, 3450.
- (259) Wang, Y.; Peng, W.; Liu, L.; Tang, M.; Gao, F.; Li, M. *Microchim. Acta* **2011**, *174*, 41.
- (260) Palanisamy, S.; Ku, S. H.; Chen, S. M. *Microchim. Acta* **2013**, *180*, 1037.
- (261) Teymourian, H.; Salimi, A.; Khezrian, S. *Biosens. Bioelectron.* **2013**, *49*, 1.
- (262) Liu, Q.; Zhu, X.; Huo, Z.; He, X.; Liang, Y.; Xu, M. *Talanta* **2012**, *97*, 557.
- (263) Li, S. J.; He, J. Z.; Zhang, M. J.; Zhang, R. X.; Lv, X. L.; Li, S. H.; Pang, H. *Electrochim. Acta* **2013**, *102*, 58.
- (264) Palecek, E.; Fojta, M.; Jelen, F.; Vetterl, V. *Electrochemical Analysis of Nucleic Acids*; Wiley: New York, 2002.
- (265) Ambrosi, A.; Pumera, M. *Phys. Chem. Chem. Phys.* **2010**, *12*, 8944.
- (266) Goh, M. S.; Bonanni, A.; Ambrosi, A.; Sofer, Z.; Pumera, M. *Analyst* **2011**, *136*, 4738.
- (267) Goh, M.; Pumera, M. *Anal. Chim. Acta* **2012**, *711*, 29.
- (268) Zhou, M.; Zhai, Y.; Dong, S. *Anal. Chem.* **2009**, *81*, 5603.
- (269) Akhavan, O.; Ghaderi, E.; Rahighi, R. *ACS Nano* **2012**, *6*, 2904.
- (270) Muti, M.; Sharma, S.; Erdem, A.; Papakonstantinou, P. *Electroanalysis* **2011**, *23*, 272.
- (271) Toh, R. J.; Bonanni, A.; Pumera, M. *Electrochim. Commun.* **2012**, *22*, 207.
- (272) Dong, H.; Zhu, Z.; Ju, H.; Yan, F. *Biosens. Bioelectron.* **2012**, *33*, 228.
- (273) Liu, A.-L.; Zhong, G.-X.; Chen, J.-Y.; Weng, S.-H.; Huang, H.-N.; Chen, W.; Lin, L.-Q.; Lei, Y.; Fu, F.-H.; Sun, Z.-l.; Lin, X.-H.; Lin, J.-H.; Yang, S.-Y. *Anal. Chim. Acta* **2013**, *767*, 50.
- (274) Niu, S.; Sun, J.; Nan, C.; Lin, J. *Sens. Actuators B* **2013**, *176*, 58.
- (275) Postma, H. W. C. *Nano Lett.* **2010**, *10*, 420.
- (276) Prasongkit, J.; Grigoriev, A.; Pathak, B.; Ahuja, R.; Scheicher, R. H. *Nano Lett.* **2011**, *11*, 1941.
- (277) Qiu, H.; Guo, W. *Appl. Phys. Lett.* **2012**, *100*, 083106.
- (278) Avdoshenko, S. M.; Nozaki, D.; da Rocha, C. G.; Gonzalez, J. W.; Lee, M. H.; Gutierrez, R.; Cuniberti, G. *Nano Lett.* **2013**, *13*, 1969.
- (279) Garaj, S.; Hubbard, W.; Reina, A.; Kong, J.; Branton, D.; Golovchenko, J. A. *Nature* **2010**, *467*, 190.
- (280) Merchant, C. A.; Healy, K.; Wanunu, M.; Ray, V.; Peterman, N.; Bartel, J.; Fischbein, M. D.; Venta, K.; Luo, Z.; Johnson, A. T. C.; Drndic, M. *Nano Lett.* **2010**, *10*, 2915.
- (281) Freedman, K. J.; Ahn, C. W.; Kim, M. J. *ACS Nano* **2013**, *7*, 5008.
- (282) Schneider, G. F.; Xu, Q.; Hage, S.; Luik, S.; Spoor, J. N. H.; Malladi, S.; Zandbergen, H.; Dekker, C. *Nat. Commun.* **2013**, *4*, 2619.
- (283) Xie, Y.; Chen, A.; Du, D.; Lin, Y. *Anal. Chim. Acta* **2011**, *699*, 44.
- (284) Du, D.; Zou, Z.; Shin, Y.; Wang, J.; Wu, H.; Engelhard, M. H.; Liu, J.; Aksay, I. A.; Lin, Y. *Anal. Chem.* **2010**, *82*, 2989.
- (285) Du, D.; Wang, L.; Shao, Y.; Wang, J.; Engelhard, M. H.; Lin, Y. *Anal. Chem.* **2011**, *83*, 746.
- (286) Zhu, Q.; Chai, Y.; Yuan, R.; Zhuo, Y.; Han, J.; Li, Y.; Liao, N. *Biosens. Bioelectron.* **2013**, *43*, 440.
- (287) Zhao, L.; Li, S.; He, J.; Tian, G.; Wei, Q.; Li, H. *Biosens. Bioelectron.* **2013**, *49*, 222.
- (288) Li, H.; He, J.; Li, S.; Turner, A. P. F. *Biosens. Bioelectron.* **2013**, *43*, 25.
- (289) Han, J.; Ma, J.; Ma, Z. *Biosens. Bioelectron.* **2013**, *47*, 243.
- (290) Loo, A. H.; Bonanni, A.; Pumera, M. *Nanoscale* **2013**, *5*, 7844.
- (291) Guo, C. X.; Zheng, X. T.; Lu, Z. S.; Lou, X. W.; Li, C. M. *Adv. Mater.* **2010**, *22*, 5164.
- (292) Wu, X. M.; Hu, Y. J.; Jin, J.; Zhou, N. L.; Wu, P.; Zhang, H.; Cai, C. X. *Anal. Chem.* **2010**, *82*, 3588.
- (293) Wu, Y. F.; Xue, P.; Kang, Y. J.; Hui, K. M. *Anal. Chem.* **2013**, *85*, 3166.
- (294) Castillo, J. J.; Svendsen, W. E.; Rozlosnik, N.; Escobar, P.; Martínez, F.; Castillo-León, J. *Analyst* **2013**, *138*, 1026.
- (295) Aragay, G.; Merkoçi, A. *Electrochim. Acta* **2012**, *84*, 49.

- (296) Li, J.; Guo, S. J.; Zhai, Y. M.; Wang, E. K. *Anal. Chim. Acta* **2009**, *649*, 196.
- (297) Li, J.; Guo, S. J.; Zhai, Y. M.; Wang, E. K. *Electrochim. Commun.* **2009**, *11*, 1085.
- (298) Gong, J. M.; Zhou, T.; Song, D. D.; Zhang, L. Z. *Sens. Actuators B Chem.* **2010**, *150*, 491.
- (299) Wonsawat, W.; Chuanuwatanakul, S.; Dungchai, W.; Punrat, E.; Motomizu, S.; Chailapakul, O. *Talanta* **2012**, *100*, 282.
- (300) Zhao, Z. Q.; Chen, X.; Yang, Q.; Liu, J. H.; Huang, X. J. *Electrochim. Commun.* **2012**, *23*, 21.
- (301) Gao, C.; Yu, X. Y.; Xu, R. X.; Liu, J. H.; Huang, X. J. *ACS Appl. Mater. Interfaces* **2012**, *4*, 4672.
- (302) Zhang, W.; Wei, J.; Zhu, H. J.; Zhang, K.; Ma, F.; Mei, Q. S.; Zhang, Z. P.; Wang, S. H. *J. Mater. Chem.* **2012**, *22*, 22631.
- (303) Brownson, D. A. C.; Lacombe, A. C.; Kampouris, D. K.; Banks, C. E. *Analyst* **2012**, *137*, 420.
- (304) O'Mahony, A. M.; Wang, J. *Anal. Method* **2013**, *5*, 4296.
- (305) Wang, J. *Anal. Chim. Acta* **2004**, *507*, 3.
- (306) Chua, C. K.; Pumera, M. *Electroanalysis* **2011**, *23*, 2350.
- (307) Chua, C. K.; Pumera, M.; Rulisek, L. *J. Phys. Chem. C* **2012**, *116*, 4243.
- (308) Poh, H. L.; Pumera, M. *Chem.—Asian J.* **2012**, *7*, 412.
- (309) Tan, S. M.; Poh, H. L.; Sofer, Z.; Pumera, M. *Analyst* **2013**, *138*, 4885.
- (310) Goh, M. S.; Pumera, M. *Anal. Bioanal. Chem.* **2011**, *399*, 127.
- (311) Ong, B. K.; Poh, H. L.; Chua, C. K.; Pumera, M. *Electroanalysis* **2012**, *24*, 2085.
- (312) Tan, S. M.; Chua, C. K.; Pumera, M. *Analyst* **2013**, *138*, 1700.
- (313) Seah, T. H.; Poh, H. L.; Chua, C. K.; Sofer, Z.; Pumera, M. *Electroanalysis* **2014**, *26*, 62.
- (314) Yang, S.; Luo, S.; Liu, C.; Wei, W. *Colloids Surf., B* **2012**, *96*, 75.
- (315) Gong, J.; Miao, X.; Zhou, T.; Zhang, L. *Talanta* **2011**, *85*, 1344.
- (316) Du, D.; Liu, J.; Zhang, X.; Cui, X.; Lin, Y. *J. Mater. Chem.* **2011**, *21*, 8032.
- (317) Gong, J.; Miao, X.; Wan, H.; Song, D. *Sens. Actuators B* **2012**, *162*, 341.
- (318) Wang, K.; Li, H.-N.; Wu, J.; Ju, C.; Yan, J.-J.; Liu, Q.; Qiu, B. *Analyst* **2011**, *136*, 3349.
- (319) Li, Y.; Bai, Y.; Han, G.; Li, M. *Sens. Actuators B* **2013**, *185*, 706.
- (320) Wang, K.; Liu, Q.; Dai, L.; Yan, J.; Ju, C.; Qiu, B.; Wu, X. *Anal. Chim. Acta* **2011**, *695*, 84.
- (321) Orazem, M. E.; Tribollet, B. *Electrochemical Impedance Spectroscopy*; Wiley-Interscience: Hoboken, NJ, 2008.
- (322) Bonanni, A.; Loo, A. H.; Pumera, M. *Trends Anal. Chem.* **2012**, *37*, 12.
- (323) Katz, E.; Willner, I. *Electroanalysis* **2003**, *15*, 913.
- (324) Bonanni, A.; Esplandiu, M. J.; Pividori, M. I.; Alegret, S.; del Valle, M. *Anal. Bioanal. Chem.* **2006**, *385*, 1195.
- (325) Loo, A. H.; Bonanni, A.; Pumera, M. *Chem.—Asian J.* **2013**, *8*, 198.
- (326) Loo, A. H.; Bonanni, A.; Pumera, M. *Electrochim. Commun.* **2013**, *28*, 83.
- (327) Dubuisson, E.; Yang, Z.; Loh, K. P. *Anal. Chem.* **2011**, *83*, 2452.
- (328) Bonanni, A.; Pumera, M. *ACS Nano* **2011**, *5*, 2356.
- (329) Giovanni, M.; Bonanni, A.; Pumera, M. *Analyst* **2012**, *137*, 580.
- (330) Yang, T.; Li, Q.; Li, X.; Wang, X.; Du, M.; Jiao, K. *Biosens. Bioelectron.* **2013**, *42*, 415.
- (331) Wang, Z.; Zhang, J.; Chen, P.; Zhou, X.; Yang, Y.; Wu, S.; Niu, L.; Han, Y.; Wang, L.; Boey, F.; Zhang, Q.; Liedberg, B.; Zhang, H. *Biosens. Bioelectron.* **2011**, *26*, 3881.
- (332) Bonanni, A.; Ambrosi, A.; Pumera, M. *Chem.—Eur. J.* **2012**, *18*, 4541.
- (333) Hu, Y.; Li, F.; Bai, X.; Li, D.; Hua, S.; Wang, K.; Niu, L. *Chem. Commun.* **2011**, *47*, 1743.
- (334) Yang, T.; Li, Q.; Meng, L.; Wang, X.; Chen, W.; Jiao, K. *ACS Appl. Mater. Interfaces* **2013**, *5*, 3495.
- (335) Luo, L.-q.; Zhang, Z.; Ding, Y.-p.; Deng, D.-m.; Zhu, X.-l.; Wang, Z.-x. *Nanoscale* **2013**, *5*, 5833.
- (336) Bonanni, A.; Chua, C. K.; Pumera, M. *Chem.—Eur. J.* **2014**, *20*, 217.
- (337) Hu, Y.; Hua, S.; Li, F.; Jiang, Y.; Bai, X.; Li, D.; Niu, L. *Biosens. Bioelectron.* **2011**, *26*, 4355.
- (338) Chen, Y.; Jiang, B.; Xiang, Y.; Chai, Y.; Yuan, R. *Chem. Commun.* **2011**, *47*, 12798.
- (339) Tombelli, S.; Minunni, A.; Mascini, A. *Biosens. Bioelectron.* **2005**, *20*, 2424.
- (340) Roy, S.; Soin, N.; Bajpai, R.; Misra, D. S.; McLaughlin, J. A.; Roy, S. S. *J. Mater. Chem.* **2011**, *21*, 14725.
- (341) Loo, A. H.; Bonanni, A.; Ambrosi, A.; Poh, H. L.; Pumera, M. *Nanoscale* **2012**, *4*, 921.
- (342) Loo, A. H.; Bonanni, A.; Pumera, M. *Nanoscale* **2012**, *4*, 143.
- (343) Hou, L.; Cui, Y.; Xu, M.; Gao, Z.; Huang, J.; Tang, D. *Biosens. Bioelectron.* **2013**, *47*, 149.
- (344) Gutes, A.; Lee, B.-Y.; Carraro, C.; Mickelson, W.; Lee, S.-W.; Maboudian, R. *Nanoscale* **2013**, *5*, 6048.
- (345) Feng, L. Y.; Chen, Y.; Ren, J. S.; Qu, X. G. *Biomaterials* **2011**, *32*, 2930.
- (346) Yang, G.; Cao, J.; Li, L.; Rana, R. K.; Zhu, J.-J. *Carbon* **2013**, *51*, 124.
- (347) Zhang, D.; Zhang, Y.; Zheng, L.; Zhan, Y.; He, L. *Biosens. Bioelectron.* **2013**, *42*, 112.
- (348) Bard, A. J.; Faulkner, L. R. *Electrochemical Methods*; Wiley: New York, 1980.
- (349) Duzgun, A.; Zelada-Guillen, G. A.; Crespo, G. A.; Macho, S.; Riu, J.; Rius, F. X. *Anal. Bioanal. Chem.* **2011**, *399*, 171.
- (350) Fouskaki, M.; Chaniotakis, N. *Analyst* **2008**, *133*, 1072.
- (351) Lai, C.-Z.; Fierke, M. A.; Stein, A.; Bühlmann, P. *Anal. Chem.* **2007**, *79*, 4621.
- (352) Crespo, G. A.; Macho, S.; Rius, F. X. *Anal. Chem.* **2008**, *80*, 1316.
- (353) Crespo, G. A.; Macho, S.; Bobacka, J.; Rius, F. X. *Anal. Chem.* **2009**, *81*, 676.
- (354) Ping, J. F.; Wang, Y. X.; Wu, J.; Ying, Y. B. *Electrochim. Commun.* **2011**, *13*, 1529.
- (355) Ping, J. F.; Wang, Y. X.; Ying, Y. B.; Wu, J. *Anal. Chem.* **2012**, *84*, 3473.
- (356) Jaworska, E.; Lewandowski, W.; Mieczkowski, J.; Maksymiuk, K.; Michalska, A. *Analyst* **2012**, *137*, 1895.
- (357) Hernandez, R.; Riu, J.; Bobacka, J.; Valles, C.; Jimenez, P.; Benito, A. M.; Maser, W. K.; Rius, F. X. *J. Phys. Chem. C* **2012**, *116*, 22570.
- (358) Jaworska, E.; Lewandowski, W.; Mieczkowski, J.; Maksymiuk, K.; Michalska, A. *Analyst* **2013**, *138*, 2363.
- (359) Pumera, M. *Energy Environ. Sci.* **2011**, *4*, 668.
- (360) Kim, T.; Lim, S.; Kwon, K.; Hong, S.-H.; Qiao, W.; Rhee, C.; Yoon, S.-H.; Mochida, I. *Langmuir* **2006**, *22*, 9086.
- (361) Pumera, M.; Smid, B.; Veltruska, K. *J. Nanosci. Nanotechnol.* **2009**, *9*, 2671.
- (362) Stoller, M. D.; Magnuson, C. W.; Zhu, Y.; Murali, S.; Suk, J. W.; Piner, R.; Ruoff, R. S. *Energy Environ. Sci.* **2011**, *4*, 4685.
- (363) Goh, M. S.; Pumera, M. *Electrochim. Commun.* **2010**, *12*, 1375.
- (364) Buglione, L.; Chng, E. L. K.; Ambrosi, A.; Sofer, Z.; Pumera, M. *Electrochim. Commun.* **2012**, *14*, S.
- (365) Bonanni, A.; Pumera, M. *Electrochim. Commun.* **2013**, *26*, 52.
- (366) Song, W.; Ji, X.; Deng, W.; Chen, Q.; Shen, C.; Banks, C. E. *Phys. Chem. Chem. Phys.* **2013**, *15*, 4799.
- (367) Buglione, L.; Bonanni, A.; Ambrosi, A.; Pumera, M. *ChemPlusChem* **2012**, *77*, 71.
- (368) Byon, H. R.; Lee, S. W.; Chen, S.; Hammond, P. T.; Shao-Horn, Y. *Carbon* **2011**, *49*, 457.
- (369) Lu, T.; Pan, L.; Li, H.; Nie, C.; Zhu, M.; Sun, Z. *J. Electroanal. Chem.* **2011**, *661*, 270.
- (370) Qiu, L.; Yang, X.; Gou, X.; Yang, W.; Ma, Z.-F.; Wallace, G. G.; Li, D. *Chem.—Eur. J.* **2010**, *16*, 10653.

- (371) Cheng, Q.; Tang, J.; Ma, J.; Zhang, H.; Shinya, N.; Qin, L.-C. *Phys. Chem. Chem. Phys.* **2011**, *13*, 17615.
- (372) Kim, K.-S.; Park, S.-J. *Electrochim. Acta* **2011**, *56*, 1629.
- (373) Yang, S.-Y.; Chang, K.-H.; Tien, H.-W.; Lee, Y.-F.; Li, S.-M.; Wang, Y.-S.; Wang, J.-Y.; Ma, C.-C. M.; Hu, C.-C. *J. Mater. Chem.* **2011**, *21*, 2374.
- (374) Buglione, L.; Pumera, M. *Electrochim. Commun.* **2012**, *17*, 45.
- (375) Stoller, M. D.; Park, S.; Zhu, Y.; An, J.; Ruoff, R. S. *Nano Lett.* **2008**, *8*, 3498.
- (376) Tang, L. A. L.; Lee, W. C.; Shi, H.; Wong, E. Y. L.; Sadovoy, A.; Gorelik, S.; Hobley, J.; Lim, C. T.; Loh, K. P. *Small* **2012**, *8*, 423.
- (377) Marsh, H.; Rodríguez Reinoso, F. *Activated Carbon*; Elsevier Ltd.: New York, 2006.
- (378) Zhu, Y.; Murali, S.; Stoller, M.; Ganesh, K.; Cai, W.; Ferreira, P.; Pirkle, A.; Wallace, R.; Cychoń, K.; Thommes, M.; Su, D.; Stach, E.; Ruoff, R. *Science* **2011**, *332*, 1537.
- (379) Seredyć, M.; Koscinski, M.; Sliwińska-Bartkowiak, M.; Bandosz, T. J. *ACS Sustainable Chem. Eng.* **2013**, *1*, 1024.
- (380) El-Kady, M. F.; Strong, V.; Dubin, S.; Kaner, R. B. *Science* **2012**, *335*, 1326.
- (381) Yang, X.; Cheng, C.; Wang, Y.; Qiu, L.; Li, D. *Science* **2013**, *341*, 534.
- (382) Brownson, D. A. C.; Banks, C. E. *Chem. Commun.* **2012**, *48*, 1425.
- (383) Seredyć, M.; Hulicova-Jurcakova, D.; Lu, G. Q.; Bandosz, T. J. *Carbon* **2008**, *46*, 1475.
- (384) Kim, W.; Joo, J. B.; Kim, N.; Oh, S.; Kim, P.; Yi, J. *Carbon* **2009**, *47*, 1407.
- (385) Zhao, L.; Fan, L.-Z.; Zhou, M.-Q.; Guan, H.; Qiao, S.; Antonietti, M.; Titirici, M.-M. *Adv. Mater.* **2010**, *22*, 5202.
- (386) Paraknowitsch, J. P.; Zhang, J.; Su, D.; Thomas, A.; Antonietti, M. *Adv. Mater.* **2010**, *22*, 87.
- (387) Zhang, L. L.; Zhao, X.; Ji, H. X.; Stoller, M. D.; Lai, L. F.; Murali, S.; McDonnell, S.; Cleveger, B.; Wallace, R. M.; Ruoff, R. S. *Energy Environ. Sci.* **2012**, *5*, 9618.
- (388) Han, J.; Zhang, L. L.; Lee, S.; Oh, J.; Lee, K. S.; Potts, J. R.; Ji, J. Y.; Zhao, X.; Ruoff, R. S.; Park, S. *ACS Nano* **2013**, *7*, 19.
- (389) Seredyć, M.; Bandosz, T. J. *J. Mater. Chem. A* **2013**, *1*, 11717.
- (390) Chen, S.; Zhu, J.; Wu, X.; Han, Q.; Wang, X. *ACS Nano* **2010**, *4*, 2822.
- (391) Zhao, X.; Zhang, L.; Murali, S.; Stoller, M. D.; Zhang, Q.; Zhu, Y.; Ruoff, R. S. *ACS Nano* **2012**, *6*, 5404.
- (392) Choi, B. G.; Yang, M.; Hong, W. H.; Choi, J. W.; Huh, Y. S. *ACS Nano* **2012**, *6*, 4020.
- (393) Zhang, B.; Yu, B.; Zhou, F.; Liu, W. *J. Mater. Chem. A* **2013**, *1*, 8587.
- (394) Seredyć, M.; Bandosz, T. J. *J. Mater. Chem.* **2012**, *22*, 23525.
- (395) Perera, S. D.; Liyanage, A. D.; Nijem, N.; Ferraris, J. P.; Chabal, Y. J.; Balkus, K. J., Jr. *J. Power Sources* **2013**, *230*, 130.
- (396) Wang, H.; Casalongue, H. S.; Liang, Y.; Dai, H. J. *Am. Chem. Soc.* **2010**, *132*, 7472.
- (397) Chang, J.; Xu, H.; Sun, J.; Gao, L. *J. Mater. Chem.* **2012**, *22*, 11146.
- (398) Lee, K. K.; Deng, S.; Fan, H. M.; Mhaisalkar, S.; Tan, H. R.; Tok, E. S.; Loh, K. P.; Chin, W. S.; Sow, C. H. *Nanoscale* **2012**, *4*, 2958.
- (399) Zhang, K.; Zhang, L. L.; Zhao, X. S.; Wu, J. *Chem. Mater.* **2010**, *22*, 1392.
- (400) Lee, J.-S.; Lee, T.; Song, H.-K.; Cho, J.; Kim, B.-S. *Energy Environ. Sci.* **2011**, *4*, 4148.
- (401) Duan, J.; Zheng, Y.; Chen, S.; Tang, Y.; Jaroniec, M.; Qiao, S. *Chem. Commun.* **2013**, *49*, 7705.
- (402) Cheng, Q.; Tang, J.; Ma, J.; Zhang, H.; Shinya, N.; Qin, L.-C. *Carbon* **2011**, *49*, 2917.
- (403) Liang, Y. Y.; Wang, H. L.; Diao, P.; Chang, W.; Hong, G. S.; Li, Y. G.; Gong, M.; Xie, L. M.; Zhou, J. G.; Wang, J.; Regier, T. Z.; Wei, F.; Dai, H. J. *J. Am. Chem. Soc.* **2012**, *134*, 15849.
- (404) Giovanni, M.; Poh, H. L.; Ambrosi, A.; Zhao, G. J.; Sofer, Z.; Sanek, F.; Khezri, B.; Webster, R. D.; Pumera, M. *Nanoscale* **2012**, *4*, 5002.
- (405) Toh, R. J.; Poh, H. L.; Sofer, Z.; Pumera, M. *Chem.—Asian J.* **2013**, *8*, 1295.
- (406) Parvez, K.; Yang, S.; Hernandez, Y.; Winter, A.; Turchanin, A.; Feng, X.; Müllen, K. *ACS Nano* **2012**, *6*, 9541.
- (407) Li, Y.; Zhou, W.; Wang, H.; Xie, L.; Liang, Y.; Wei, F.; Idrobo, J.-C.; Pennycook, S. J.; Dai, H. *Nat. Nanotechnol.* **2012**, *7*, 394.
- (408) Yang, S.; Feng, X.; Wang, X.; Müllen, K. *Angew. Chem., Int. Ed.* **2011**, *50*, 5339.
- (409) Lin, Z.; Waller, G. H.; Liu, Y.; Liu, M.; Wong, C.-p. *Carbon* **2013**, *53*, 130.
- (410) Yang, Z.; Yao, Z.; Li, G.; Fang, G.; Nie, H.; Liu, Z.; Zhou, X.; Chen, X. a.; Huang, S. *ACS Nano* **2011**, *6*, 205.
- (411) Poh, H. L.; Šimek, P.; Sofer, Z.; Pumera, M. *ACS Nano* **2013**, *7*, 5262.
- (412) Jeon, I.-Y.; Zhang, S.; Zhang, L.; Choi, H.-J.; Seo, J.-M.; Xia, Z.; Dai, L.; Baek, J.-B. *Adv. Mater.* **2013**, *25*, 6138.
- (413) Liang, J.; Jiao, Y.; Jaroniec, M.; Qiao, S. Z. *Angew. Chem., Int. Ed.* **2012**, *51*, 11496.
- (414) Su, Y.; Zhang, Y.; Zhuang, X.; Li, S.; Wu, D.; Zhang, F.; Feng, X. *Carbon* **2013**, *62*, 296.
- (415) Sheng, Z.-H.; Gao, H.-L.; Bao, W.-J.; Wang, F.-B.; Xia, X.-H. *J. Mater. Chem.* **2012**, *22*, 390.
- (416) Choi, C. H.; Chung, M. W.; Kwon, H. C.; Park, S. H.; Woo, S. I. *J. Mater. Chem. A* **2013**, *1*, 3694.
- (417) Wang, L.; Sofer, Z.; Šimek, P.; Tomandl, I.; Pumera, M. *J. Phys. Chem. C* **2013**, *117*, 23251.
- (418) Zheng, Y.; Jiao, Y.; Ge, L.; Jaroniec, M.; Qiao, S. Z. *Angew. Chem., Int. Ed.* **2013**, *52*, 3110.
- (419) Yin, Z. Y.; Zhu, J. X.; He, Q. Y.; Cao, X. H.; Tan, C. L.; Chen, H. Y.; Yan, Q. Y.; Zhang, H. *Adv. Energy Mater.* **2014**, *4*, 1300574.
- (420) Jariwala, D.; Sangwan, V. K.; Lauhon, L. J.; Marks, T. J.; Hersam, M. C. *Chem. Soc. Rev.* **2013**, *42*, 2824.
- (421) Kavan, L.; Yum, J. H.; Grätzel, M. *Phys. Status Solidi B* **2013**, *250*, 2643.
- (422) Grätzel, M. *J. Photochem. Photobiol., C* **2003**, *4*, 145.
- (423) Kavan, L.; Yum, J.-H.; Grätzel, M. *Electrochim. Acta* **2014**, *128*, 349.
- (424) Wang, X.; Zhi, L.; Mullen, K. *Nano Lett.* **2007**, *8*, 323.
- (425) Lee, K. S.; Lee, Y.; Lee, J. Y.; Ahn, J.-H.; Park, J. H. *ChemSusChem* **2012**, *5*, 379.
- (426) Kavan, L.; Yum, J.-H.; Nazeeruddin, M. K.; Grätzel, M. *ACS Nano* **2011**, *5*, 9171.
- (427) Kavan, L.; Yum, J. H.; Grätzel, M. *Nano Lett.* **2011**, *11*, 5501.
- (428) Kavan, L.; Yum, J. H.; Grätzel, M. *ACS Nano* **2011**, *5*, 165.
- (429) Kavan, L.; Yum, J. H.; Grätzel, M. *ACS Appl. Mater. Interfaces* **2012**, *4*, 6998.
- (430) Dai, L. *ChemSusChem* **2010**, *3*, 797.
- (431) Guo, C. X.; Yang, H. B.; Sheng, Z. M.; Lu, Z. S.; Song, Q. L.; Li, C. M. *Angew. Chem., Int. Ed.* **2010**, *49*, 3014.
- (432) Xiao, F. X.; Miao, J. W.; Liu, B. *J. Am. Chem. Soc.* **2014**, *136*, 1559.
- (433) Bi, H.; Huang, F.; Liang, J.; Xie, X.; Jiang, M. *Adv. Mater.* **2011**, *23*, 3202.
- (434) Seol, M.; Youn, D. H.; Kim, J. Y.; Jang, J. W.; Choi, M.; Lee, J. S.; Yong, K. *Adv. Energy Mater.* **2014**, *4*, 1300775.
- (435) Lin, T.; Huang, F.; Liang, J.; Wang, Y. *Energy Environ. Sci.* **2011**, *4*, 862.
- (436) Wu, J.; Becerril, H. A.; Bao, Z.; Liu, Z.; Chen, Y.; Peumans, P. *Appl. Phys. Lett.* **2008**, *92*, 263302.
- (437) Becerril, H. A.; Mao, J.; Liu, Z.; Stoltzberg, R. M.; Bao, Z.; Chen, Y. *ACS Nano* **2008**, *2*, 463.
- (438) Yin, Z.; Sun, S.; Salim, T.; Wu, S.; Huang, X.; He, Q.; Lam, Y. M.; Zhang, H. *ACS Nano* **2010**, *4*, 5263.
- (439) De Arco, L. G.; Zhang, Y.; Schlenker, C. W.; Ryu, K.; Thompson, M. E.; Zhou, C. *ACS Nano* **2010**, *4*, 2865.

- (440) Zhang, D.; Xie, F.; Lin, P.; Choy, W. C. H. *ACS Nano* **2013**, *7*, 1740.
- (441) Liu, J.; Durstock, M.; Dai, L. *Energy Environ. Sci.* **2014**, *7*, 1297.
- (442) Li, S.-S.; Tu, K.-H.; Lin, C.-C.; Chen, C.-W.; Chhowalla, M. *ACS Nano* **2010**, *4*, 3169.
- (443) Jeon, Y.-J.; Yun, J.-M.; Kim, D.-Y.; Na, S.-I.; Kim, S.-S. *Sol. Energy Mater. Sol. Cells* **2012**, *105*, 96.
- (444) Ye, Y.; Dai, L. *J. Mater. Chem.* **2012**, *22*, 24224.
- (445) Li, X.; Zhu, H.; Wang, K.; Cao, A.; Wei, J.; Li, C.; Jia, Y.; Li, Z.; Li, X.; Wu, D. *Adv. Mater.* **2010**, *22*, 2743.
- (446) Feng, T.; Xie, D.; Lin, Y.; Zhao, H.; Chen, Y.; Tian, H.; Ren, T.; Li, X.; Li, Z.; Wang, K.; Wu, D.; Zhu, H. *Nanoscale* **2012**, *4*, 2130.
- (447) Miao, X.; Tongay, S.; Petterson, M. K.; Berke, K.; Rinzler, A. G.; Appleton, B. R.; Hebard, A. F. *Nano Lett.* **2012**, *12*, 2745.
- (448) Zhang, Z. X.; Guo, Y. X.; Wang, X. J.; Li, D.; Wang, F. L.; Xie, S. S. *Adv. Funct. Mater.* **2014**, *24*, 835.
- (449) Behura, S. K.; Nayak, S.; Mukhopadhyay, I.; Jani, O. *Carbon* **2014**, *67*, 766.
- (450) Scrosati, B.; Garche, J. *J. Power Sources* **2010**, *195*, 2419.
- (451) Nishi, Y. *J. Power Sources* **2001**, *100*, 101.
- (452) Etacheri, V.; Marom, R.; Elazari, R.; Salitra, G.; Aurbach, D. *Energy Environ. Sci.* **2011**, *4*, 3243.
- (453) Liu, J.; Liu, X.-W. *Adv. Mater.* **2012**, *24*, 4097.
- (454) Han, S.; Wu, D.; Li, S.; Zhang, F.; Feng, X. *Small* **2013**, *9*, 1173.
- (455) Liu, C.; Li, F.; Ma, L.-P.; Cheng, H.-M. *Adv. Mater.* **2010**, *22*, E28.
- (456) Dahn, J. R.; Zheng, T.; Liu, Y.; Xue, J. S. *Science* **1995**, *270*, 590.
- (457) Sato, K.; Noguchi, M.; Demachi, A.; Oki, N.; Endo, M. *Science* **1994**, *264*, 556.
- (458) Yata, S.; Kinoshita, H.; Komori, M.; Ando, N.; Kashiwamura, T.; Harada, T.; Tanaka, K.; Yamabe, T. *Synth. Met.* **1994**, *62*, 153.
- (459) Pan, D.; Wang, S.; Zhao, B.; Wu, M.; Zhang, H.; Wang, Y.; Jiao, Z. *Chem. Mater.* **2009**, *21*, 3136.
- (460) Lian, P.; Zhu, X.; Liang, S.; Li, Z.; Yang, W.; Wang, H. *Electrochim. Acta* **2010**, *55*, 3909.
- (461) Yoo, E.; Kim, J.; Hosono, E.; Zhou, H.-s.; Kudo, T.; Honma, I. *Nano Lett.* **2008**, *8*, 2277.
- (462) Mukherjee, R.; Thomas, A. V.; Krishnamurthy, A.; Koratkar, N. *ACS Nano* **2012**, *6*, 7867.
- (463) Reddy, A. L. M.; Srivastava, A.; Gowda, S. R.; Gullapalli, H.; Dubey, M.; Ajayan, P. M. *ACS Nano* **2010**, *4*, 6337.
- (464) Wu, Z.-S.; Ren, W.; Xu, L.; Li, F.; Cheng, H.-M. *ACS Nano* **2011**, *5*, 5463.
- (465) Wang, H.; Zhang, C.; Liu, Z.; Wang, L.; Han, P.; Xu, H.; Zhang, K.; Dong, S.; Yao, J.; Cui, G. *J. Mater. Chem.* **2011**, *21*, 5430.
- (466) Zhang, C.; Mahmood, N.; Yin, H.; Liu, F.; Hou, Y. *Adv. Mater.* **2013**, *25*, 4932.
- (467) Xu, C.; Xu, B.; Gu, Y.; Xiong, Z.; Sun, J.; Zhao, X. S. *Energy Environ. Sci.* **2013**, *6*, 1388.
- (468) Zhao, X.; Hayner, C. M.; Kung, M. C.; Kung, H. H. *Adv. Energy Mater.* **2011**, *1*, 1079.
- (469) Wang, X.-L.; Han, W.-Q. *ACS Appl. Mater. Interfaces* **2010**, *2*, 3709.
- (470) Xue, D.-J.; Xin, S.; Yan, Y.; Jiang, K.-C.; Yin, Y.-X.; Guo, Y.-G.; Wan, L.-J. *J. Am. Chem. Soc.* **2012**, *134*, 2512.
- (471) Wang, G.; Wang, B.; Wang, X.; Park, J.; Dou, S.; Ahn, H.; Kim, K. *J. Mater. Chem.* **2009**, *19*, 8378.
- (472) Luo, B.; Wang, B.; Li, X.; Jia, Y.; Liang, M.; Zhi, L. *Adv. Mater.* **2012**, *24*, 3538.
- (473) Qin, J.; He, C.; Zhao, N.; Wang, Z.; Shi, C.; Liu, E.-Z.; Li, J. *ACS Nano* **2014**, *8*, 1728.
- (474) Chang, K.; Chen, W. *ACS Nano* **2011**, *5*, 4720.
- (475) Cao, X.; Shi, Y.; Shi, W.; Rui, X.; Yan, Q.; Kong, J.; Zhang, H. *Small* **2013**, *9*, 3433.
- (476) Kucinskis, G.; Bajars, G.; Kleperis, J. *J. Power Sources* **2013**, *240*, 66.
- (477) Ding, Y.; Jiang, Y.; Xu, F.; Yin, J.; Ren, H.; Zhuo, Q.; Long, Z.; Zhang, P. *Electrochim. Commun.* **2010**, *12*, 10.